8-1-1990

Merging panchromatic multispectral images for enhanced image analysis

Curtis K. Munechika

MERGING PANCHROMATIC AND MULTISPECTRAL IMAGES FOR ENHANCED IMAGE ANALYSIS

by:

CURTIS K. MUNECHIKA, Captain, USAF

A thesis submitted in partial fulfillment of the requirements for the degree of Master of Science in the Center for Imaging Science in the College of Graphic Arts and Photography at the Rochester Institute of Technology

August 1990

Signature of the Author Curtis K. Munechika

Accepted by _____

Coordinator, M.S. Degree Program

Center for Imaging Science
College of Graphic Arts and Photography
Rochester Institute of Technology
Rochester, New York

CERTIFICATE OF APPROVAL

M.S. DEGREE THESIS

The M.S. degree thesis of Curtis Munechika
has been examined and approved by the thesis
committee as satisfactory for the thesis requirement
for the Master of Science degree

Dr. John R. Schott, Thesis Advisor

Lt. Col. Phil Datema

Mr. Carl Salvaggio

23 AUG 90
Date

Center for Imaging Science
College of Graphic Arts and Photography
Rochester Institute of Technology
Rochester, New York

THESIS RELEASE PERMISSION FORM

Title of Thesis: Merging Panchromatic and Multispectral Images for Enhanced Image Analysis

I, Curtis K. Munechika grant permission to the Wallace Memorial Library of the Rochester Institute of Technology to reproduce this thesis in whole or in part provided any reproduction will not be of commercial use or for profit.

Curtis K. Munechika

23 AUG 90

Date

MERGING PANCHROMATIC AND MULTISPECTRAL IMAGES FOR ENHANCED IMAGE ANALYSIS

by

Curtis K. Munechika

Submitted to the Center for Imaging Science in
partial fulfillment of the requirements for the
Master of Science degree at the
Rochester Institute of Technology

ABSTRACT

This study evaluates several methods that enhance the spatial resolution of multispectral images using a finer resolution panchromatic image. The resultant hybrid, high resolution, multispectral data set has increased visible interpretation and improved classification accuracy, while preserving the radiometry of the original multispectral images. These methods can therefore be applied to create simulated high resolution multispectral data, as well as to enhance image analysis.

ACKNOWLEDGEMENTS

This work could not have been completed without the support of many people. I would first like to thank the United States Air Force for allowing me the opportunity to study at the Center of Imaging Science. The experience has been exceptionally rewarding.

I would also like to thank my committee members for all their assistance:

to Dr. John Schott, for providing the overall guidance, focus, and an occasional kick in the pants;

to Lt Col Phil Datema, for his time, patience, and support in maintaining a long distance working relationship; and

to Carl Salvaggio, for answering all of my not-so-quick questions.

Special thanks also to: Jim Warnick who first started this study and was my best sounding board; to Dr. Roger Easton whose company at the oddest hours was appreciated; to Steve Schultz who rescued my work from a terminally ill computer; and to Laura Abplanalp and Leslie Genther who helped in putting this together.

Lastly I wish to acknowledge my comrades-in-arms for their encouragement, assistance, and abuse: Ranjit Bhaskar, Betsy Fry, Gopal Sundaramoorthy, Wendy Rosenblum, Steve Wear, and the many others in the classes of 88 - 90.

DEDICATION

This work is dedicated to my family...

To my parents, for instilling my desire to learn (and for their babysitting);
To my brother, for his insight and time (as well as use of his computer);
and especially

to
Jan, Kristen, and Lauren

Table of Contents

List of Figures

List of Tables

1.0 INTRODUCTION

Spatial resolution is an important parameter in image interpretation. However, to capture multispectral images or images within a narrower spectral bandpass, spatial resolution is often diminished. In general, if a sensing system has fine spectral discrimination, then it is physically difficult to also have fine spatial resolution.

The emphasis of this study is to enhance the spatial resolution of multispectral images using data from another sensor. In particular, this study evaluates several techniques to merge the medium resolution Thematic Mapper (TM) multispectral images with a high resolution panchromatic image captured from the SPOT satellite. The performance of each merging technique is measured by classification accuracy on the hybrid images, as well as on how well the hybrid images maintain the radiometric and spectral information of the TM data.

The results of this study show that these merging techniques can produce high resolution multispectral images for enhanced image analysis. Not only is visible interpretation clearly improved, but classification accuracy is also increased. In addition, the resultant hybrid images adequately maintain the TM radiometry.

For the remainder of this introductory chapter, section 1.1 discusses some concepts on resolution in the remote sensing arena. It covers the effects that different types of resolution have on classification accuracy, as well as the design trade-offs between these types of resolution. Section 1.2 looks at previous work done on merging remotely sensed data.

1.1 Spatial, Spectral, and Radiometric Resolution

In general terms, resolution can be thought of as the ability of a system to distinguish fine detail. Most often, we think of resolution in terms of "*spatial resolution*", or how well we can resolve the spatial detail in an image. As such, there are many ways to measure or quantify the spatial resolution of an imaging system (i.e. by the modulation transfer function, ground resolvable distance, etc).

For simplicity, the ground instantaneous field-of-view (GIFOV) is used in this study. The GIFOV is the projection of the limiting detector aperture onto the ground. It is similar to the ground sample distance and has units of length. Thus the smaller the GIFOV, the smaller the sampling distance on the ground, and the finer the spatial resolution of the system.

However, in the field of remote sensing, and especially with multispectral data, there are other forms of resolution that are equally as important.

"*Radiometric resolution*" is determined by the number of effective grey levels that are available to the system to represent the scene brightness. For example, an 8-bit system would be able to record an image in 256 levels of brightness. Its radiometric resolution would be finer and more precise than a 6-bit system which can only work with 64 levels.

"*Spectral resolution*" can be thought of as the width of the bandpass over which radiance is measured. The more narrow this wavelength interval, the finer the spectral resolution. Intuitively, the finer your spectral resolution, the more spectral bands we could obtain over a given spectral range. The more spectral bands available for analysis, the

more spectral information will be available.

1.1.1 Resolution and Classification Accuracy

The effect of these three types of resolution on classifying images has been studied, particularly since the introduction of the Thematic Mapper.

The Thematic Mapper (TM) was launched aboard Landsat-4 on July 16, 1982. In comparison with the older Multispectral Scanners (MSS), TM provided finer spatial resolution, narrower and more optimally placed spectral bands, and finer radiometric precision. A comparison chart is shown below.

Table 1-1

A Comparison of Multispectral Scanners (MSS) and Thematic Mapper (TM)

	MSS	TM
G IFOV (m)	8 0	30 (bands 1-5, 7) 120 (band 6)
Spectral Bandpass (micron)	0.5 - 0.6 0.6 - 0.7 0.7 - 0.8 0.8 - 1.1	0.45 - 0.52 0.52 - 0.60 0.63 - 0.69 0.76 - 0.90 1.55 - 1.75 10.40 - 12.50 2.08 - 2.35
Quantization Levels	64 (6 bits)	256 (8 bits)

With these improvements in resolution, numerous studies were conducted to

determine their effect on classification accuracy. Even before the TM was launched, Sadowski et al [77] used simulated data to find that classification accuracy would be significantly enhanced with the additional TM spectral bands and the increased number of quantization levels. However, they also discovered that classification accuracy actually decreased as spatial resolution became finer. These results were corroborated by Morgenstern et al [77], Latty and Hoffer [81], Markham and Townshend [81], and Williams et al [84].

The reason behind the apparent lack of effect that finer spatial resolution has on classification is because of two offsetting effects. Improving spatial resolution will sharpen boundaries and reduce the amount of mixed pixels in an image. This reduction in mixed pixels contributes to an increase in classification accuracy. However, improving spatial resolution also increases the within-class spectral variance causing a decrease in classification accuracy [Landgrebe 77, and Irons et al 85]. Thus depending on the input image, increasing spatial resolution may or may not aid in computer classification -- even though the advantages of increased spatial resolution appear obvious when conducting manual photointerpretation.

Many of these studies concluded that the commonly-used per-pixel Gaussian maximum likelihood (GML) classifier did not effectively use the additional information that increased spatial resolution provides. However, in these cases, only spectral bands were used as input to the GML classifier.

To better use this information in high spatial resolution images, current classifiers have been following either of two paths, one using the textural features found in the image and the other using context to support classification. For two of the more well-known papers on using texture and context for classification, refer to Haralick [79] and Gurney and Townshend [81] respectively.

Using these types of classifiers which apply spatial information, classification accuracies have increased with more spatial detail [Di Zenzo et al 87, Hjort and Mohn 84, Warnick et al 89]. Rosenblum [90] found that the optimal set of input features for classification of high resolution air photos contain both spectral and textural information.

Generally, if a classifier can effectively use all spatial, spectral, and radiometric information, classification accuracies can be improved with finer spatial, spectral, and radiometric resolution.

1.1.2 Resolution Trade-offs

Unfortunately, as in many relationships, there are trade-offs between the different types of resolution. For example, if we wished to have a system with fine spatial resolution, it would be very difficult for this system to additionally have fine spectral resolution. To improve the spatial resolution of our scanning system, we would require a smaller GIFOV. A smaller GIFOV means the energy reaching the sensor has originated from a smaller ground area -- and if other parameters remain constant -- this means less energy reaching the sensor. Lower levels of energy means a lower signal level available to the sensor, resulting in a lower signal-to-noise ratio (SNR). To produce useful output, the sensor must be at or above a threshold SNR to distinguish a signal from the noise. To compensate this lower SNR due to a smaller GIFOV we could broaden the spectral bandpass to allow more energy through -- i.e., spectral resolution is sacrificed to compensate for the gain in spatial resolution.

Conversely, if we wished our data to be captured within a narrower spectral band, again less energy would be incident on the detector. Increasing the GIFOV (losing spatial resolution) would increase the number of incident photons on the detector so that an

acceptable SNR is maintained.

Another trade-off mentioned by Green [88] is a simple data handling problem. Suppose we had 8 Mbits of digital storage. We could approximately store either a:

1000 x 1000 pixel image, 8 bits/pixel, 1 spectral band;

or

380 x 380 pixel images, 8 bits/pixel, 7 spectral bands;

or

1000 x 1000 pixel images, 4 bits/pixel, 2 spectral bands.

The first system provides high spatial resolution but limited spectral information. The second example provides a significant amount of spectral data, but at a low spatial resolution. The third system provides some spectral resolution at high spatial resolution, but at much lower radiometric precision than the first two systems. Other similar data handling constraints that could drive information trade-offs are limitations in transmission and acquisition time.

All these system trade-offs are dependent on the current state of technology. With time and technological advances, information trade-offs will become less severe. But given existing data and existing remote sensing systems, we can overcome these current trade-offs by combining data from two complementary systems. The resultant hybrid data set would contain the "best" characteristics of the individual systems.

1.2 Historical Overview on Merging Images

To improve the relatively coarse spatial resolution of multispectral images, the idea of merging data from different sensors has been attempted. Early studies reported successful merging with the Landsat MSS images (80 m GIFOV). Radar images from airborne systems and the Shuttle Imaging Radar (SIR-A) have been merged with MSS images to enhance geological interpretation [Daily 79; Chavez 83]. Lauer and Todd [81] combined MSS and RBV images to obtain a hybrid product, while Schowengerdt [82] merged MSS with the Heat Capacity Mapping Mission (HCCM) data.

With the introduction of the TM and SPOT sensor systems which have finer spatial and spectral resolutions, further studies on merging were reported. All of these merging techniques, as well as those done with MSS images, could basically be classified into 3 categories.

1.2.1 Merging for Display

Price [87] coined the first category of merging techniques as the "ad hoc" approaches. Since the primary concern of these methods was to optimize image display, some unusual operations were done on the data. However, the resultant hybrid images appeared to have increased spatial resolution. Welsh et al [87] summarized these ad hoc methods into two equations:

$$M_i' = a_i \times \left(M_i \times P\right)^{1/2} + b_i \qquad (1\text{-}1)$$

or

$$M_i' = a_i \times \left(\omega_1 M_i \oplus \omega_2 P\right) + b_i \qquad (1\text{-}2)$$

where:

M_i' = the digital count (DC) for a pixel in the i-th band of the merged image;

M_i = DC for the corresponding pixel in the i-th multispectral image;

P = DC for the corresponding panchromatic reference image pixel;

ω_1 , ω_2 = weighting factors;

a_1 , b_1 = scaling factors to optimize the dynamic range; and

$\oplus$ = operator which could be addition, subtraction, multiplication, ratio, etc.

Using these methods and simulated SPOT data, Cliche [85] integrated the panchromatic channel into the multispectral channels to significantly improve visible interpretation. Chavez [84] added edge enhanced (simulated) SPOT data to TM images. Chavez [86] also merged TM data with a digitized panchromatic photograph. Hashim [88] simply "overlaid" registered TM and MSS images to obtain a hybrid product.

Currently, many Geographical Information Systems (GIS) which contain layers of information in their database, implement some sort of data combination for display to the user [Welsh 85; Walsh et al 87]. Since a high priority of a GIS is to optimize image display, "ad hoc" approaches to merging are frequently used. One of the more simpler methods for an enhanced RGB display is to place the high resolution panchromatic image into the green channel, and two low resolution multispectral bands into the red and blue channels. Since the green channel contributes the most to the intensity component, the overall display looks sharper.

1.2.2 Merging by separate manipulation of spatial information

A multispectral image can be thought of as having a spectral component and a spatial component. The second type of merging algorithm first tries to separate these components, then manipulates the spatial component to obtain spatially enhanced images without touching the spectral information.

One way to separate spatial/spectral information is by looking at the spatial frequencies of the image. An image, according to Schowengerdt, can also be considered to be the sum of a low spatial frequency component and a high spatial frequency component [Schowengerdt 80].

$$\text{image} = \text{lowpass}(\text{image}) + \text{highpass}(\text{image}) \qquad (1\text{-}3)$$

The primary assumption in this technique is that the spectral information is contained in the lowpass component and that the spatial information is in the highpass component. If the edges, or the high spatial frequencies of the images to be merged are correlated, then the highpass component of the finer spatial resolution image could be substituted for the highpass component of the lower spatial resolution image. Assuming that the majority of the spectral information is contained in the low frequency component, then the resultant hybrid image would maintain its spectral content while gaining improved spatial resolution.

Schowengerdt used this technique to reconstruct compressed MSS images by extrapolating the edge information from the high resolution bands to the low resolution (compressed) bands. Tom et al [85] used a variation of this technique to sharpen TM band 6 (120 m GIFOV) by using the TM bands that have a 30 m GIFOV.

Another way to separate spatial and spectral information is based on the intensity-hue-saturation (IHS) color transformation [Hayden et al 82]. The IHS transformation allows spatial information, contained in the intensity component, to be treated separately from the spectral information which is embedded in the hue and saturation components. The user can then manipulate the spatial information via the intensity component while maintaining overall color balance of the original scene.

With the IHS method, three carefully selected multispectral bands are transformed into the IHS domain. The digital counts (DC) of the intensity component can then be modified using the high resolution (panchromatic) reference image DCs. The modified data is then transformed back into the red-green-blue (RGB) color domain and displayed.

Using IHS methods, Carper et al [87] and Welsh and Ehlers [87] obtained visually superior results than those obtained using Cliche's (ad hoc) methods. Care has to be taken though, to ensure that the high spatial resolution reference image is highly correlated to the other input images. Having high correlation between two images means that the linear relationship between the images is very strong.

1.2.3 Merging and Maintaining Radiometry

All of these methods up to now produced visually enhanced images. Spatial resolution appeared to take on the reference (panchromatic) image resolution while retaining most of the spectral information. However, in all cases, the specific radiometric values of the multispectral images were lost. The third type of merging algorithm is similar to the ad hoc approach, but is more statistically-based and attempts to maintain radiometric integrity.

One method suggested by Pradines [86] to keep radiometric quality of the multispectral images is illustrated on the next page:

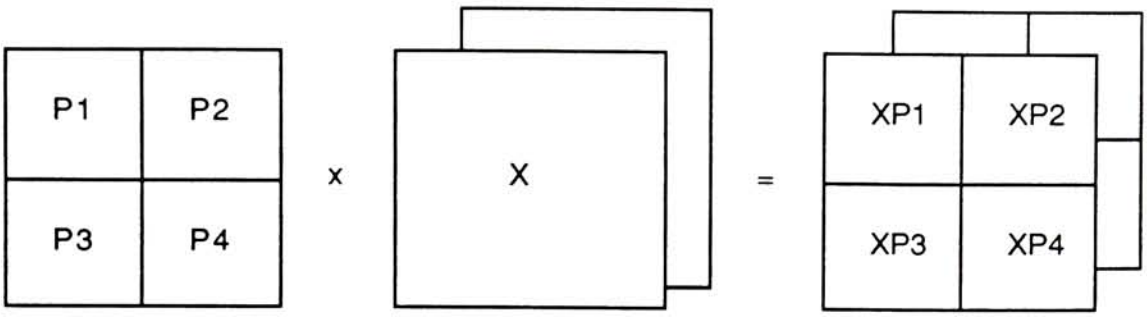

where $XP(J) = X \times \frac{P(J)}{P1 + P2 + P3 + P4}$, $J = 1..4$

Figure 1-1. Pradine's Merging Method

By using this method, the aggregate of the four hybrid pixels will return the radiometry of the original multispectral image. However, the high spatial resolution image (panchromatic channel) must be correlated with the individual multispectral images. For those bands not correlated with the reference image, this merging algorithm cannot be used.

Two other merging techniques which try to maintain the radiometry of the multispectral images are the Price [87] and the DIRS methods [Warnick 89]. These methods are described in more detail in the following section.

2.0 MERGING METHODS AND MODIFICATIONS

This study evaluates the third type of merging techniques -- those techniques which attempt to preserve the integrity of the multispectral data. The two primary techniques under test are the DIRS and the Price methods. In addition, several modifications and enhancements have been incorporated to address some of the known short-comings of these techniques. These modified versions are also included for comparison.

2.1 The DIRS Method

The Digital Imaging and Remote Sensing Laboratory (DIRS) conducted a proof-of-concept study on merging multi-date-multi-sensor-multi-resolution images for enhanced image analysis [Warnick, et al, 1989]. Specifically they merged a high resolution panchromatic image (SPOT-1 panchromatic channel, 10m GIFOV) with medium resolution multispectral images (Landsat-5, TM bands 1-5, 7, 30m GIFOV).

The DIRS method can be summarized in the following steps:

(1) The SPOT image is geometrically registered to the TM images.

(2) A medium resolution panchromatic image is created from a weighted average of TM bands 1 through 4. This synthetic image approximates the same spectral characteristics as the high resolution SPOT panchromatic channel.

(3) The histogram of the SPOT panchromatic image is then linearly adjusted to the histogram of the synthetic TM panchromatic image. This transformation will, to the first order, account for the differing atmospheric and sensor effects between the SPOT and the Landsat TM images.

(4) The images are then merged to create a high resolution, multiband hybrid image. The merging algorithm is:

$$DC_{\text{Hybrid Multiband}}(i) = DC_{\text{SPOT Pan}} \cdot \left(\frac{DC_{TM}(i)}{DC_{\text{Syn TM Pan}}} \right) \qquad (2\text{-}1)$$

where:

$DC_{\text{Hybrid Multiband}}$ (i) is the digital count of the i-th band in the hybrid multiband image;

$DC_{\text{SPOT Pan}}$ is the digital count in the adjusted panchromatic SPOT image;

DC_{TM}(i) is the DC in the i-th band of the original multispectral image; and

$DC_{\text{Syn TM Pan}}$ is the digital count in the synthetic TM panchromatic image.

The DIRS method is applied on a pixel-by-pixel basis, and therefore each of the above terms also has a pixel location. These locations are left off for easier reading.

2.1.1 Results Using the DIRS Merging Method

In addition to the visible improvement of the images, the overall classification accuracy was approximately 10 percentage points higher for the hybrid data set than for the original TM images.

2.1.2 Concerns on the DIRS Merging Method

Because the DIRS method was developed only as a proof-of- concept study, the authors identified several areas for further study.

(1) Concerns on creating the synthetic TM panchromatic image:

The synthetic, medium resolution panchromatic image was produced as a weighted average of TM bands 1 through 4. The weighting factor for each band is determined by finding the common area of the TM spectral response curve and the SPOT panchromatic spectral response curve. The common area under the two curves is then divided by the total area under the TM curve considered. The resultant quotient is the weighting factor for that TM band. By using integration to determine areas, the weighting factor can be represented as:

$$w_i' = \frac{\int_{-\infty}^{\infty} \min\left(TM_{RSR,\,i}(\lambda),\ SPOT_{RSR}(\lambda)\right) d(\lambda)}{\int_{-\infty}^{\infty} TM_{RSR,\,i}(\lambda)\ d\lambda} \qquad (2\text{-}2)$$

where:

i refers to the TM band number, i = 1..4;

w_i' is the weighting factor for the i-th band;

$TM_{RSR,\,i}(\lambda)$ is the relative spectral response curve of the i-th band of the TM scene; and

$SPOT_{RSR}(\lambda)$ is the relative spectral response curve of the SPOT panchromatic channel.

Once the weighting factors are determined for the 4 TM bands, the factors are normalized as:

$$w_i = \frac{w_i'}{\sum_{i=1}^{4} w_i'} \tag{2-3}$$

The synthetic TM panchromatic image can now be created as:

$$TM_{Syn\ Pan} = \sum_{i=1}^{4} w_i \times TM_i \tag{2-4}$$

However, it was found that the synthetic TM panchromatic image was not sensitive in the 700 to 750 nm range, while the SPOT panchromatic sensor is still relatively responsive. Since the reflectivity of vegetation is active in this region, the SPOT panchromatic image responds to this vegetation reflectance information while the synthetic TM panchromatic did not.

To correct this discrepancy, the spectral response curve for TM band 4 was "shifted" from a bandpass of (760, 900) nm down to (710, 850) nm. This shift increased the weighting factor for TM band 4, thereby increasing the responsivity in this region and providing a "truer" approximation of the SPOT panchromatic image. However, the authors suggested that another method of producing a synthetic TM panchromatic image should be explored.

(2) Concerns on the weak correlation between the SPOT panchromatic channel and TM bands 4, 5, and 7:

The merging algorithm used in the DIRS method as previously shown in equation (2-1) is:

$$DC_{\text{Hybrid Multiband}}(i) = DC_{\text{SPOT Pan}} \cdot \left(\frac{DC_{TM}(i)}{DC_{\text{Syn TM Pan}}} \right)$$

where i represents the TM bands 1 through 5 and 7. The concern is when the images for TM bands 4, 5, and 7 are merged with the SPOT panchromatic image. These bands are only weakly correlated with the SPOT panchromatic channel and should probably be merged in a different fashion.

(3) Concerns on Radiometry:

The high resolution, multiband hybrid images can be thought of as TM multiband images that have been spatially enhanced. The enhancement is the result of the integration of the SPOT panchromatic image, but the resultant mean radiances should still be the same as the original TM data. As illustrated below, the original TM images have one pixel to describe a 30m by 30m area, while the hybrid image has 9 pixels to describe the same area. For consistent nomenclature, the 30m by 30m area will be referred to as a "superpixel"; and a 10m by 10m pixel as a "subpixel".

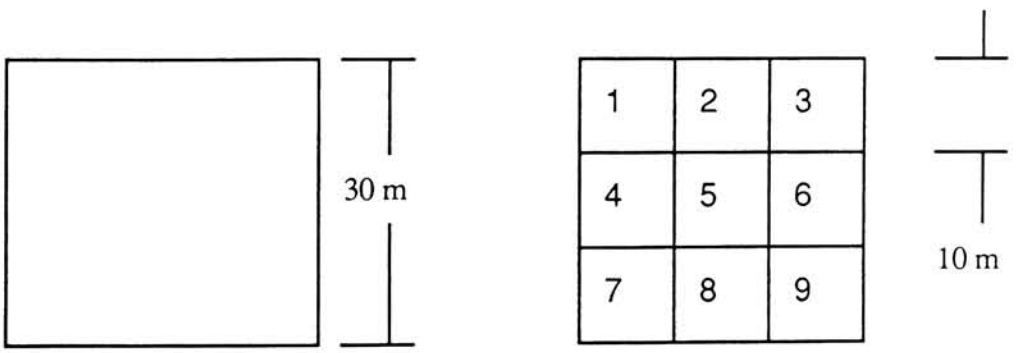

Figure 2-1 Superpixel and subpixels

Assuming linear modeling, the following condition must hold to maintain radiometric integrity.

$$DC_{TM} = \frac{1}{9} \sum_{j=1}^{9} DC_{Hybrid}(j) \qquad (2\text{-}5)$$

However, no such check was made or enforced in the DIRS method.

2.2 General Modifications to the DIRS Method

This section describes three general modifications to the DIRS method which address some of the concerns raised in the previous section. These modifications are grouped together because they do not alter the merging algorithm. Instead, they affect either the input images to the merging algorithm, or the hybrid output images.

2.2.1 Creating a TM panchromatic image

In the DIRS study, the weighting factors for each TM band were obtained by computing the overlapping areas of the SPOT panchromatic and the TM bands spectral response curves. However, the synthetic TM panchromatic image had a lack of sensitivity in the 700-750 nm region. Consequently the TM band 4 spectral response curve was "shifted" to provide a stronger weighting factor and more responsivity in that bandpass.

Another method to obtain the weighting factors has been used by Suits [Suits et al 88] to substitute signals from one sensor for the signals of another. By slightly modifying

Suit's approach, new TM weighting factors were computed using a multivariate regression on estimated sensor signals.

Estimating Sensor Signals

Given the reflectance spectrum of a target, some atmospheric parameters, and an atmospheric model (such as LOWTRAN) we can estimate the radiance that reaches the sensor in a bandpass of interest. This radiance parameter is designated L_λ , and is a function of wavelength, λ. With L_λ we can cascade the sensor's spectral response function, $\beta(\lambda)$, to get the effective radiance seen by the sensor. This effective radiance, L_s is computed as:

$$L_s = \frac{\int_0^\infty L_\lambda \cdot \beta(\lambda)\ d\lambda}{\int_0^\infty \beta(\lambda)\ d\lambda} \qquad (2\text{-}6)$$

The output signal (in DCs) can now be estimated using L_s and the known gain and offset of each sensor.

$$\widehat{DC}_i = \frac{L_{s\text{-}i} - \text{offset}_i}{\text{gain}_i} \qquad (2\text{-}7)$$

where: $\widehat{DC}_i$ = estimated DC of TM band i ;

$L_{s\text{-}i}$ = effective radiance seen by the i-th band; and

gain_i , offset_i = the gain and offset of the i-th band.

These simulated signals are then regressed to determine the weighting factors. This regression can be represented as:

$$\begin{bmatrix} \widehat{DC}_{SPOT\text{-}1} \\ \widehat{DC}_{SPOT\text{-}2} \\ \widehat{DC}_{SPOT\text{-}3} \\ \vdots \\ \widehat{DC}_{SPOT\text{-}n} \end{bmatrix} = \begin{bmatrix} \widehat{DC}_{TM1\text{-}1} & \widehat{DC}_{TM2\text{-}1} & \widehat{DC}_{TM3\text{-}1} & \widehat{DC}_{TM4\text{-}1} \\ \widehat{DC}_{TM1\text{-}2} & \widehat{DC}_{TM2\text{-}2} & \widehat{DC}_{TM3\text{-}2} & \widehat{DC}_{TM4\text{-}2} \\ \widehat{DC}_{TM1\text{-}3} & \widehat{DC}_{TM2\text{-}3} & \widehat{DC}_{TM3\text{-}3} & \widehat{DC}_{TM4\text{-}3} \\ \vdots & \vdots & \vdots & \vdots \\ \widehat{DC}_{TM1\text{-}n} & \widehat{DC}_{TM2\text{-}n} & \widehat{DC}_{TM3\text{-}n} & \widehat{DC}_{TM4\text{-}n} \end{bmatrix} \begin{bmatrix} \omega_1 \\ \omega_2 \\ \omega_3 \\ \omega_4 \end{bmatrix} + \begin{bmatrix} \varepsilon_1 \\ \varepsilon_2 \\ \varepsilon_3 \\ \vdots \\ \varepsilon_n \end{bmatrix} \quad (2\text{-}8)$$

where: $\widehat{DC}$ is the estimated signal of the subscripted sensor;

ω_m , m = 1..4 is the weighting factors for TM1, TM2, TM3, and TM4 respectively;

n is the number of samples in the regression; and

ε is the error vector which is minimized when solving for ω.

To compute the simulated signals from TM1, TM2, TM3, TM4 and SPOT, LOWTRAN 7 (an atmospheric propagation model) was modified. The first modification to LOWTRAN 7 was to allow the program to access a target reflectance spectrum. LOWTRAN 7 in its original form uses only one reflectance value (called the surface albedo or 'SALB') for all wavelengths. This limitation implies that all target reflectance spectra are uniform and flat. The modified version now allows LOWTRAN 7 to access a file containing reflectance information. A reflectance value is then accessed (or computed via interpolation) for each wavelength run by LOWTRAN.

The second modification was available from previous work by Carl Salvaggio. His modification integrated the sensor's spectral response curves with the radiance values computed by LOWTRAN 7. The output signal (in DC) was then computed following

equation (2-7).

Having modified LOWTRAN 7 to produce simulated sensor DCs, 25 target reflectance spectra were chosen. These 25 targets were comprised of 5 major classes -- urban, soil, water, trees, and grass -- with 5 samples each. These spectra are plotted in figures 2-2 through 2-6 on the following pages.

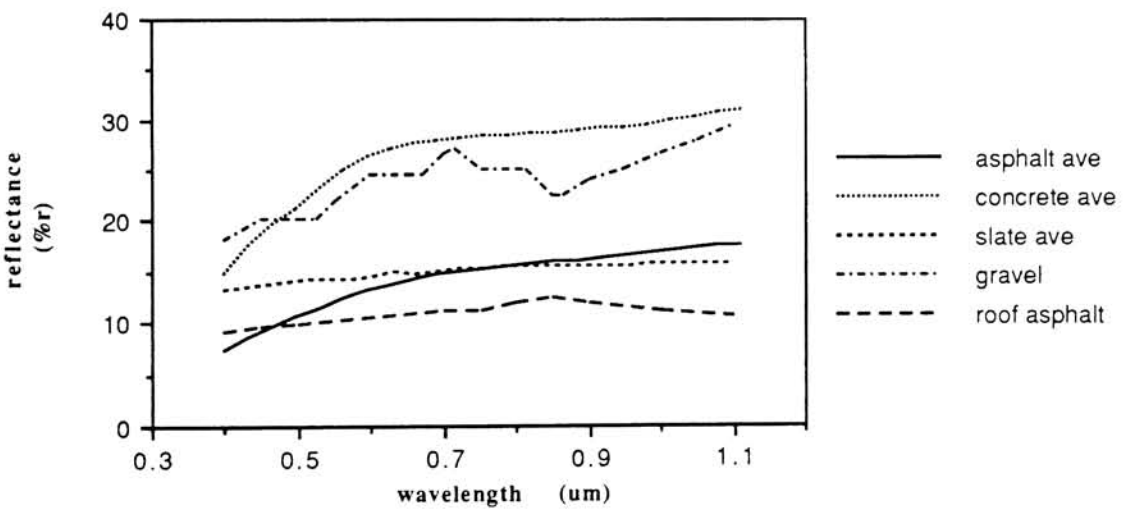

Figure 2-2 Reflectance Spectra for Selected Urban Targets

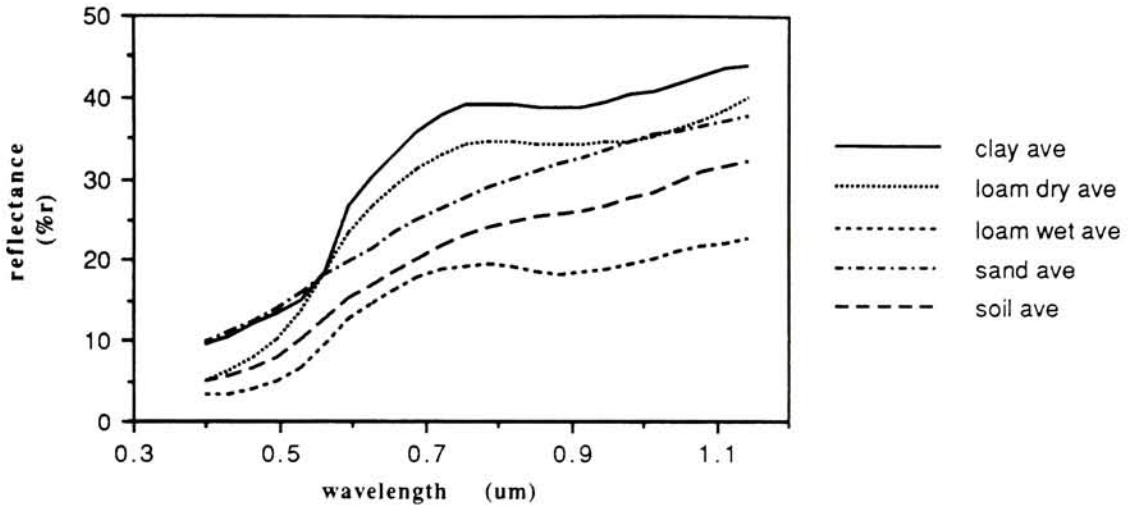

Figure 2-3 Reflectance Spectra of Selected Soil Targets

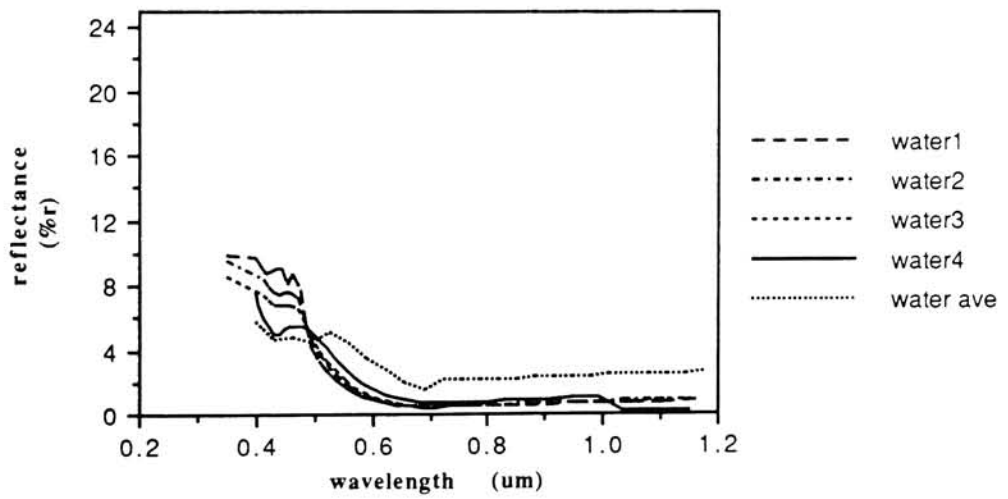

Figure 2-4 Reflectance Spectra of Selected Water Targets

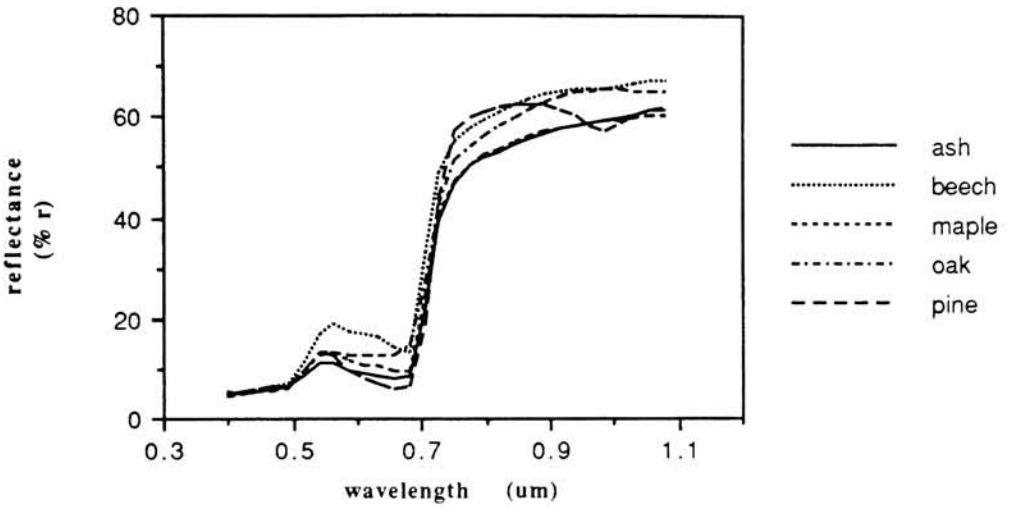

Figure 2-5 Reflectance Spectra of Selected Tree Targets

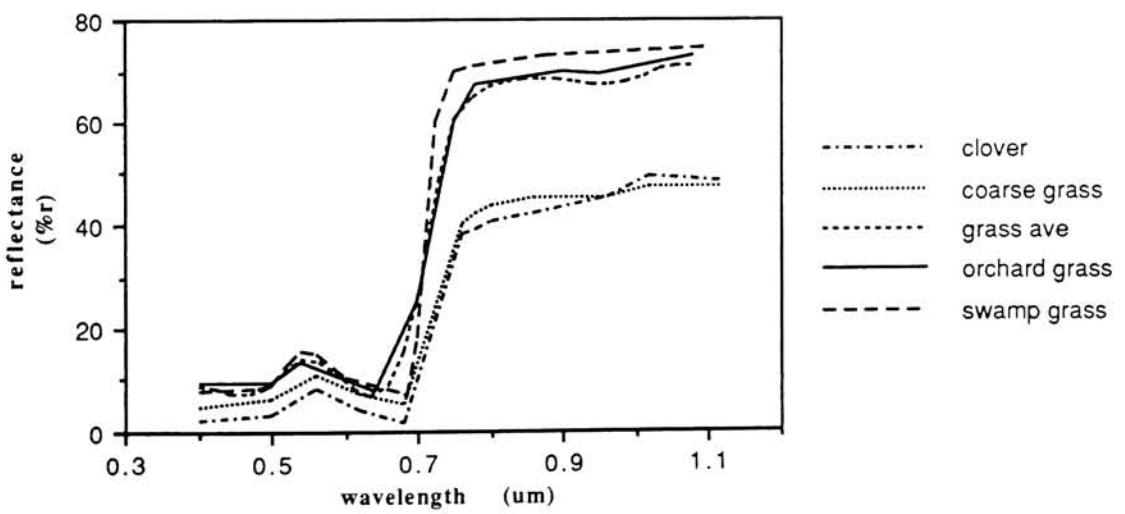

Figure 2-6 Reflectance Spectra of Selected Grass Targets

The modified LOWTRAN 7 was then run with these 25 reflectance spectra at 3 different atmospheres of varying haze. These 75 samples were then regressed via equation (2-8) and new weighting factors for TM1, TM2, TM3 and TM4 were obtained. These results are described in section 4.1. For further information on the LOWTRAN input parameters, the spectral targets, and the sensor parameters please see Appendix H.

2.2.2 Interpolated Input Images

In the original DIRS method, each TM 30m superpixel was replicated into nine smaller 10m pixels to match the SPOT's pixel resolution (see figure 2-7).

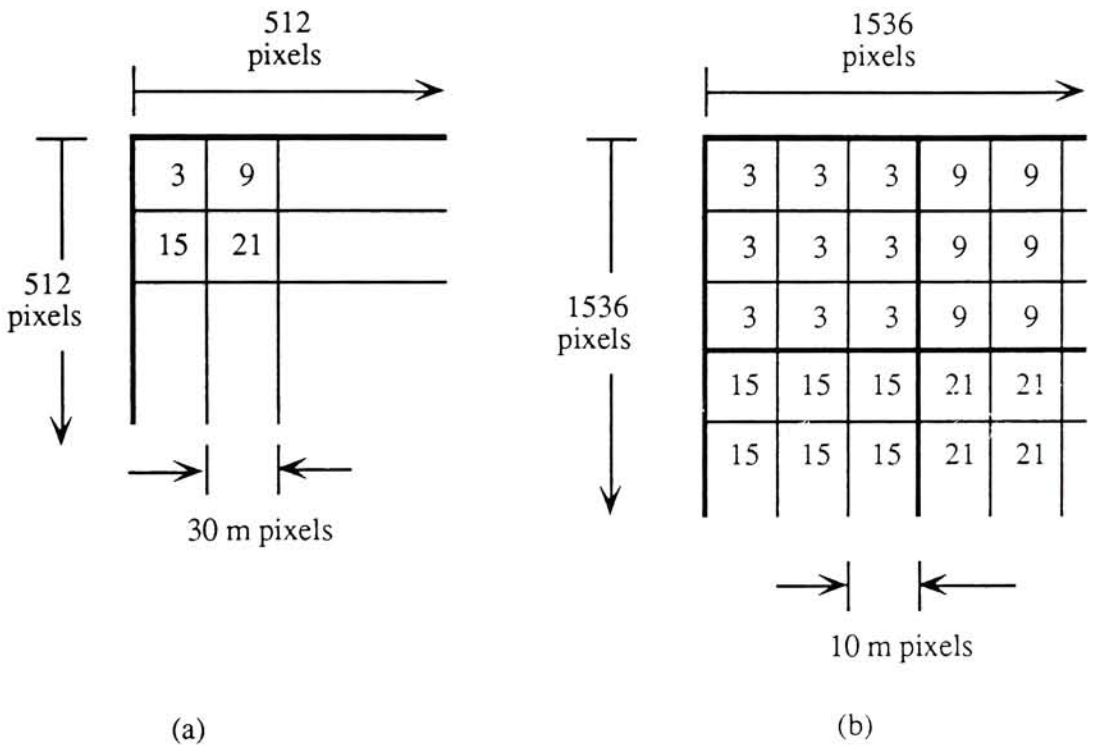

Figure 2-7 Pixel Replication
(a) 512 by 512 original TM image with 30m pixels.
(b) After replication, the image is now 1536 by 1536 with 10m pixels. The covered ground area is the same.

These replicated TM images were then used as input to the merging algorithm. In hopes of reducing the subsequent "blocky" appearance in the hybrid images (caused in part by the blocky input images), a 3 by 3 averaging filter was convolved with the replicated

input images. This simple filtering technique has been used to reduce the blocky appearance when enlarging images [Bernstein 79], and when merging multi-resolution images [Chavez 84, 86]. Thus, given a replicated image as in Figure 2-7, the resultant input image is shown in Figure 2-8 below.

1	1	1
1	1	1
1	1	1

(a) 3 by 3 averaging kernel

3	3	5	7	9
3	3	5	7	9
7	7	9	11	13
11	11	13	15	17
15	15	17	19	21

(b) resultant interpolated input

Figure 2-8 Interpolated Input

By using these averaged TM inputs, the merging algorithm does not change, although the term $DC_{TM}(i)$ no longer has the same value over the entire superpixel.

For this study, these replicated images that were smoothed by the averaging filter are referred to as the "interpolated" input images. This term is used to distinguish these images from other images that will be "blurred", "smoothed", or "averaged".

2.2.3 A Technique for Radiometric Post-correction

Although the interpolation of the input data reduces the blocky appearance, the average of the 9 pixels within the superpixel of the filtered input image may no longer equal

the original data -- radiometric integrity is lost. In addition, the DIRS method does not check or enforce whether the average DC within the SPOT panchromatic superpixel equals the corresponding superpixel in the synthetic TM panchromatic image. Again, the precise radiometric value is lost.

Rather than alter the basic merging algorithm of the DIRS method (or any method), radiometric integrity can be restored at the superpixel level by multiplying each hybrid superpixel (a block of 9 10m pixels) by a correction factor. This correction factor is defined as:

$$C.F. = \frac{TM_{i\text{ - }30m}}{\left(\frac{1}{9}\right)\sum_{j=1}^{9} Hybrid(j)_{i\text{ - }10m}} \qquad (2\text{-}9)$$

where:

$TM_{i\text{ -}30m}$ = DC from one original 30 m pixel from TM band i

$Hybrid(j)_{i\text{ - }10m}$ = DC from the j-th 10 m pixel (out of 9) from the hybrid superpixel that corresponds to TM_i.

This post-fix operation corrects for differences in the SPOT panchromatic and the synthetic TM panchromatic images, as well as the radiometric change to the interpolated TM input images. This correction, however, re-introduces some of the block appearances since the correction factor is constant over a superpixel.

2.3 The DIRS Enhancement 1 Merging Method

In a simple effort to reduce the "blocky" appearance of the hybrid data, the DIRS report suggested implementing a nearest neighbor-type of correction scheme. In this correction routine, each subpixel was compared to its own superpixel's center value and to its neighbors center value (see Figure 2-9).

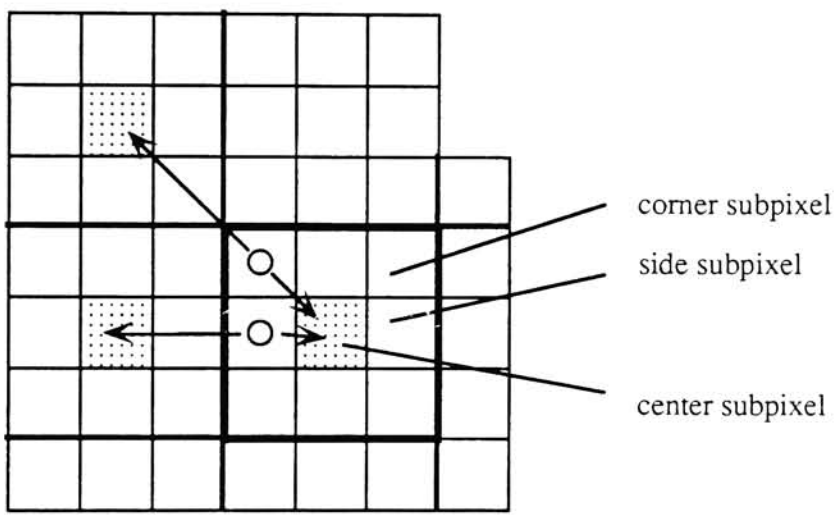

Figure 2-9 DIRS nearest neighbor correction routine.

Corner subpixels compared values with the diagonal neighbor, and side subpixels compared to the adjacent neighbor superpixel's center value. If the subpixel's DC was closer to its own center pixel's value, then the merging algorithm remained the same as in equation (2-1):

$$DC_{\text{Hybrid Multiband}}(i) = DC_{\text{SPOT Pan}} \cdot \left(\frac{DC_{TM}(i)}{DC_{\text{Syn TM Pan}}} \right)$$

If the subpixel's DC was closer to the neighbor's DC, than the neighbor's ratio was used in the merging algorithm:

$$DC_{\text{Hybrid Multiband}}(i) = DC_{\text{SPOT Pan}} \cdot \left(\frac{DC_{\text{Neighbor TM}}(i)}{DC_{\text{Neighbor Syn TM Pan}}} \right) \qquad (2\text{-}10)$$

The DIRS Enhancement 1 merging method follows this same correction scheme, except that the corner pixels also compare their values against its adjacent superpixel's center values (not just the diagonal superpixel). The comparison scheme for one corner subpixel looks as below:

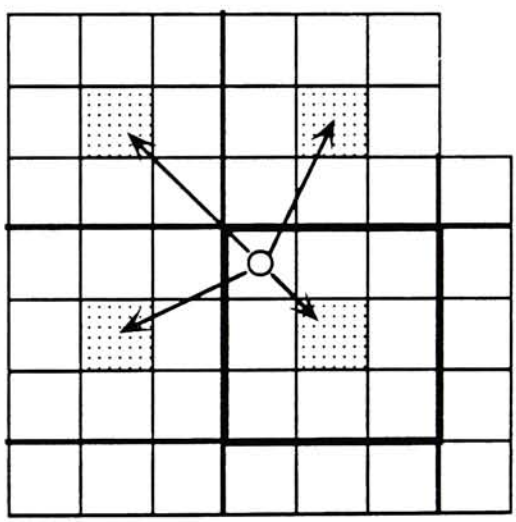

Figure 2-10 DIRS Enhancement 1 Correction Routine

The superpixel whose center pixel value was closest to the subpixel value contributed the ratio in the merging algorithm.

The reason why the adjacent pixels were included in the comparison for the corner

subpixels is because the correlation between adjacent pixels is much higher than between diagonal pixels [Ahern 86]. This better correlation means there is an increased chance that a corner subpixel will find a better, more accurate match for substituting ratios. Correcting the corner subpixels obviously reduces the overall block appearance.

Despite these changes, the DIRS Enhancement 1 method still has several limitations. These include:

- The center subpixel of a superpixel is never changed and will always use its own ratio.

- Each and every non-center subpixel is checked, regardless if it resides in a non-varying superpixel, or if the neighboring superpixels have a high variance.

- TM bands 4,5, and 7 are still handled as though they are correlated to the SPOT panchromatic image.

- Radiometry is still not precisely preserved.

2.4 DIRS Enhancement 2 Merging Method

DIRS Enhancement 2 is an attempt to correct some of the deficiencies in previous DIRS methods. This method is described below and can be followed in the flow chart diagram in Figure 2-12 at the end of this section.

The basic premise of this method is that the high resolution SPOT panchromatic image provides the spatial information on which segmentation and computational decisions are made. The inputs to the method are the replicated TM and the SPOT panchromatic

images. The SPOT panchromatic image is handled in 3 by 3 blocks which correspond to the replicated TM input image superpixels.

The steps for each 3 by 3 panchromatic block are outlined as follows:

1. Check to see if the SPOT block is "mixed" or "pure". A block is considered mixed if the variance among its nine pixels is higher than an established threshold. A "pure" block would be one with a variance lower than this threshold.

a) If the superpixel block is pure, then the DIRS original merging algorithm (section 2.1) with a post-fix correction routine (section 2.2.3) is run to create the corresponding hybrid block. This merging operation will be referred to as the "pure merge" in this algorithm.

b) If the block has a high variance, then the algorithm continues processing the mixed block.

2. Check if all the neighboring blocks are also mixed. If all are mixed, then the algorithm defaults to do the pure merge (the original DIRS method) over the superpixel block of interest. If some of the neighboring superpixel blocks are "pure", then the algorithm continues.

3. Connect the panchromatic superpixel. Each subpixel within the pan superpixel is compared to its adjacent subpixels. If the difference between the 2 subpixels is lower than a set threshold, then they are considered "connected". If two subpixels are connected, then each subpixel is allowed to compare to the others adjacent subpixels for further connections. Thus a network of the superpixel can be constructed. An exploded view of the potential connections for a center subpixel is shown in Figure 2-11.

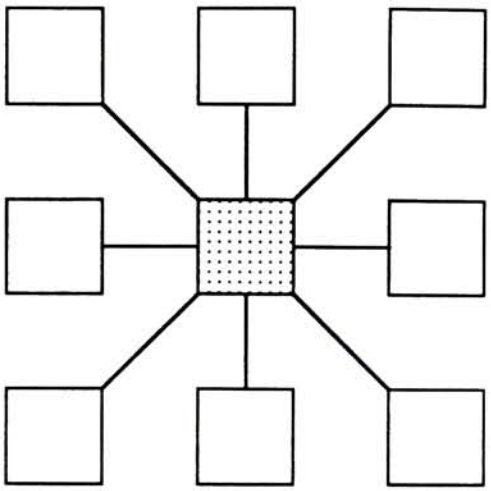

Figure 2-11. Connections between the center subpixel

4. Find the subpixels within the mixed SPOT block that can be matched to a pure neighboring superpixel. A match can occur when the subpixel DC and the neighboring superpixel's mean value are within a set threshold. Rather than limit the subpixels to compare only with those neighboring superpixels they can touch (as in DIRS Enhancement 1), this method also allows the subpixels to compare to any of the eight neighboring superpixels provided that: (a) the neighboring superpixel is pure; and (b) the subpixel can be "connected" to the superpixel. If the subpixel has more than one superpixel to which it could be matched, then the superpixel whose mean value is the closest to the subpixel value is chosen. These matched subpixels are then referenced as "pure" subpixels.

5. Create the corresponding TM hybrid subpixels by merging these pure subpixels using the matching superpixel's ratio and correction factor. This merge is similar to the DIRS Enhancement 1 method by substituting ratios of neighboring superpixels.

6. Derive a new TM value for the remaining (mixed) subpixels by removing the hybrid values computed in the step before. This can be described as:

$$NewTM_i = \frac{9 \cdot (TM_i) - \sum_{j=1}^{n} hybrid_i(j)}{(9 - n)} \qquad (2\text{-}11)$$

where: $NewTM_i$ = New DC for the remaining (mixed) subpixels within the superpixel of interest in TM band i;

TM_i = Original DC of the superpixel of interest in TM band i;

n = number of pure subpixels;

$hybrid_i(j)$ = those hybrid subpixels computed from the pure subpixels;

If all the subpixels were found to be pure, (n = 9), then this step is skipped to step 10.

7. Check to see if the new TM values are valid. The new TM values cannot be less than 0 or greater than 255.

a) If the values are invalid, then the least pure hybrid subpixel is removed and reclassified as a mixed subpixel. The least pure hybrid subpixel is the subpixel which has the largest difference between itself and its matching superpixel mean. The least pure hybrid subpixel will continue to be removed until there are no pure hybrid subpixels left, or new valid values for TM are computed. If there are no pure hybrid subpixels left, then the algorithm defaults to do a pure merge on the superpixel.

8. Compute a new synthetic TM_{pan} value for the remaining subpixels using the new

TM DCs. Using the new valid TM DCs and the weighting factors developed in section 2.1.1, the new synthetic TM panchromatic can be described as:

$$NewTM_{Syn\ Pan} = \sum_{i=1}^{4} w_i \times NewTM_i \qquad (2\text{-}12)$$

9. The remaining subpixels are now merged using the new TM DC and the new synthetic TM_{pan} DC using the same basic DIRS algorithm:

$$DC_{Hybrid(i)} = DC_{SPOT\ Pan} \cdot \left(\frac{DC_{NewTM(i)}}{DC_{NewTMSynPan}} \right) \qquad (2\text{-}13)$$

10. Radiometrically correct these mixed hybrid subpixels generated in step 9 using the post-fix operation.

11. Check to see if this final hybrid block (pure and mixed subpixels) is "reasonable". Some checks for being reasonable are: (a) if the hybrid band is correlated with the SPOT panchromatic image, the order of the 9 hybrid subpixels should be the same as the order of the original SPOT subpixels; (b) the standard deviation among the subpixels of the hybrid superpixel should be within a threshold factor of the standard deviation of the original SPOT superpixel.

12. If the hybrid superpixel is found to be unreasonable, then the least pure subpixel is removed and the algorithm returns to step 6. If the hybrid superpixel is found to be reasonable, then the algorithm is done and a new superpixel is started.

Note that with this new method, the following improvements to DIRS Enhancement 1 were made:

(1) The center subpixel is not constrained to only use its superpixel ratio and correction factor. If it can match to a connecting superpixel, then the center subpixel can use the matching superpixel's parameters. In addition, the other subpixels can also match with any of the eight neighboring superpixels provided that a connection exists between the two and the superpixel is pure.

(2) Rather than running comparisons for all subpixels, only those SPOT pan superpixel blocks that are identified as "mixed" (have a large variance) will be processed. In addition, only those neighboring superpixels that are pure will be able to contribute their ratio and correction factor. These changes should help in speed and in avoiding improper substitutions for superpixel parameters.

(3) Radiometry is preserved. Those subpixels that are identified as 'pure' (are matched to a pure neighboring superpixel) produce the pure hybrid subpixels. The remaining subpixels are then computed to maintain the radiometric value of the original TM value. In simplistic terms, it can be described as:

$$\text{known\_answer} = \text{pure\_values}_{\text{subpix}} + \text{mixed\_values}_{\text{subpix}}$$

Given a known answer (original TM value) and the pure subpixel component (determined), the mixed component is simply what's left.

However, DIRS Enhancement 2 still does not handle the weakly correlated TM bands 4, 5, and 7 any differently.

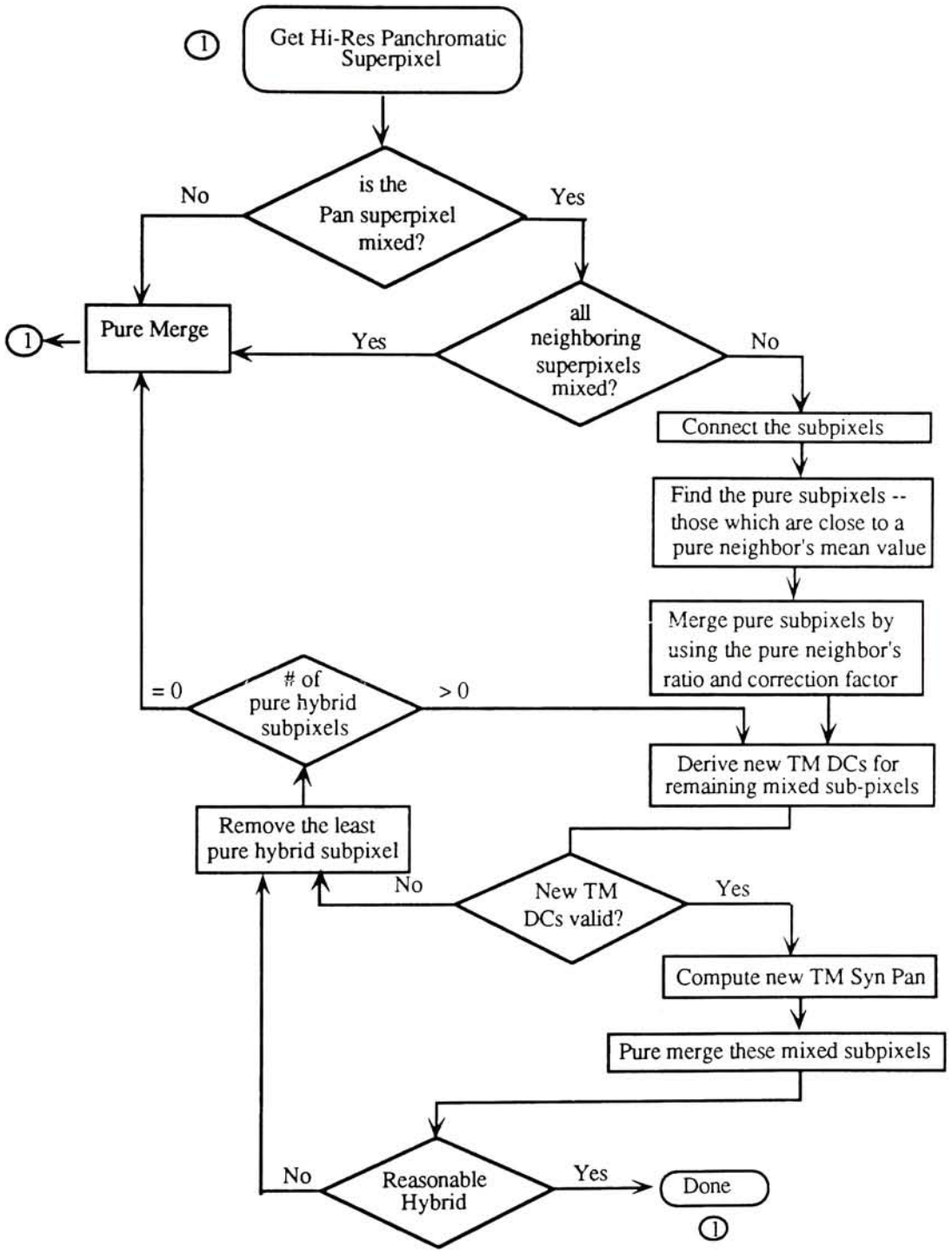

Figure 2-12 Flow Diagram of DIRS Enhancement 2 Merging Method

2.4.1 A Modification to the DIRS Enhancement 2 Method

This small modification is a quick fix to handle the TM bands that are weakly correlated to the panchromatic image. For this modification, the only change to the DIRS Enhancement 2 method is to the "pure merge" operation for the weakly correlated bands. Instead of pure merging these bands using the DIRS method:

$$DC_{\text{Hybrid Multiband}}(i) = DC_{\text{SPOT Pan}} \cdot \left(\frac{DC_{TM}(i)}{DC_{\text{Syn TM Pan}}} \right)$$

the hybrid value now simply takes the value of the original TM superpixel:

$$DC_{\text{Hybrid UncorrelatedBand}}(i) = DC_{TM}(i)$$

Thus if a subpixel is matched to a neighboring pure superpixel, the hybrid subpixel for these weakly correlated bands would contain the TM value for that matching superpixel.

All other (correlated) bands are manipulated in the identical fashion as before.

These methods described so far in section 2 are variations of the basic DIRS merging algorithm. The remainder of this section describes Price's merging method and some of its variations. The results of all these methods will be presented in section 4.

2.5 Price's Merging Technique

Price's technique for merging multispectral and panchromatic images is split into two cases. The first case is for multispectral bands that are correlated with the panchromatic image. The second case is for weakly correlated bands.

2.5.1 Case 1 -- Correlated Input Images

Because the images are correlated, the relationship can be described as linear. On an individual band basis, the linear coefficients can be determined using a simple linear regression. This is illustrated in Figure 2-13, where the DCs of an averaged SPOT panchromatic image are plotted against the DCs of a Thematic Mapper (TM) band.

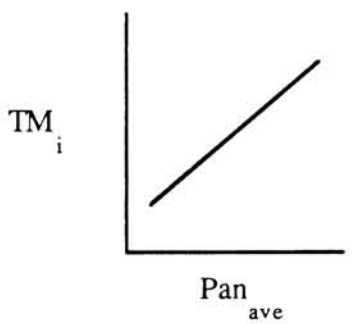

$$TM_i = (a_i \times Pan_{ave}) + b_i$$

Figure 2-13. Linear Regression of TM bands and the Panchromatic Image

where: TM_i = DC of a superpixel in the TM i-th band;

Pan_{ave} = the average of the DCs in the corresponding superpixel of the SPOT panchromatic image;

a_i , b_i = linear coefficients for the i-th TM band.

After solving for a_i and b_i we can compute a high resolution estimate of the i-th band using the original high resolution panchromatic channel:

$$\widehat{TM}_i = a_i \cdot Pan_{10m} + b_i \qquad (2\text{-}14)$$

The merging algorithm then uses the high resolution estimate to create the hybrid image:

$$Hybrid_i = \frac{TM_i \cdot \widehat{TM}_i}{\widehat{TM}_{i\text{-}ave}} \qquad (2\text{-}15)$$

where: $Hybrid_i$ = DC of the hybrid i-th band;

TM_i = DC from the original TM i-th band;

$\widehat{TM}_i$ = DC from the high resolution estimate of TM i-th band;

$\widehat{TM}_{i\text{-}ave}$ = average of the DCs in the corresponding $\widehat{TM}_i$ image corresponding to the TM_i pixel.

For example, the merging of TM multispectral images (30 m GIFOV) with a SPOT panchromatic image (10 m GIFOV), is illustrated below in Figure 2-14:

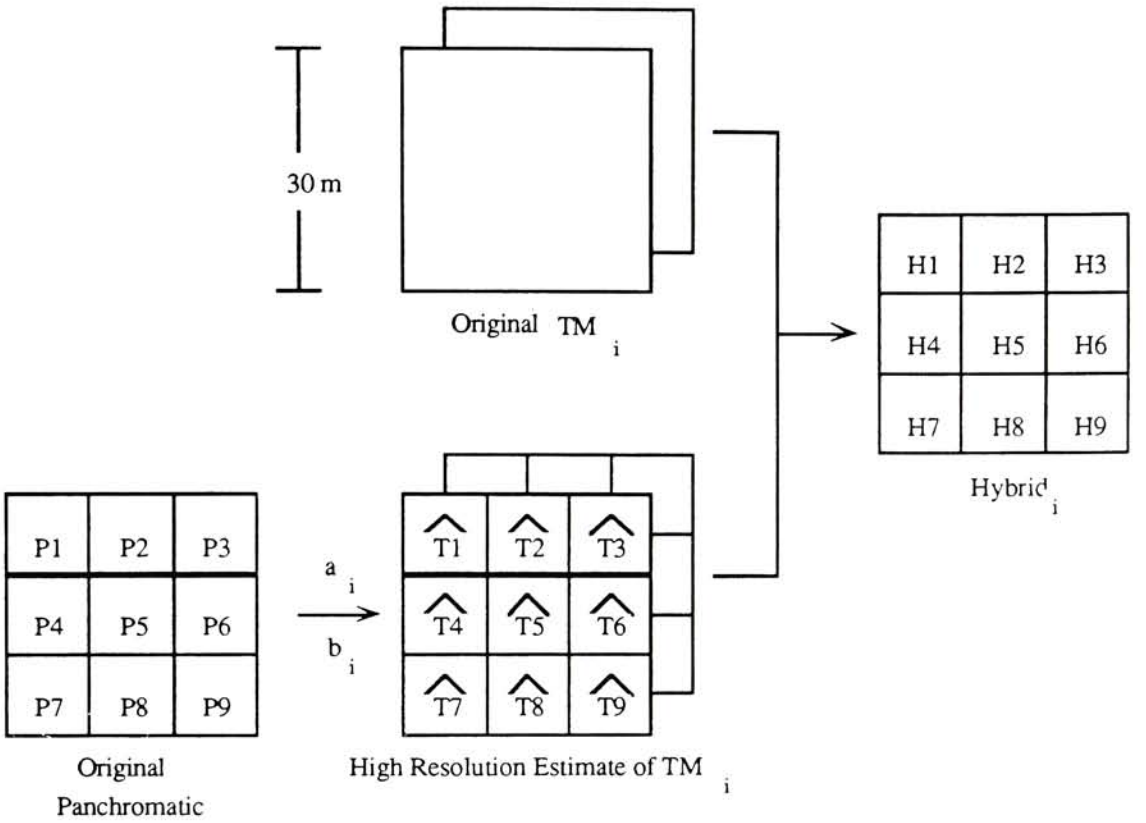

Figure 2-14 Price's Merging Method -- Case 1

where:

$$H(J)_i = \frac{TM_i \cdot \widehat{T(J)_i}}{\widehat{TM}_{i\text{-}ave}} \qquad , J = 1,..9$$

and $$\widehat{TM}_{i\text{-}ave} = \frac{1}{9}\sum_{J=1}^{9} \hat{T}(J)_i$$

Note the similarity to Pradines' method, except that Price is using an estimate of a multispectral band instead of the panchromatic data directly for the merging operation. In addition, Price's resulting hybrid image has an average DC the same as the original

multispectral band, while Pradine has the sum of the hybrid DCs equal the original multispectral value. Finally, Price suggests a method to handle multispectral bands that are weakly correlated with the panchromatic channel.

2.5.2 Case 2 - Weakly Correlated Bands

Because some bands are not linearly related (ie visible and near infrared channels), a more general relationship was used by Price. After registering the images, Price again averaged the panchromatic channel to the same spatial resolution as the multispectral images. Price then computed the expected (mean) value for the weakly correlated band for each given value in the 30m panchromatic image.

For example, Price would find all the pixels in the 30m panchromatic image that had a DC of X (0 to 255). He would then find the average of the DCs of the corresponding pixels in the weakly correlated band. Thus a simple look-up-table (LUT) can be generated. This process is depicted in Figure 2-15 on the following page. Using this LUT, a high resolution estimate of the multispectral band can be computed from the original high resolution panchromatic image. This high resolution estimate is now used as in the correlated case, and is merged with the original multispectral data.

2.5.3 Price's Results

Price tested his procedure using SPOT simulation data with a 10 m panchromatic and three 20m multispectral channels. He then averaged the channels to obtain 20m panchromatic and 40m multispectral channels. Applying the above procedures to the averaged data, Price produced hybrid 20m values which were then compared to the original (true) values at 20m resolution.

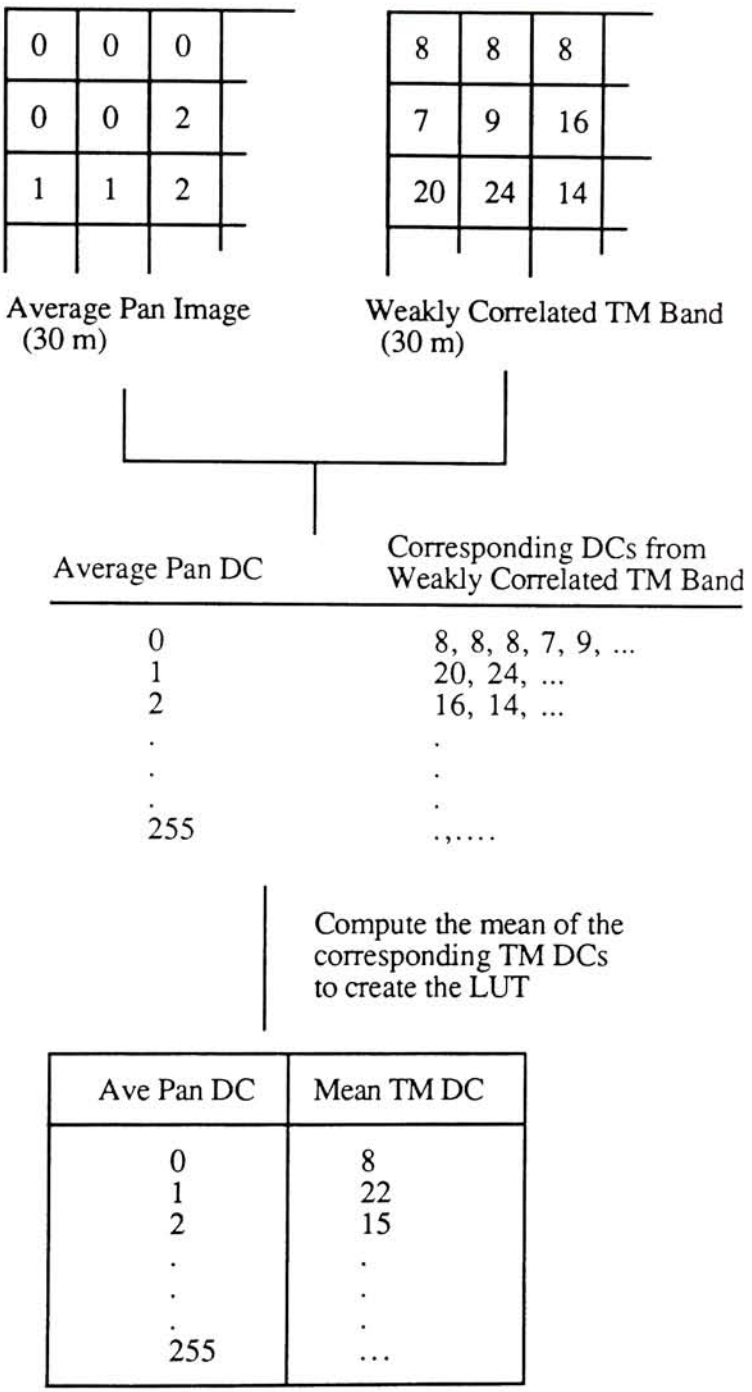

Figure 2-15 Creation of a Look-up Table (LUT)

Multispectral channels 1 and 2 were highly correlated with the panchromatic channel, and produced residual errors of around two digital counts. This is quite accurate since the standard deviation of the original data was around 20 DCs.

For the third channel which is not correlated, the procedure was only "moderately successful". The predicted values accounted only for about 75% of the variance in the original data, as compared to 99% in the correlated case.

Price did not test the effect his technique had on classification accuracy.

2.6 Price Modification -- A Method of Handling Weakly Correlated Input Images

One of the biggest concerns in all of the merging techniques to date has been the merging of multispectral images that are weakly correlated with the reference panchromatic channel. In our case, TM bands 4, 5, and 7 are not strongly correlated with the panchromatic channel.

This modification to Price's technique implements a method by Tom et al [85]. In his paper, Tom improved the spatial resolution of the TM band 6 from 120 m to 30 m using the other TM bands. His technique is based on an adaptive multiband least squares method which computes an optimal image estimate. His approach relies on the assumption that registered TM data are correlated across the bands in small local areas. By using the local correlation property, Tom used visible and IR bands to predict the thermal IR image data (band 6) in 30 m resolution. The thermal image estimate was formed by a weighted linear combination of reference images in which the weights changed adaptively over the entire

image.

By modifying Tom's technique, we could obtain high resolution estimates of TM bands 4,5, and 7. To compute the high resolution TM band 7 estimate, the adaptive multiband enhancement procedure would take these general steps:

(1) Average filter the panchromatic channel to obtain 30 m resolution.

(2) Using the averaged 30 m panchromatic image and the original TM 1, 2, and 3 images as input, we can implement the adaptive least squares method to generate the linear prediction coefficients for band 7 at each pixel location. For a given location of the sliding 3 by 3 window, we can represent this as:

$$\begin{bmatrix} TM7_1 \\ TM7_2 \\ TM7_3 \\ \vdots \\ TM7_9 \end{bmatrix} = \begin{bmatrix} 1 & TM1_1 & TM2_1 & TM3_1 & Pan_1 \\ 1 & TM1_2 & TM2_2 & TM3_2 & Pan_2 \\ 1 & TM1_3 & TM2_3 & TM3_3 & Pan_3 \\ \vdots & \vdots & \vdots & \vdots & \vdots \\ 1 & TM1_9 & TM2_9 & TM3_9 & Pan_9 \end{bmatrix} \begin{bmatrix} b_0 \\ b_1 \\ b_2 \\ b_3 \\ b_4 \end{bmatrix} + \begin{bmatrix} e_1 \\ e_2 \\ e_3 \\ \vdots \\ e_9 \end{bmatrix} \qquad (2\text{-}16)$$

The least square solution is computed by solving for the set of coefficients (the vector **b**) that minimizes the error vector (**e**). Note that each pixel location will have its own set of coefficients. One way to handle this data is to have matching coefficient "images" for each input/reference image.

(3) Obtain 10 m resolution estimates of TM bands 1, 2, and 3 by previous methods. (i.e., Price or DIRS methods)

(4) Generate an optimal estimate of TM band 7 using the prediction coefficients and the high resolution input images (panchromatic, Hybrid bands 1, 2, 3). For each 10m pixel this can be represented as:

$$\widehat{TM7} = (b_1 \cdot Hyb_1) + (b_2 \cdot Hyb_2) + (b_3 \cdot Hyb_3) + (b_4 \cdot Pan_{10m}) + b_o \qquad (2\text{-}17)$$

where Hyb_1 , Hyb_2 , and Hyb_3 are the 10m hybrid pixels derived from using Price's technique for correlated bands.

(5) Merge this high resolution estimate of TM band 7 with the original band 7 using Price's method with correlated images (section 2.5.1) to obtain a 10m Hyb_7 image.

After obtaining Hyb_7, we can use this band as another input reference to compute Hyb_5. As before, a vector **b** is determined, this time with one more dimension for the additional input reference image.

$$\begin{bmatrix} TM5_1 \\ TM5_2 \\ TM5_3 \\ \vdots \\ TM5_9 \end{bmatrix} = \begin{bmatrix} 1 & TM1_1 & TM2_1 & TM3_1 & TM7_1 & Pan_1 \\ 1 & TM1_2 & TM2_2 & TM3_2 & TM7_2 & Pan_2 \\ 1 & TM1_3 & TM2_3 & TM3_3 & TM7_3 & Pan_3 \\ \vdots & \vdots & \vdots & \vdots & \vdots & \vdots \\ 1 & TM1_9 & TM2_9 & TM3_9 & TM7_9 & Pan_9 \end{bmatrix} \begin{bmatrix} b_0 \\ b_1 \\ b_2 \\ b_3 \\ b_4 \\ b_5 \end{bmatrix} + \begin{bmatrix} e_1 \\ e_2 \\ e_3 \\ \vdots \\ e_9 \end{bmatrix} \qquad (2\text{-}18)$$

With this vector **b**, the high resolution estimate for TM5 can be computed similar to equation (2-17):

$$\begin{aligned} \widehat{TM5} = {} & (b_1 \cdot Hyb_1) + (b_2 \cdot Hyb_2) + (b_3 \cdot Hyb_3) + \\ & (b_4 \cdot Hyb_7) + (b_5 \cdot Pan_{10m}) + b_o \end{aligned} \qquad (2\text{-}19)$$

The hybrid image for TM5 is then obtained by merging this high resolution estimate of TM5 with the original TM5 image using Price's method with correlated images. Once the hybrid for TM5 (Hyb_5)is found, this band as well as Hyb_7 are used to compute the high resolution hybrid for TM band 4.

The order of computing band 7, 5, and then 4 is chosen because this is the order of decreasing band correlation with the panchromatic image. Tom et al [85] additionally showed that increasing the number of input reference bands decreased the high resolution estimate error. Therefore, band 4 -- the weakest correlated band -- is computed last to use the 2 additional reference bands.

Section 2 described the two primary methods of merging that are investigated in this study -- the DIRS and the Price methods. In addition, several modifications and enhancements have also been introduced. The following section describes how these methods were tested and compared.

3.0 EXPERIMENTAL APPROACH

In comparing these merging methods, several variations of the input images were used. These variations are described in section 3.1. The two primary tests for evaluation -- classification accuracy and radiometric error -- are described in sections 3.2 and 3.3 respectively. Finally, the procedure for this study is presented in section 3.4.

3.1 Selection and Preparation of Test Imagery

The SPOT and TM images selected for this study are the identical images used in the DIRS proof-of-concept study [Warnick 89]. The images were selected from a scene of greater Rochester, NY, acquired in June of 1987. The acquisition and ephemeris data for these scenes are presented below:

Table 3-1
Scene Acquisition and Ephemeris Data [from Warnick 89]

Scene Parameter	SPOT Pan	Landsat-5 TM
Date	10 June 87	15 June 87
Time of Day	16:06:21 GMT	15:26:01 GMT
Sensor View Angle	9.7°	--
Sun Elevation	65.9°	59.0°
Scene ID	1618263870610160621 1P	Y5120115221X0

Some of the image statistics are listed in Table 3-2 :

Table 3-2
Scene Statistics

Band	mean (DC)	Std Dev
TM1	98.14	13.55
TM2	39.94	7.49
TM3	41.40	12.73
TM4	97.82	21.85
TM5	81.36	17.08
TM7	31.64	11.23
SPOT	47.74	11.98

3.1.1 Registration of Images

The SPOT panchromatic image was registered to the TM data set on two separate occasions using two different transformation coefficients. This provided two variations of the SPOT image to use in comparing the merging techniques. With their differences in registration, some of the effects of mis-registration can be addressed.

The SPOT panchromatic image is registered to the lower resolution TM data set to preserve the multispectral information. Registration is conducted by first selecting ground control points in both the panchromatic and TM images. The geometric transformation coefficients are then computed using multiple regression techniques on the selected control points. With these coefficients, the panchromatic image is geometrically resampled using cubic convolution. For more information on standard registration techniques, refer to

Schowengerdt [83] or the ERDAS Users Guide.

For the DIRS proof-of-concept study, the SPOT panchromatic image was registered to the TM data set using a first order transformation matrix. Eighteen ground control points were used to determine the coefficients. Using these control points and the coefficients, a residual analysis determined that a maximum error of 0.916 SPOT pixels (or 9.16 meters of error) remained after the transformation of these control points. These transformation coefficients are shown in table 3-3.

Table 3-3
Transformation Coefficients used for the Resampling of the SPOT Image
for the Original DIRS Study

Coefficient	x	y
Intercept	474.6330	275.7023
X	0.01939835	0.9500315
Y	0.9497908	-0.0191019

Another set of transformation coefficients were computed in an effort to reduce the registration error. Sixteen ground control points were used to solve a second order transformation. The resultant residual analysis showed that the maximum error dropped to 0.459 SPOT pixels, or less than 5 meters of error. These coefficients are shown in Table 3-4 below.

Table 3-4
New (second order) Transformation Coefficients
used for the Resampling of the SPOT Image

Coefficient	x	y
Intercept	0.3064387	0.2884292
X^2	0.9446802	0.0203343
XY	- 0.0195416	0.9464509
Y^2	0.0032847	- 0.197969
X	- 0.0012493	0.825885
Y	0.1723889	0.196619

3.1.2 Blurred Image Sets

The original SPOT and TM images were blurred to 30m and 90m GIFOV respectively. By using these lower spatial resolution images as input for the merging techniques, each algorithm can be compared and evaluated as to how well it "recovers" the original (30m) TM images.

Since the ground instantaneous field-of-view (GIFOV) is used as the measure of spatial resolution, the method of blurring these image sets should be consistent with its use. The definition of GIFOV is simply the projection of the limiting detector aperture onto the ground. Optical blur and electronics are not taken into account. Thus to simulate an image acquired with a lower resolution system, the pixels that extend over the new, lower resolution projection (or footprint) are averaged to get a mean signal over the area. This mean value is then replaced into all the pixels under the area, or the block is subsampled to

get one pixel that represents a larger area (a superpixel) that contains the mean value. This averaging over the "superpixel" of interest assumes a linear radiance mixing model which has been found to be a reasonable approximation [Merickel 83, Chhikara 84].

Thus to blur a SPOT 10m GIFOV image into a 30m image, nonoverlappping, 3 by 3 blocks of 9 pixels are averaged to get one 30m superpixel.

3.1.3 Figures of Images

The following figures show the original TM data set at 30m GIFOV, the blurred TM data set at 90m GIFOV, and the original SPOT image after registration to 0.459 pixel error.

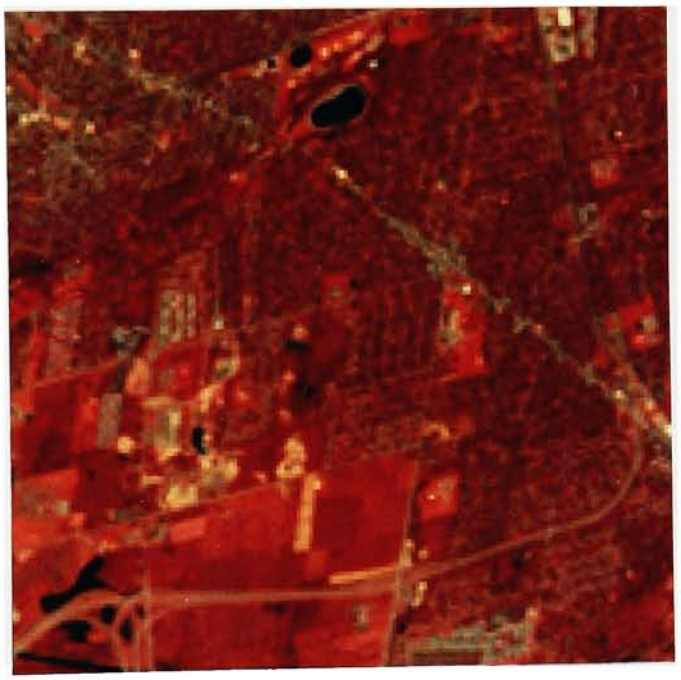

Figure 3-1 Original TM (30m GIFOV) bands 5, 3, 2 displayed in RGB

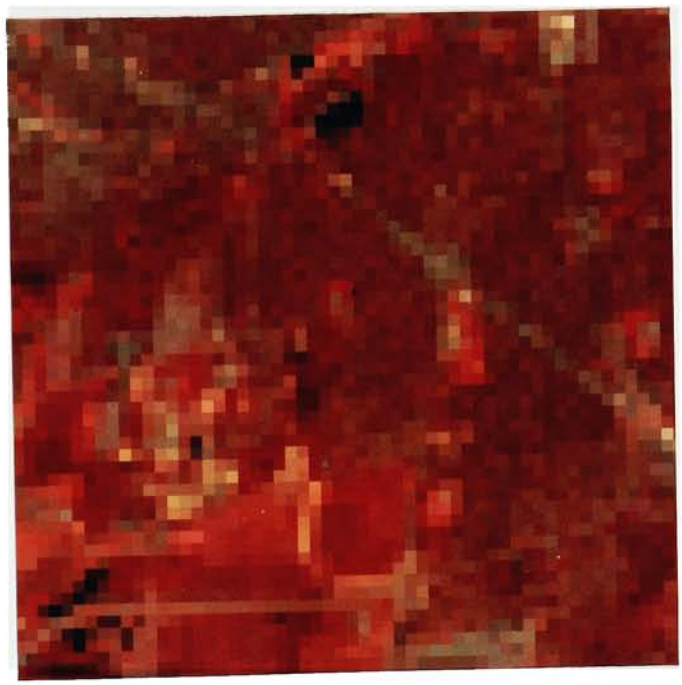

Figure 3-2 Blurred TM (90m GIFOV) bands 5, 3, 2 displayed in RGB

Figure 3-3 Original SPOT panchromatic image (10m GIFOV)

3.2 Classification of Test Imagery

All the data sets are classified using the standard Gaussian Maximum Likelihood (GML) classifier with eight bands of input. These eight bands are comprised of the TM bands (or hybrid equivalent) 1, 2, 3, 4, 5, and 7, as well as a 5/3 ratio band, and a *texture* band. The texture band is a statistical feature band computed from the equivalent TM band 4. Each pixel in the texture band is the standard deviation of the DCs in a 3 by 3 window around the corresponding pixel in the equivalent band 4.

3.2.1 Training Samples for Classification

All the data sets are classified using the same training sites. The training sites were carefully chosen to get the best classification of the original TM data set, while permitting the blurred TM data set (90m GIFOV) to also classify well. The majority of the training samples were selected from the original 30m data set with special considerations to ensure that the sample remains "pure" when blurred to a lower resolution. However. it was found that a few training samples taken in highly busy areas were required for adequate classification accuracy of the original TM data set..

In all, there were 17 classes to which the GML classifier could segment -- 4 classes of urban, 1 class of soil, 2 classes of water, 5 classes of trees, and 5 classes of grass.

3.2.2 Measuring Classification Accuracy

After classification, the classified image is recoded from 17 separate classes into the 5 primary classes: urban, soil, water, trees, and grass. These classified images are then subjected to one or more of the following accuracy tests.

(1) Classification Accuracy using a Random Data Set. In this interactive test, random pixel locations for each class are chosen from the classified image. These pixels locations are then presented to the user who is viewing the original (or a registered, higher resolution) data set. The user classifies the pixel at that location. If the user is unsure of the class to which the pixel belongs, then the user can opt to discard that pixel. The program will then randomly select another pixel location. A confusion matrix is then constructed plotting these user inputs as ground truth, against the results of the classified image.

(2) Classification Accuracy using Independent Data Set 1. This data set has user selected sample *areas* (rather than random pixels) against which classification is checked. It is an independent data set in that none of the samples comes from the training set. The advantage to this test is that the same pixel classifications can be quickly compared against all techniques. The disadvantage to this technique is that the selected data set may not be a fair representation of the classification.

(3) Classification Accuracy using Independent Data Set 2. This independent data set was specifically designed to test the spatial resolution of the classifier.

Rather than using selected sample areas as in Independent Data Set 1, each sample was selected one pixel at a time. Fifty samples per class were chosen. All samples were selected in areas where finer spatial resolution would help -- examples include urban pixels taken from minor side streets, trees within suburban areas, and pixels near boundaries or edges. As an independent data set, the same advantages and disadvantages apply.

3.2.3 Testing the Significance of Overall Classification Accuracies

Using the confusion matrix obtained from any of the three accuracy tests above, an overall classification accuracy value can be computed for a classified image. For this study, the overall classification accuracy is defined as the average of the percent correctly classified for each class (i.e. the average of the diagonal of the confusion matrix).

For those accuracy tests with an equal number of samples per class (Random and Independent Data Set 2), two statistical tests of significance can be conducted.

The first test is a check whether the overall classification accuracies from each of the methods are statistically (significantly) different from one another. Using an r x c table analysis as presented by Freund [88], a chi-square (χ^2) value is obtained. If χ^2 is larger than a threshold χ^2 (based on degrees of freedom and significance level), then the methods can be considered different from one another. An example is presented in Appendix G.

The second test determines if a merging method produces an overall classification accuracy that is statistically better than the classification accuracy obtained from the input (un-merged) TM data set. This test calculates a threshold classification accuracy value,

above which is considered significantly different from the classification accuracy obtained from an un-merged TM data set. The threshold value is computed using standard test statistics concerning the difference between two proportions [Freund 88]. An example is presented in Appendix G.

3.3 Radiometric Error Analysis

Radiometric error analysis is conducted on the hybrid data sets when the input images are the blurred SPOT panchromatic (30m GIFOV) and the blurred TM data set (90m GIFOV). These hybrid data sets (at approximately 30m GIFOV) can now be compared to the original TM 30m data to see how well they "recovered" the true TM values. For each band, error is measured as:

$$\varepsilon_{DC} = \sqrt{\frac{\sum_{j=1}^{n} (\text{Hybrid}(j) - \text{TM}(j))^2}{n}} \qquad (3\text{-}1)$$

where:

ε_{DC} is the RMS error in digital counts (DC);

Hybrid(j) is the hybrid DC at pixel j;

TM(j) is the original TM DC at pixel j; and

n is the number of pixels used in the error calculation (generally all the pixels in the image).

Because each band has different DC distribution characteristics (i.e., mean value, standard deviation, etc), comparing the RMS error in DCs among the various bands is not

appropriate. A better means of interband comparison (as well as inter-image comparison) is to express the error in reflectance units rather than in digital counts.

Computing the Error in Reflectance Units

The error can be computed in reflectance units if reflectance data is available. For this study, the error in reflectance units is computed for bands 1, 2, 3,and 4. The method is as follows:

(1) Several control points on the original TM data set (bands 1..4) are identified and their digital counts (DC) are recorded.

(2) A reflectance unit is then estimated for that particular point at the bandpass of the sensor based on standard reflectance curves. (see figures 2-2 to 2-6)

(3) The DCs for each band and their respective (estimated) reflectance values are then linearly regressed to determine the best fit line. The line can be described as:

$$DC_i = m_i \cdot r_i + b_i \tag{3-2}$$

where:

DC_i is the digital count in band i;

m_i , b_i is the slope and offset of the best-fit line for band i; and

r_i is the estimated reflectance for the digital count.

(4) Using the slope m found above, along with ε_{DC} , the error in reflectance units can now be computed as:

$$\varepsilon_r = \frac{\varepsilon_{DC}}{m} \tag{3-3}$$

3.4 Running Methods and Modifications

This section describes the parameters (such as threshold limits) that were used for this study.

3.4.1 Running DIRS Enhancement 2

In this method, the panchromatic image is grouped into 3 by 3 blocks that correspond to the TM superpixels. The standard deviation of each 9 pixel block is computed. The average of all these block standard deviations ($\overline{x}_\sigma$), as well as the standard deviation of these block standard deviations (σ_σ) are then computed and presented to the user. The user is prompted to enter a standard deviation threshold value to differentiate the pure from the mixed 3 by 3 blocks. Those blocks that have a standard deviation greater than the threshold are considered to be mixed. Those panchromatic blocks that have a standard deviation less than the threshold are considered pure.

For the SPOT panchromatic image, the following are the block standard deviation statistics and the threshold standard deviation used:

	$\bar{x}_\sigma$	σ_σ	σ_T
SPOT registration error of 0.916 pixels			
Original SPOT image (10m GIFOV):	5.311	4.335	8.235
Blurred SPOT image (30m GIFOV):	5.788	3.793	8.347
SPOT registration error of 0.459 pixels			
Original SPOT image (10m GIFOV):	4.891	3.952	7.559
Blurred SPOT image (30m GIFOV):	5.575	3.682	8.060

The thresholds were chosen so that approximately 25% of the blocks would be classified as 'mixed'. These thresholds can be calculated by assuming that the standard deviation of the blocks follow a normal distribution. Thus, by providing a z-score, the threshold can be computed using the standard (z-score) equation and tables

$$z = (\sigma_T - \bar{x}_\sigma) / \sigma_\sigma \tag{3-4}$$

For a mixed block rate of 25%, $z_{.25} = 0.675$; and the threshold, σ_T, can now be computed.

This σ_T is also used to determine if a subpixel is connected to another subpixel, or if it can be matched to a neighboring superpixel. It can be shown that the standard deviation between two values is equal to the absolute value of their difference divided by the square root of two (Appendix I):

$$\sigma_{1,2} = \frac{|x_1 - x_2|}{\sqrt{2}} \tag{3-5}$$

If $\sigma_{1,2}$ is smaller than σ_T, then the two samples are considered connected.

3.5 Experimental Procedure

The experimental procedure is broken down into three parts. In the first part, the merging methods were run on blurred resolution image sets -- the SPOT panchromatic image and the TM bands were blurred to 30m and 90m GIFOV respectively. The hybrids were evaluated on radiometric error and classification accuracy.

In the second part, the methods were again tested using blurred image sets, but the input SPOT image was the image that had a registration error of less than 5 meters. In this manner, the differences in results from Part 1 and Part 2 can be attributed to registration differences.

In the third part, the methods are run on original resolution images and the hybrids are evaluated on classification accuracy alone. In all three parts, the classification accuracies of the hybrids were compared to the classification accuracy of the un-merged (input) TM data set. Whenever possible, the hybrid classification accuracies were evaluated to see if they were significantly different than the un-merged TM data set classification accuracy.

3.5.1 Part 1 -- Merging with Coarser Resolution Input Data Sets

In the first part, 10 of the merging methods were run on the blurred image sets. The

TM data set was blurred to 90m and the SPOT panchromatic image (0.916 pixel registration error) was blurred to 30m. These 10 methods were the:

(1) DIRS original method;

(2) DIRS method with the new synthetic panchromatic image;

(3) DIRS method with the interpolated input *;

(4) DIRS method with the interpolated input and post-fixing *;

(5) DIRS Enhancement 1 method *;

(6) DIRS Enhancement 1 method with post-fixing *;

(7) DIRS Enhancement 2 method *;

(8) DIRS Enhancement 2 method with TM4 modification *;

(9) Price's method (with a look-up table for TM4, TM5, TM7); and

(10) Price's modified method (with adaptive weighting).

* -- uses the new synthetic panchromatic image.

For a quick review, Table 3-5 contains a brief summary of each of these methods.

The hybrid data sets, as well as the blurred and original TM data sets, were then checked for radiometric errors, and classified. Classification accuracy was determined using independent data set 1. Those methods that provided the most encouraging and interesting results were then selected for further testing.

Table 3-5
Summary Table of Merging Methods

Method	Comments
1 - DIRS Original Method	$DC_{Hybrid}(i) = DC_{SPOT\ Pan} \cdot \left(\frac{DC_{TM}(i)}{DC_{Syn\ TM\ Pan}}\right)$ (section 2.1)
2 - DIRS with new synthetic pan image	Replace $DC_{Syn\ TM\ Pan}$ with $DC_{New\ Syn\ TM\ Pan}$ (section 2.2.1)
3 - DIRS with Interpolated Input	Rather than pixel replicate, the coarser resolution input images are interpolated. (section 2.2.2)
4 - DIRS with Interpolated Input and Post-fixing	Takes output from (3) and post-fixes -- ensures that the average of the hybrid superpixel area equals the original TM DC. (section 2.2.2 and 2.2.3)
5 - DIRS Enhancement 1	Same as (1) but substitutes the superpixel ratio with a neighbor superpixel ratio if the subpixel is closer to the neighbor's center subpixel value. (section 2.3)
6 - DIRS Enhancement 1 with Post-fixing	Takes output from (5) and post-fixes. (section 2.3 and 2.2.3)
7 - DIRS Enhancement 2	Segments the superpixel based on the pan image and on user input thresholds. (section 2.4)
8 - DIRS Enhancement 2 with TM4 mod	Only weakly correlated bands are handled differently. The hybrid subpixel takes the value of the original TM DC (or a neighboring TM DC) (section 2.4.1)
9 - Price's Method	Creates a hi-res estimate of the band, then post-fixes. Correlated Bands -- estimate created by linear transform of pan image. Weakly Correlated Bands -- estimate created by LUT. (section 2.5)
10 - Price's Modified Method (adaptive weights)	Same as (9) except when obtaining estimate for weakly correlated bands. Instead of LUT, uses adaptive weights. (section 2.6)

3.5.2 Part 2 -- Merging with Coarser Resolution Data Sets with a Lower Registration Error

In this phase of the study, six of the methods were again tested at the blurred resolutions, but the input SPOT image was the image that had a registration error of less than 5 meters. The resultant hybrid data sets were then radiometrically checked and the classification accuracies were determined using both independent data set 1 and a random data set.

3.5.3 Part 3 -- Merging with Original Resolution Data Sets

This last phase used the original resolution data sets to create hybrid data sets with approximately 10m GIFOV. The classification accuracies of these hybrid data sets were then determined using the independent data sets 1 and 2, as well as a random data set.

4.0 RESULTS

4.1 Creating the New Synthetic Panchromatic Image

The weights for TM bands 1 through 4 using the technique described in section 2.2.1 are:

ω_{TM1} = - 0.0134;

ω_{TM2} = 0.6417;

ω_{TM3} = 0.3175;

ω_{TM4} = 0.0311; with an r^2 value of 0.9999

Because TM bands 1, 2, and 3 are highly correlated to one another, there is redundant information between them. Because of this, TM1 only provides a weak contribution to the overall weighting. Since TM1 contributes a relatively small, and negative amount, the regression was run again this time without TM1 as an input. These weightings are now:

ω_{TM2} = 0.5931;

ω_{TM3} = 0.3310;

ω_{TM4} = 0.0345; also with an r^2 value of 0.9999

A summary chart is shown below:

Table 4-1
Summary of Weighting Factors used to Generate the TM Panchromatic Image

	DIRS weighting	LOWTRAN Set 1	LOWTRAN Set 2
TM1	0.0617	- 0.0134	--
TM2	0.4550	0.6417	0.5931
TM3	0.3818	0.3175	0.3310
TM4	0.1015	0.0311	0.0345

The resultant TM panchromatic images have the following characteristics:

Table 4-2
Summary of the Histogram Statistics for the Panchromatic Images

	Mean	Std Dev
Original SPOT pan image	47.71	11.97635
SPOT pan image blurred to 30m	47.71	10.08628
TM pan image (DIRS weighting)	49.96	8.35087
TM pan image (LOWTRAN 1 weighting)	40.50	8.37877
TM pan image (LOWTRAN 2 weighting)	40.77	8.33082

Since the the differences between the two LOWTRAN-derived weights are minimal, the second set of weights (without TM1) was used to create the synthetic TM panchromatic image.

The SPOT pan image is then linearly adjusted to the TM synthetic pan image to account for the atmospheric differences between the acquisition times. The coefficients for the linear adjustment are determined as:

$$m = \frac{\sigma_2}{\sigma_1} \; ; \; b = \bar{x}_2 - m \cdot \bar{x}_1$$

where: σ_2 , $\bar{x}_2$ are the standard deviation and the mean of the TM pan image;

σ_1 , $\bar{x}_1$ are the standard deviation and the mean of the SPOT pan image to be adjusted.

The SPOT image can now be adjusted as:

$$SPOT_{adjusted} = m \cdot SPOT_{orig} + b$$

A quick check was done to see if there was a difference between using the blurred SPOT pan image statistics or the original pan image statistics (to provide σ_1 and $\bar{x}_1$) to derive the linear coefficients for atmospheric adjustment. These results are summarized below:

Table 4-3
Summary of the Linear Coefficients used for Adjustment

	m	b
Original SPOT input:		
LOWTRAN syn TM pan	0.6956	7.5826
DIRS syn TM pan	0.6973	16.6928
Averaged SPOT input:		
LOWTRAN syn TM pan	0.8260	1.3637
DIRS syn TM pan	0.8279	10.4588

These adjusted SPOT images were then blurred to 30m and compared to the synthetic TM pan image. To obtain hybrid images that are radiometrically precise, there should be no difference between the blurred, adjusted SPOT pan image and the synthetic TM pan image. However, there were some RMS error differences as shown in Table 4-4:

Table 4-4
Summary of the Error Differences

	RMS error (DC)	error normalized to input image
Original SPOT input:		
LOWTRAN syn TM pan	3.77	5.42
DIRS syn TM pan	3.97	5.69
Averaged SPOT input:		
LOWTRAN syn TM pan	3.80	4.60
DIRS syn TM pan	4.04	4.87

These results indicate that the synthetic TM pan image created from the LOWTRAN-derived weights will provide a better radiometric hybrid than from the TM pan image using the DIRS weights. In addition, it initially appears that using the original SPOT image to derive the adjustment coefficients gives slightly better radiometric results.

However, these results may be due simply to the standard deviation of the images used to obtain the coefficient m. The larger m is, the more variation in the adjusted SPOT image, and the larger the difference is between the adjusted SPOT image and the synthetic TM pan image. Thus, if either σ_2 gets larger, or if σ_1 gets smaller, m becomes larger and so does the error. These errors in DC can be converted to DC error in the SPOT input by dividing by their respective m's (similar to computing the reflectance error in section 3.3). With these normalized errors shown in the second column in Table 4-4, the linear coefficients derived from an averaged SPOT pan image now results in lower errors.

Despite which synthetic TM pan image is used, however, it is apparent that radiometry will not be exactly preserved if the DIRS merging method(s) are unchanged.

4.2 Computing the Error in Reflectance

Over 30 control points were taken over the original TM data set (bands 1..4). These points are listed below.

Table 4-5
Selected Control Points

Screen Location		TM1 DC	TM2 DC	TM3 DC	TM4 DC
Road1	102,71	100	38	43	41
	168,48	101	37	41	41
	75,80	96	35	38	44
	59,82	105	42	46	48
Road2	297,167	119	49	60	53
	304,178	116	49	60	55
	309,185	115	47	58	57
Concrete	417,41	174	77	101	77
	502,333	187	79	110	86
	422,6	182	81	100	81
Soil	221,402	125	62	88	85
	225,385	125	59	86	91
	222,395	123	58	85	80
	258,439	126	60	89	86
Water	142,327	81	31	27	6
	37,449	84	31	27	8
	261,84	98	32	23	11
	267,78	95	31	20	13
	220,44	81	30	26	9

(Table 4-5 continued on the next page)

Table 4-5 (continued)
Selected Control Points

Screen Location		TM1 DC	TM2 DC	TM3 DC	TM4 DC
Trees	83,428	82	29	26	139
	295,55	81	29	24	132
	129,144	80	28	22	120
	94,232	81	32	25	142
	110,157	82	29	24	131
Grass1	285,374	92	39	36	116
	247,387	88	35	32	127
	180,404	92	41	40	117
	287,368	90	39	35	128
	143,480	91	39	35	124
Grass2	150,406	95	43	40	155
	215,381	93	39	36	148
	233,468	89	39	32	148

The subgroups under Table 4-5 were then averaged and their reflectances were estimated for each band. The reflectance estimates were based on the spectral curves shown in Figures 2-2 through 2-6. These results are listed in Table 4-6 below.

Table 4-6
Averaged DC and Estimated Reflectance

	Ave TM1 DC	% r	Ave TM2 DC	% r	Ave TM3 DC	% r	Ave TM4 DC	% r
Road1	101	8	38	10	42	11	43	13
Road2	117	10	48	12	59	15	55	17
Concrete	181	19	79	24	104	25	81	28
Soil	125	12	60	17	87	20	86	35
Water	88	6	31	5	25	6	9	2
Trees	81	5	29	6	24	11	133	55
Grass1	91	7	39	9	36	9	122	44
Grass2	92	7	40	9	36	9	150	62

The four separate plots and regressions for Table 4-6 are shown in the figures on the following pages.

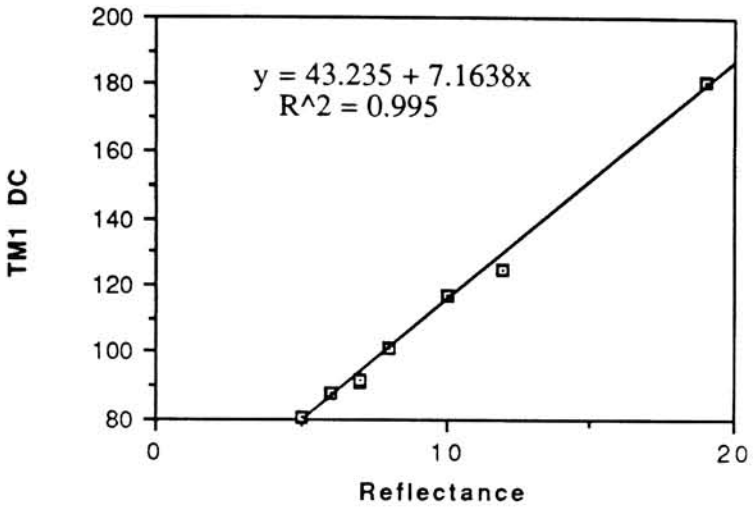

Figure 4-1 Plot of TM1 DC versus estimated Reflectance

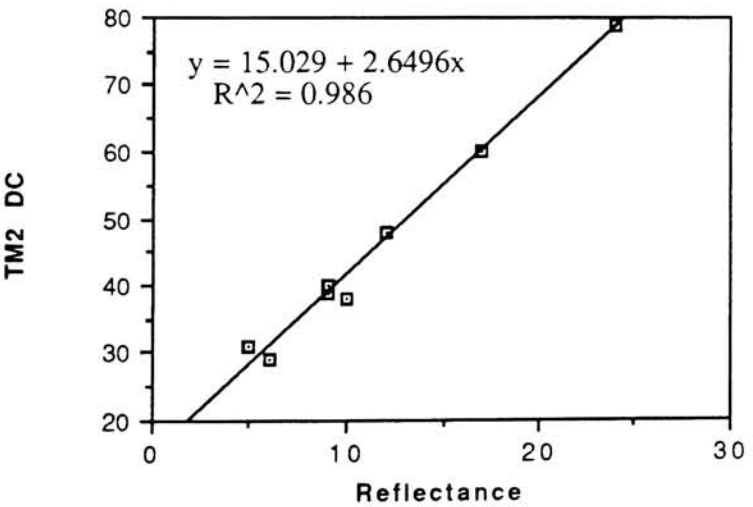

Figure 4-2 Plot of TM2 DC versus estimated Reflectance

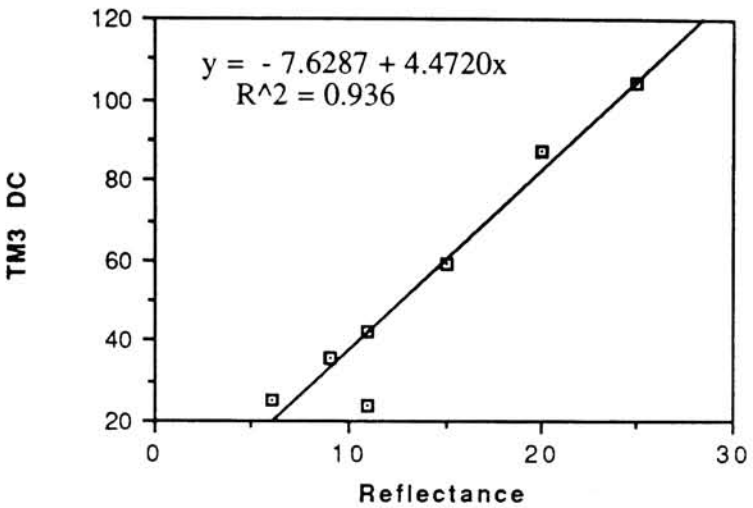

Figure 4-3 Plot of TM3 DC versus estimated Reflectance

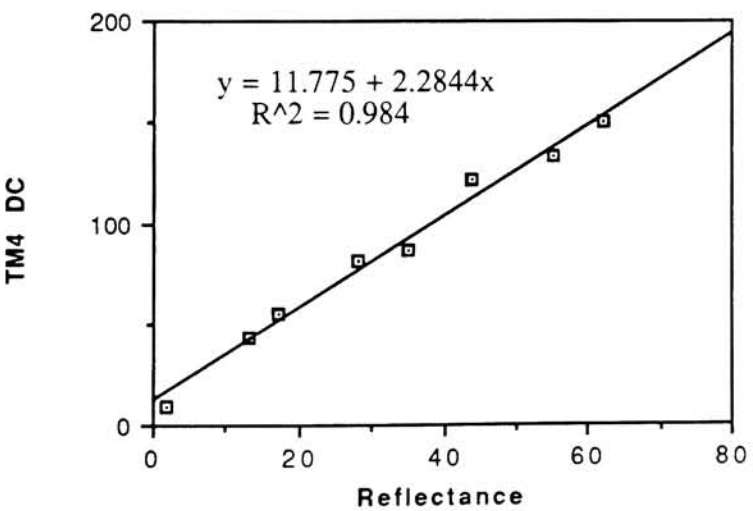

Figure 4-4 Plot of TM4 DC versus estimated Reflectance

Thus, to transform the error from DC to reflective units:

$$\varepsilon_{r\text{-}i} = \frac{\varepsilon_{DC\text{-}i}}{m_i}$$

where: i is the TM band 1..4; and

$m_1 = 7.1638;$

$m_2 = 2.6496;$

$m_3 = 4.4720;$

$m_4 = 2.2844;$

4.3 Results for Part 1 -- Merging with Coarser Resolution Input Sets

In this part of the study, 10 of the merging methods were run on the blurred image sets. The TM data set was blurred to 90m and the SPOT panchromatic image was blurred to 30m. The summary of these results are shown in Tables 4-7a through 4-7c on the following pages. For the further details on these results, refer to Appendices B and C.

Table 4-7a
Summary of Classification Breakdown by Percentage (30m hybrid)

	urban	soil	water	trees	grass
Original TM (30m)	42.34	3.32	0.53	34.17	19.64
Blurred TM (90m)	66.48	1.30	0.49	8.23	23.49
DIRS Method					
- Orig Syn Pan	55.38	4.64	1.26	15.87	22.86
- New Syn Pan	56.25	3.38	1.03	12.80	26.56
- Interpolated Input	47.06	1.66	0.69	25.65	24.94
- Interpolated and post-fixed	50.53	1.71	0.66	14.50	32.60
DIRS Enhancement 1					
- No post-fix	41.99	0.35	0.61	12.50	44.58
- With post-fix	47.84	0.68	0.63	15.58	35.27
DIRS Enhancement 2					
- No modification	54.27	1.93	0.73	14.70	28.37
- modified for TM4, 5	50.21	3.61	0.77	12.00	33.42
Price Method					
- LUT	39.51	4.19	1.12	16.07	39.11
- Adaptive Weights	45.23	2.51	1.34	12.97	39.98

Table 4-7b
Summary of Classification Accuracy with
Independent Data Set 1 (30m hybrid)

	urban	soil	water	trees	grass	overall ave
Original TM (30m)	92.5	100.0	62.3	61.9	99.1	83.2
Blurred TM (90m)	73.6	0	30.2	37.7	90.9	46.5
DIRS Method						
- Orig Syn Pan	63.2	100.0	88.7	14.9	94.2	72.2
- New Syn Pan	96.2	96.7	100.0	27.2	93.6	82.7
- Interpolated Input	95.2	100.0	100.0	51.0	99.1	88.5
- Interpolated and post-fixed	96.2	100.0	88.7	22.3	99.7	81.4
DIRS Enhancement 1						
- No post-fix	76.4	85.2	90.6	9.9	97.9	72.0
- With post-fix	96.2	93.4	98.1	19.3	99.7	81.3
DIRS Enhancement 2						
- No modification	98.1	95.1	77.3	29.7	93.6	78.8
- modified for TM4, 5	90.6	96.7	88.7	39.6	99.4	83.0
Price Method						
- LUT	71.7	96.7	98.1	48.0	99.1	82.7
- Adaptive Weights	76.4	93.4	88.7	29.2	99.1	77.4

where: $\text{overall ave} = \frac{\text{urban} + \text{soil} + \text{water} + \text{trees} + \text{grass}}{5}$

Table 4-7
Summary Table for 30 m Hybrid Results

	Classification Accuracy using Independent Data Set 1	Total RMS Error (DC)
Original TM (30m)	83.2%	reference
Blurred TM (90m)	46.5%	45.8
DIRS Method		
- Orig Syn Pan	72.2%	47.8
- New Syn Pan	82.7%	51.2
- Interpolated Input	88.5%	50.8
- Interpolated then post-fixed	81.4%	43.6
DIRS Enhancement 1		
- No post-fix	72.0%	49.7
- With post-fix	81.3%	43.5
DIRS Enhancement 2	78.8%	44.6
- modified for TM4, TM5	83.0%	43.6
Price Method		
- LUT for TM4, 5, 7	82.7%	43.1
- Adaptive weights for TM4, 5, 7	77.4%	38.4

where:

$$\text{Classification Accuracy} = \text{overall ave} = \frac{\text{urban} + \text{soil} + \text{water} + \text{trees} + \text{grass}}{5}$$

$$\text{Total RMS Error} = \varepsilon_{band1} + \varepsilon_{band2} + \varepsilon_{band3} + \varepsilon_{band4} + \varepsilon_{band5} + \varepsilon_{band7}$$

4.3.1 Observations from Part 1 -- Merging with Coarser Resolution Input Sets

Visible interpretation markedly improved as did classification accuracy (using independent data set 1). In every case classification accuracy increased from 46.5% to at least 72.0%. In several cases, the classification accuracy approached, or even exceeded the classification accuracy of the original TM (30 m) data set. This significant improvement is primarily due to the improved classification of water and soil.

As for radiometric errors, the goal was to improve (or at least not significantly degrade) the difference associated between the blurred TM data set and the original TM data set. A successful method would lower the 45.8 DC total error while sharpening the image.

The two methods that best recovered the original TM radiometry were the Price techniques. For the DIRS techniques, unless they included the post-fixing operation, the errors were higher than the blurred TM data set. The primary band that contributes these errors is TM (or hybrid equivalent) band 4. Even in the blurred TM data set, the error in reflectance units for TM4 are over 3 times greater than for the other reflective bands (see Appendix C).

The primary reason for this high error in band 4 is its high standard deviation (or high contrast) within the image. (Refer to section 3.1 on the selection of the imagery). For this reason, plus the fact that TM4 is not highly correlated with the panchromatic image, it is not surprising that the DIRS methods have high radiometric errors in band 4.

4.4 Results for Part 2 -- Merging with Coarser Resolution Data Sets with a Lower Registration Error

In this phase of the study, six of the methods were again tested at the blurred resolutions, but the input SPOT image that was used had a registration error of less than 5 meters. The summary of these results are shown in Tables 4-8a through 4-8d below. For further details on these results, please refer to Appendices D and E.

Table 4-8a
Summary of Classification Breakdown by Percentage (Re-registered 30m hybrid)

	urban	soil	water	trees	grass
Original TM (30m)	42.34	3.32	0.53	34.17	19.64
Blurred TM (90m)	66.48	1.30	0.49	8.23	23.49
DIRS Method					
- Interpolated Input	47.37	1.20	0.66	20.32	30.45
- Interpolated and post-fixed	49.65	1.98	0.67	11.96	35.74
DIRS Enhancement 1					
- With post-fix	55.94	1.10	0.66	17.01	25.30
DIRS Enhancement 2					
- modified for TM4, 5	57.91	4.24	0.63	12.36	24.87
Price Method					
- LUT	41.94	5.11	0.79	30.06	22.10
- Adaptive Weights	46.32	2.98	0.87	17.79	32.06

Table 4-8b
Summary of Classification Accuracy with
Independent Data Set 1 (Re-registered 30m hybrid)

	urban	soil	water	trees	grass	Overall ave
Original TM (30m)	92.5	100	62.3	61.9	99.1	83.2
Blurred TM (90m)	73.6	0	30.2	37.6	90.9	46.5
DIRS Method						
- Interpolated Input	95.3	100	100	44.1	97.9	87.5
- Interpolated and post-fixed	89.6	100	88.7	19.3	99.7	79.5
DIRS Enhancement 1						
- With post-fix	97.2	88.5	100	43.6	95.8	85.0
DIRS Enhancement 2						
- modified for TM4, 5	83.0	95.1	77.4	45.0	93.9	78.9
Price Method						
- LUT	56.6	96.7	92.5	75.2	97.3	83.7
- Adaptive Weights	80.2	98.4	88.7	28.2	95.2	78.1

where: $\text{overall ave} = \frac{\text{urban} + \text{soil} + \text{water} + \text{trees} + \text{grass}}{5}$

Table 4-8c
Summary of Classification Accuracy with
Random Data Set (Re-registered 30m hybrid)

	urban	soil	water	trees	grass	Overall ave
Original TM (30m)	76.0	35.0	100	68.0	92.0	74.2
Blurred TM (90m)	62.0	22.0	82.0	54.0	72.0	58.4
DIRS Method						
- Interpolated Input	64.0	48.0	100	74.0	52.0	67.6
- Interpolated and post-fixed	62.0	38.0	100	82.0	58.0	68.0
DIRS Enhancement 1						
- With post-fix	62.0	34.0	92.0	66.0	70.0	64.8
DIRS Enhancement 2						
- modified for TM4, 5	64.0	10.0	96.0	86.0	60.0	63.2
Price Method						
- LUT	72.0	14.0	88.0	70.0	76.0	64.0
- Adaptive Weights	66.0	35.0	76.0	83.0	58.0	63.6

where: overall ave $= \frac{\text{urban + soil + water + trees + grass}}{5}$

Statistical Test 1: $\chi^2 = 4.795$ (< 11.070) No significant differences among the methods ($\alpha = 0.05$)

Statistical Test 2: Those methods with overall classification accuracies > 63.5% are significantly better than 58.4%. ($\alpha = 0.05$)

Table 4-8d
Summary Table for Selected 30 m Hybrid Sets
using a Re-registered SPOT image as input

	Classification Accuracy using Independent Data Set 1	Classification Accuracy using a Random Data Set	Total RMS Error (DC)
Original TM (30m)	83.2%	74.2%	reference
Blurred TM (90m)	46.5%	58.4%	45.8
DIRS Method			
- Interpolated Input	87.5%	67.6%	48.8
- Interpolated then post-fixed	79.5%	68.0%	41.1
DIRS Enhancement 1			
- With post-fix	85.0%	64.8%	40.7
DIRS Enhancement 2			
- modified for TM4, TM5	78.9%	63.2%	41.8
Price Method			
- LUT for TM4, 5, 7	83.7%	64.0%	38.4
- Adaptive weights for TM4, 5, 7	78.1%	63.6%	36.2

where:

$$\text{Classification Accuracy} = \text{overall ave} = \frac{\text{urban} + \text{soil} + \text{water} + \text{trees} + \text{grass}}{5}$$

$$\text{Total RMS Error} = \varepsilon_{band1} + \varepsilon_{band2} + \varepsilon_{band3} + \varepsilon_{band4} + \varepsilon_{band5} + \varepsilon_{band7}$$

4.4.1 Observations in Part 2 -- Merging with Coarser Resolution Data Sets with a Lower Registration Error

The improved registration resulted in better radiometry for every method in every band, except for the DIRS Enhancement 2 band 4. However in this case, the radiometric error is only slightly higher.

For classification accuracy using independent data set 1, three methods slightly improved, while the other three methods showed slightly poorer results. At this resolution, it does not appear that registration differences between 1 pixel error and 0.5 pixel error have any significant effect on classification.

Using the classification accuracies derived from random data sets, we can now see that no method was able to surpass the accuracy of the original TM data set. The primary difference between independent data set 1 and a random data set are the results for soil. The classifiers for all these hybrids basically overclassified on the soil. Thus the soil sample chosen for the independent data set was always correctly classified (near 100% accuracies); but with a random set, the overclassification was detected.

Although none of these methods were able to outperform the overall classification accuracy (using a random data set) of the original TM data set, they all were able to improve the classification accuracy of the blurred TM data set. In addition, several methods were able to outperform the original TM data set in classifying trees and soil.

4.5 Results for Part 3 -- Merging with Original Resolution Data Sets

This last phase used the original resolution data sets to create hybrid data sets with approximately 10m GIFOV. The summary of these results are shown in Tables 4-9a through 4-9e below. For the further details on these results, please refer to Appendix F.

Table 4-9a
Summary of Classification Breakdown by Percentage (10m hybrid)

	urban	soil	water	trees	grass
Original TM (30m)	42.34	3.32	0.53	34.17	19.64
DIRS Method					
- Interpolated Input	51.08	1.50	0.56	23.83	23.03
- Interpolated and post-fixed	48.86	1.86	0.55	28.36	20.39
DIRS Enhancement 1					
- With post-fix	49.74	1.24	0.59	27.86	20.59
DIRS Enhancement 2					
- modified for TM4, 5	47.76	2.28	0.54	29.98	19.43
Price Method					
- LUT	47.32	1.76	0.58	30.52	19.82
- Adaptive Weights	47.62	1.62	0.59	29.35	20.83

Table 4-9b
Summary of Classification Accuracy with
Random Data Set (10m hybrid)

	urban	soil	water	trees	grass	overall ave
Original TM (30m)	76.0	35.0	100	68.0	92.0	74.2
DIRS Method						
- Interpolated Input	72.0	66.0	100	89.0	77.0	80.8
- Interpolated and post-fixed	71.0	47.0	100	62.0	88.0	73.8
DIRS Enhancement 1						
- With post-fix	74.0	66.0	100	82.0	82.0	80.8
DIRS Enhancement 2						
- modified for TM4, 5	64.0	37.0	100	81.0	81.0	72.6
Price Method						
- LUT	76.0	56.0	100	77.0	89.0	79.6
- Adaptive Weights	71.0	57.0	100	88.0	89.0	81.0

where: $\text{overall ave} = \frac{\text{urban} + \text{soil} + \text{water} + \text{trees} + \text{grass}}{5}$

Statistical Test 1: $\chi^2 = 22.112$ (> 11.070) The differences among the classification accuracies are significant. The methods are not equal. ($\alpha = 0.05$)

Statistical Test 2: Those methods with overall classification accuracies > 76.5% are significantly better than 74.2%. ($\alpha = 0.05$). For $\alpha = 0.01$, the threshold for significance is 80.4%

Table 4-9c
Summary of Classification Accuracy with
Independent Data Set 1 (10m hybrid)

	urban	soil	water	trees	grass	overall ave
Original TM (30m)	92.5	100	62.3	61.9	99.1	83.2
DIRS Method						
- Interpolated Input	98.1	100	100	81.2	99.4	95.7
- Interpolated and post-fixed	97.2	100	62.3	77.7	99.1	87.3
DIRS Enhancement 1						
- With post-fix	99.1	100	88.7	76.7	97.6	92.4
DIRS Enhancement 2						
- modified for TM4, 5	97.2	100	81.1	76.2	99.1	90.7
Price Method						
- LUT	99.1	100	88.7	88.6	99.1	95.1
- Adaptive Weights	99.1	100	79.2	71.8	98.8	89.8

where: $\text{overall ave} = \frac{\text{urban} + \text{soil} + \text{water} + \text{trees} + \text{grass}}{5}$

Table 4-9d
Summary of Classification Accuracy with
Independent Data Set 2 (10m hybrid)

	urban	soil	water	trees	grass	overall ave
Original TM (30m)	50.0	100	60.0	70.0	78.0	71.6
DIRS Method						
- Interpolated Input	82.0	100	74.0	94.0	92.0	88.4
- Interpolated and post-fixed	76.0	98.0	62.0	78.0	88.0	80.4
DIRS Enhancement 1						
- With post-fix	86.0	100	72.0	80.0	76.0	82.8
DIRS Enhancement 2						
- modified for TM4, 5	76.0	96.0	60.0	80.0	74.0	77.2
Price Method						
- LUT	94.0	98.0	74.0	80.0	82.0	85.6
- Adaptive Weights	90.0	100	66.0	86.0	82.0	84.8

where: overall ave $= \frac{\text{urban + soil + water + trees + grass}}{5}$

Statistical Test 1: $\chi^2 = 14.194$ (> 11.070) The differences among the classification accuracies are significant. The methods are not equal. ($\alpha = 0.05$)

Statistical Test 2: Those methods with overall classification accuracies > 78.0% are significantly better than 71.6%. ($\alpha = 0.05$). For $\alpha = 0.01$, the threshold for significance is 80.5%

Table 4-9
Summary Table of Classification Accuracies for Selected 10 m Hybrid Sets using a Re-registered SPOT image as input

	Random Data Set	Independent Data Set 1	Independent Data Set 2
Original TM (30m)	74.2%	83.2%	71.6%
DIRS Method			
- Interpolated Input	80.8%	95.7%	88.4%
- Interpolated then post-fixed	73.8%	87.3%	80.4%
DIRS Enhancement 1			
- With post-fix	80.8%	92.4%	82.8%
DIRS Enhancement 2			
- modified for TM4, TM5	72.6%	90.7%	77.2%
Price Method			
- LUT for TM4, 5, 7	79.6%	95.1%	85.6%
- Adaptive weights for TM4, 5, 7	81.0%	89.8%	84.8%

where:

$$\text{Classification Accuracy} = \text{overall ave} = \frac{\text{urban} + \text{soil} + \text{water} + \text{trees} + \text{grass}}{5}$$

4.5.1 Observations for Part 3 -- Merging with Original Resolution Data Sets

Using independent data set 2, it becomes quite clear that the hybrid data classifies better in the high frequency areas -- especially in the cases of urban and trees. The samples for these two classes were taken from small side roads and from suburban areas. For the other classes (water, soil, and grass) it was much more difficult to find isolated incidences, and thus these samples were taken near boundaries and edges. With these samples the original TM data set performed nearly as well.

Visually, the classification maps also confirm these results -- the roads have more definition and the soil regions are more defined (see Appendix F).

4.6 Other Comparisons Between the Merging Methods

4.6.1 Visual Comparisons

All the methods visually improved the blurred images. However, under higher magnification, the blocky appearance is readily apparent in some of the methods (see figures 4-9 through 4-14).

The most blocky hybrid set was that of the DIRS Enhancement 2 method (with TM4 and TM5 modification). This result is not surprising since the algorithm was run with a threshold that considered only 25% of the superpixel blocks as mixed. Thus at best, only one-fourth of the blocks could be further segmented into subpixels without using the pure

merging method. In addition, the algorithm's method of handling TM4 and TM5 is to insert the original TM values into the hybrid subpixels. This simple technique may not decrease the blocking, and in some cases may accentuate the blocking efffect within these bands.

Another noticed artifact was some high frequency noise in the hybrid bands created by both Price techniques. For the Price technique that uses the look up table (LUT), the high frequency noise is generated when the SPOT panchromatic transformation LUT has no value associated with a SPOT DC. This can happen since the LUT is generated with an averaged SPOT image and the TM band. In those cases, the value placed in the output image is the closest lower value on the table.

In Figure 4-13 we can see this anomaly in a grove of trees. Band 5 is placed in the red channel, and is sensitive to the vegetation so the grove is a deep red color. The panchromatic channel is only marginally sensitive to the vegetation and so its DC is much lower. In those cases where there is no match for the panchromatic DC, the nearest (and lower) value on the table corresponding to the DC is output. Thus these dark spots are noticed in the grove of red trees.

The modified Price technique also produces high frequency noise in the output images. In these instances, the multiband regression derives the (best fit) weights for a superpixel area (section 2.6). These weights however, occasionally produce an outlier (an extreme value) when applied to the individual subpixels within that superpixel. These outliers appear as speckle, or high frequency noise in the image. To reduce the speckled appearance, a simple median filter was applied to these hybrid images. A median filter maintains the edges of an image, but eliminates individual pixel noise. The resultant hybrid images after median filtering has no speckle, however, some fine structure (such as

housetops) are also lost.

Overall, the method which produces the most appealing visual hybrid is the DIRS method with an interpolated TM data set as input.

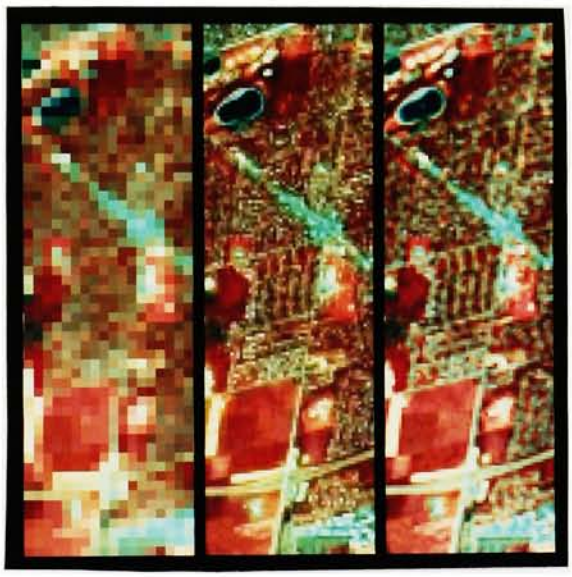

Figure 4-5. Comparison of Coarser Resolution Images
(a) Blurred TM Bands 5,3,2 (90m GIFOV)
(b) Hybrid Bands 5,3,2 produced by DIRS Method with Interpolated Input (30m GIFOV)
(c) Original TM Bands 5,3,2 (30m GIFOV)

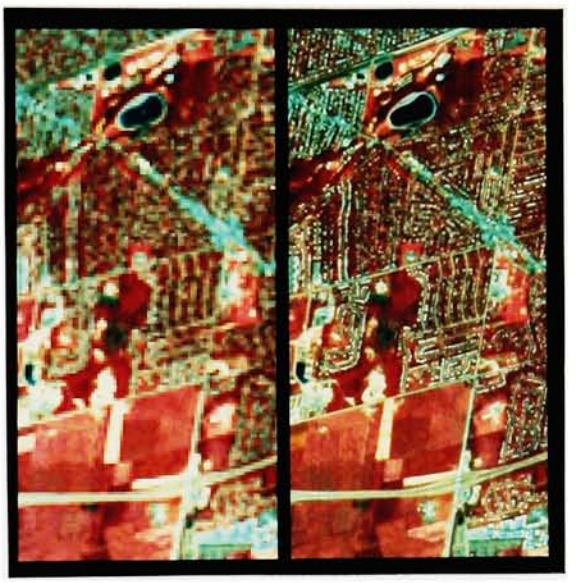

Figure 4-6. Comparison of Original Resolution Images
(a) Original TM Bands 5,3,2 (30m GIFOV)
(b) Hybrid Bands 5,3,2 produced by DIRS Method with Interpolated Input (10m GIFOV)

Figure 4-7. Replicated TM Bands 5,3,2
(30m GIFOV) (magnification = 4x)

Figure 4-8. Interpolated TM Bands 5,3,2
(30m GIFOV) (magnification = 4x)

Figure 4-9. DIRS Method with Interpolated Input
(10m GIFOV) (magnification = 4x)

Figure 4-10. DIRS Method with Interpolated Input and Post-fixing
(10m GIFOV) (magnification = 4x)

Figure 4-11. DIRS Enhancement 1 with post-fixing
(10m GIFOV) (magnification = 4x)

Figure 4-12. DIRS Enhancement 2 Method with mod to TM4 and TM5
(10m GIFOV) (magnification = 4x)

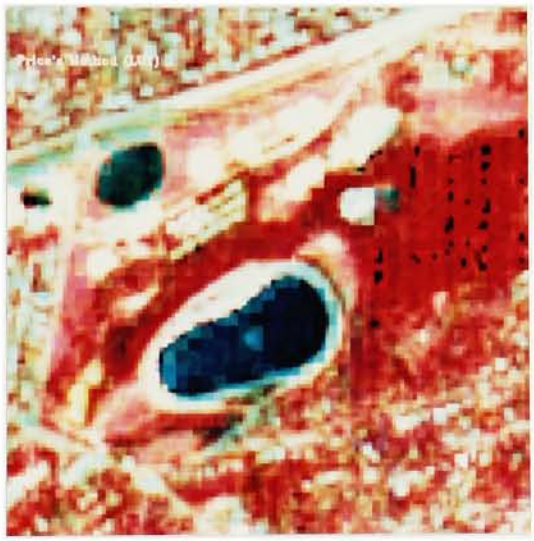

Figure 4-13. Price's Method (LUT)
(10m GIFOV) (magnification = 4x)

Figure 4-14. Modified Price's Method with Adaptive Weights
(10m GIFOV) (magnification = 4x)

4.6.2 Implementation Comparisons

Price's methods require the most time-consuming preparation. His methods first compute high resolution estimates of the TM bands, then merge these estimates to the original resolution TM images. For those bands that are correlated to the panchromatic image (TM bands 1, 2, and 3), each band must derive the linear coefficients to transform the panchromatic image into a high resolution estimate of the TM band.

While running the modified Price technique for the weakly correlated bands, the coefficients to obtain the high resolution estimates are computed for each superpixel area (hence the term *adaptive* weighting). For each band, this results in close to 300,000 multivariate regressions. In addition, the modified Price technique must also run serially, in that the high resolution estimate of TM7 must be computed first, since it is used as an input to compute the estimates for TM5 and TM4. All these coefficients are image dependent and must be computed for every scene.

The DIRS methods require some preparation before merging, but they are not as extensive as in the Price methods. First, a synthetic panchromatic image must be computed. For this study, the weights used to compute this synthetic image are general purpose weights that are not image dependent (section 2.2.1). Once the synthetic image has been created, the SPOT panchromatic histogram is linearly adjusted to this synthetic image, and the merging operation can begin.

Except for the modified Price technique, the run times for these merging methods are approximately equal, taking less than 5 minutes to run on a VAX 1170. Because the

modified Price technique is run serially and computes numerous regressions, obtaining a full bybrid data set (bands 1-5,7) takes approximately 45 minutes. However, the code for the modified Price technique, as well as the other methods, can be optimized for faster run times.

5.0 CONCLUSIONS

This study set out to determine if we could enhance our multispectral analysis by merging a higher resolution panchromatic image to a lower resolution multispectral data set while preserving the multispectral information. The results in section 4.0 clearly show that merging can enhance analysis. Visual interpretablity, as well as computer interpretability (measured via classification) is improved.

Several merging methods were compared, and each were found to have their own advantages and disadvantages. No method was found to be overwhelmingly the best in all phases of the evaluation. Listed below are the evaluation criteria and those techniques which performed well.

(1) **Best method to improve classification**: DIRS method with interpolated input. This method consistently provided the highest classification accuracy regardless of the input classification set. Other methods which performed well are the Price techniques and the DIRS Enhancement 1 with post-fixing.

(2) **Best methods to maintain radiometry**: Price and the modified Price with adaptive weights. The modified Price method was the only method to improve the radiometric error between the blurred TM4 image and the original TM4 image. The Price method using the LUT also performed well with TM4. However for bands that are strongly correlated, the DIRS methods perform slightly better. In all cases, if the registration error between the panchromatic image and the TM data set is lower, so is the radiometric error.

(3) **Best method to improve visual interpretation**: DIRS with interpolated input. Because this method does not force the radiometry to be correct over the superpixel area, there is no blocking effect observed in the hybrid images. All other methods produce images with some degree of blocking.

If the primary goal in merging panchromatic and multispectral images is improved interpretablity, then the method to merge should be the DIRS method with interpolated input. If preserving radiometry is equally important (as in situations where the hybrid data set is used as a simulated product, or as input for further processing) then the modified Price's technique with adaptive weights, or the DIRS Enhancement 1 method with post-fixing is recommended.

This study has developed and demonstrated several merging techniques which can enhance image analysis. However, there are still some short-comings among these techniques. Better methods to handle uncorrelated bands, as well as "smarter" segmentation routines to reduce block appearances are two areas which require more attention. These issues and recommendations for further studies are explored in the next section.

6.0 RECOMMENDATIONS

This section is broken down into two main parts. The first part explores some possible changes and improvements to the merging methods that were evaluated in this study. The second part is a more generalized view of the direction that future merging methods should consider.

6.1 Improvements to the Price Methods

The modified Price method with the adaptive weights for TM bands 4, 5, and 7 provided the best overall results among the methods evaluated. However, information was lost when a median filter was applied over bands 4, 5 and 7 to eliminate the speckled appearance. One improvement to this method would be to selectively (rather than comprehensively) filter the image.

The selection criteria to filter the subpixel could be based on the standard deviation of the input high resolution image(s). For example, this can be represented as:

$$\text{Threshold } (k, l) = \text{Factor} \cdot \sigma_{\text{hi-res input}}(k,l) \cdot \frac{\sigma_{TM(i)}}{\sigma_{\text{ave hi\_res input}}} \qquad (6\text{-}1)$$

where:
- $\sigma_{\text{hi-res input}}(k,l)$ = the standard deviation of the high resolution image at the area surrounding pixel location k,l;
- $\sigma_{TM(i)}$ = the standard deviation of the TM band i image;
- $\sigma_{\text{ave hi-res input}}$ = the standard deviation of the averaged high resolution image (30m GIFOV);
- Factor = weighting factor;

Threshold(k,l) = the threshold value for pixel location k,l

Thus, if the standard deviation of the 3 by 3 pixel block centered at k, l is greater than Threshold(k,l), then that pixel location should be median filtered.

6.2 Improvements to the DIRS Methods

For certain applications, the DIRS methods show considerable promise. However, when merging bands that are weakly correlated with the panchromatic image, the algorithm falls short in maintaining radiometry. Therefore, as Price concluded, the correlated and the weakly correlated bands must be handled differently if radiometry is to be preserved. Further recommendations for each of these cases are presented below.

6.2.1 Recommendations in Processing Correlated Bands

The first recommendation is in the generation and the use of the TM-based synthetic panchromatic image. In this study, image independent weights were computed and used. These weights were created by taking a best fit of 25 target samples over 3 different atmospheres (section 2.2.1). Thus, these weights were intended to approximate a SPOT panchromatic image for a general Landsat TM image set. However, for a more accurate estimate of the panchromatic image, the weights can be calculated on an image to image basis with *a priori* knowledge of the scene.

For example, in the scene used in this study, the original TM data set classified the

five major classes in the following breakdown:

urban	42.34 %
soil	3.32 %
water	0.53 %
trees	34.17 %; and
grass	19.64 %.

Before any merging, the scene clearly has limited soil and water. So rather than having each of the 25 targets weighted equally in the regression to compute the synthetic panchromatic weights, the regression can weight the samples based on their percentage of scene composition. In addition, if the atmospheric parameters are known, these too can be used to generate more accurate samples for the regression. In this manner, an image dependent weighting set can be developed to produce a more accurate panchromatic image.

With this synthetic panchromatic image, the atmospheric differences between the acquisition of the SPOT and TM images can be removed. As suggested in section 4.1, the blurred SPOT panchromatic image should be linearly adjusted to the synthetic panchromatic image. These same coefficients are then applied to the original resolution SPOT panchromatic image to transform the SPOT image into the TM aquisition domain.

After this transformation, the synthetic panchromatic image should be replaced in the DIRS merging algorithm with the blurred or averaged SPOT image. Thus instead of the DIRS merging algorithm of:

$$DC_{\text{Hybrid Multiband}}(i) = DC_{\text{SPOT Pan}} \cdot \left(\frac{DC_{TM}(i)}{DC_{\text{Syn TM Pan}}} \right) \qquad (6\text{-}2)$$

the algorithm should appear as:

$$DC_{\text{Hybrid Multiband}}(i) = DC_{\text{SPOT Pan}} \cdot \left(\frac{DC_{TM}(i)}{DC_{\text{Ave SPOT Pan}}} \right) \quad (6\text{-}3)$$

In this manner, the radiometry is correct within the superpixel for all pure merges. The synthetic panchromatic image is used only to atmospherically adjust the original SPOT panchromatic image to the TM data set.

6.2.2 Recommendation for Handling Bands that are Weakly Correlated to the Panchromatic Band

Perhaps one of the more exciting results of this study is how well the DIRS methods can sharpen and recover the TM bands that are correlated to the finer resolution input (panchromatic) band. Even the DIRS Enhancement 2 method returns a lower radiometric error in bands 2 and 3 than the Price methods (Appendix C and E). These results suggest that the high resolution input band that is used in merging with a TM multispectral band should be correlated for a more accurate and radiometrically correct hybrid.

For those multispectral bands which are weakly correlated to the high resolution panchromatic image, a recommendation is to replace the panchromatic input with a high resolution estimate of the weakly correlated band in the merging algorithm. The primary DIRS merging algorithm for these bands would look identical to the Price method. Instead of the DIRS merging algorithm shown in equation (6-2), the algorithm would be:

$$DC_{\text{Hybrid Multiband}}(i) = DC_{\text{Hi-res}}(i) \cdot \left(\frac{DC_{TM}(i)}{DC_{\text{Ave Hi-res}}} \right) \quad (6\text{-}4)$$

where: $DC_{Hi\text{-}res}(i)$ = Digital count (DC) of the high resolution estimate of TM band i;

As in the modified Price technique (section 2.6), the high resolution estimate can be computed using the Tom et al [85] technique.

The advantage of implementing this recommendation is that the DIRS methods are not limited to this primary merging algorithm. With the modifications and enhancements to the DIRS method (section 2.2 through 2.4), the merging algorithm may replace the superpixel ratio with a neighboring superpixel's ratio (see equation 2-10). By not being limited to a "pure merge" at every superpixel, the DIRS methods should provide an improvement to the Price methods.

6.2.3 Improvements to the Interpolated Input

The DIRS method using interpolated TM inputs created hybrid data sets that significantly improved interpretability. For this reason, further work in the interpolation routine can be explored.

For this study, a simple averaging kernal was used in the interpolation routine (section 2.2.2). Other standard kernals may provide a more accurate, and realistic interpolation. Two suggested kernals for future investigation are the Gaussian-weighted kernal, and a cubic convolution kernal.

6.2.4 Improvements to the DIRS Enhancement 2 Method

Although successful in only a limited sense, the concepts behind the DIRS Enhancement 2 method warrant further investigation. This method is the only method which does not employ a radiometric post-fix operation. Instead, the method works by first determining the subpixel values that most likely belong to pure surrounding areas. Those subpixels that are "left-over" are then assigned values such that radiometry is preserved over the superpixel. Conceptually, this approach should alleviate the superpixel blocking effect -- more so than a hard post-fix operation -- while maintaining radiometry. However, the implementation of this algorithm was not robust. Further work needs to be accomplished in many areas. Three suggestions are presented below.

The first recommendation is to run the DIRS Enhancement 2 method using interpolated TM input (rather than replicated input). If the threshold is set such that 25% of the superpixel areas are considered mixed, then a minimum of 75% of the image set will appear as the DIRS method with interpolated input and post-fixing. The other 25% of the image set will be sharpened with the enhanced segmentation routine. The resultant hybrid images should more radiometrically precise than the DIRS method with interpolated input and post-fixing; and should appear less blocky than the original DIRS Enhancement 2 method.

The second improvement would be modifying the thresholds used in decision-making. Currently there is only one threshold value that is of prime interest to the algorithm. This is the user defined threshold that determines whether a superpixel is mixed

or is pure. The second threshold determines if a subpixel is connected to a neighboring subpixel (or superpixel), but its value is computed from the mixed threshold (section 3.4).

Further work should untie these two thresholds to allow more flexibility. Then the algorithm should be excercised with varying threshold settings. Some preliminary work was done in varying the thresholds, but the two thresholds were tied together and only minor differences were noted.

The last suggestion for the improvement of the DIRS Enhancement 2 method is much more involved. The algorithm needs to become "smarter", and must use other information to segment and sharpen the images. Currently, all the decisions are based on the standard deviation threshold of the panchromatic (or high resolution) image.

Other information that could be used are edge information, or other textural and statistical features. The additional information does not have to be limited to spatial information. A classification map of the low resolution TM data set would be a useful input, especially when dealing with weakly correlated bands.

In essense, this third suggestion is pointing to an artificial intelligence system, and is by no means a trivial problem. However, this is the long-term and general direction that data fusion algorithms will follow.

6.3 General Considerations

This study investigated several methods that enhanced the spatial resolution of multispectral data using a higher resolution panchromatic image. The study concentrated on methods that operate in the spatial domain and work with simple linear relationships.

Other methods that work in other domains should also be studied. Work in the spatial frequency domain seems to be a natural area for concentration, but care must still be taken to separate the spatial and spectral information if maintaining radiometry is important.

Neural networks can provide an alternative to the simple linear relationships prescribed by these methods. Neural networks are inherently non-linear in describing an optimal relationship, and may be a method in handling bands that are weakly correlated to the panchromatic image.

These methods that were evaluated are relatively simple, fast, and effective. There is still some room for improvement, but the level of effort to attain further gain will be much more extensive and complex. Future methods will have to incorporate and manipulate more layers of information, including spectral, spatial, and statistical data, as well as information on context. This influx of information may lead to a multi-stage segmentation/classification scheme, or to a scheme that is iterative in nature.

Lastly, this study looked at only one image set and at one sensor pairing. The methods are expected to be applicable to other sensor sets, as well as to hyperspectral data, but further testing with varying image sets should be accomplished to ensure the robustness of these techniques.

REFERENCES

Acevedo, W., J.S.Buis, R.C.Wrigley, "Changes in Classification Accuracy Due to Varying Thematic Mapper and Multispectral Scanner Spatial, Spectral, and Radiometric Resolution," *Proceedings of the XVIIIth International Symposium on RemoteSensing of Environment*, Paris, France, pp. 27-44, 1984

Ahearn, S.C., "A Proposed Hotelling T^2 Based Unsupervised Procedure as Input to a Bayesian Classifier," *Annual Convention of American Society for Photogrammetry and Remote Sensing*, 1986, pp 350-359

Alwashe,M.A., S.Jutz, J.Zilger, "Integration of SPOT and Landsat Thematic Mapper data for Land use and Urban Mapping of At'Taif, Saudi Arabia," *Proceedings of IGARSS '88 Symposium*, Edinburgh, Scotland, 13-16 Sept 1988, p 629, 1988

Bernstein, R., J.B.Lotspiech, H.j.Myers, H.G.Kolsky, R.D.Lees, "Analysis and Processing of Landsat--4 Sensor Data Using Advanced Image Processing Techniques and Technologies," *IEEE Transactions on Geoscience and Remote Sensing*, vol GE-22, no 3, pp 192-221, 1984

Campbell, J.B., Introduction to Remote Sensing, The Guilford Press, 1987

Carper, W.J., R.W.Kiefer, T..M. Lillesand, "Enhancement of SPOT Image Resolution using an Intensity-Hue-Saturation Transformation," *1987 ASPRS Technical Papers*, pp 348-361, 1987

Chavez, P.S., Jr., G.L. Berlin, and M.A. Tarabzouni, "Discriminating Lithologies and Surficial Deposits in the AL Hisma Plateau Region of Saudi Arabia with Digitally Combined Landsat MSS and SIR-A Images," *Proceedings: National Conference on Resource Management Applications: Energy and Environment,* Vol 4, San Francisco, CA pp 22-34, 1983

Chavez, P.S., Jr., "Digital Processing Techniques for Image Mapping with Landsat TM and SPOT Simulator Data," *Proceedings of the XVIIIth International Symposium on Remote Sensing of Environment*, Paris, France, pp. 101-116, 1984

Chavez, P.S., Jr., "Digital Merging of Landsat TM and Digitized NHAP Data for 1:24,000-Scale Image Mapping," *Photogrammetric Engineering and Remote Sensing*, Vol 52, no 10, pp 1637-1646, Oct 1986

Chavez, P.S., Jr., J.A.Bowell, "Comparison of the Spectral Information Content of Landsat Thematic Mapper and Spot for Three Different Sites in the Phoenix, Arizona Region," *Photogrammetric Engineering and Remote Sensing*, vol 54, no 12, pp 1699-1708, 1988

Chhikara, R.S., "Effect of Mixed (Boundary) Pixels on Crop Proportion Estimation," *Remote Sensing of Environment*, vol 14, pp 207-218, 1984

Clark, B.P., F.G.Sadowski, A.J.Johnson, "An Approach for Emulating the Color Balance of Landsat Multispectral Scanner Images with AVHRR data," *1987 ASPRS-ACSM Fall Convention ASPRS Technical Papers*, pp 331-341

Cliche, G., F. Bonn, and P. Teillet, "Integration of the SPOT Panchromatic Channel into its Multispectral Mode for Image Sharpness Enhancement," *Photogrammetric Engineering and Remote Sensing*, Vol 51, no 3, pp 311-316, 1985

Daily, M., T. Farr, C. Elachi, and G. Schaber, "Geologic Interpretation from Composited Radar and Landsat Imagery," *Photogrammetric Engineering and Remote Sensing*, Vol 45, no 8, pp 1109-1116, 1979

Di Zenzo, S., R.Bernstein, S.D.Degloria, H.G.Kolsky, "Gaussian Maximum Likelihood and Contextual Classification Algorithms for Multicrop Classification," *IEEE Transactions on Geoscience and Remote Sensing*, vol GE-25, no 6, pp 805-814, 1987

Di Zenzo, S., S.D.Degloria, R.Bernstein, H.G.Kolsky, "Gaussian Maximum Likelihood and Contextual Classification Algorithms for Multicrop Classification Experiments Using Thematic Mapper and Multispectral Scanner Sensor Data," *IEEE Transactions on Geoscience and Remote Sensing*, vol GE-25, no 6, pp 815-824, 1987

ERDAS User's Guide, copyright (c) 1988, by ERDAS, Inc, Atlanta, GA

Freund, John E., Modern Elementary Statistics, 7th Ed., Prentice-Hall, Englewood Cliffs, New Jersey, 1988

Green, W.B., Digital Image Processing A Systems Approach, 2nd Ed, Van Nostrand Reinhold, New York, NY, 1989

Gurney, C.M., J.R.Townshend, "The use of Contextual Information in the Classification of Remotely Sensed Data," *Photogrammetric Engineering and Remote Sensing*, vol 49, pp 55-64, 1983

Haralick, R.M., "Statistical and Structural Approaches to Texture," *Proceedings of the IEEE*, vol 67, no 5, pp 786-804, 1979

Haralick, R.M. and K.S. Shanmugam,"Combined Spectral and Spatial Processing of ERTS Imagery Data," *Remote Sensing of the Environment*, vol3, pp 3-13, 1974

Hashim, M., "Crop Identification Using Merged Landsat Multispectral Scanner and Thematic Mapper Data Preliminary Attempts," *1988 ACSM-ASPRS Annual Convention*, St Louis, Missouri, Vol 4-Image Processing/Remote Sensing, pp 11-20, 1988

Hjort, N.L., E.Mohn, "A Comparison of some Contextual Methods in Remote Sensing Classification," *Proceedings of the XVIIIth International Symposium on Remote Sensing of Environment*, Paris, France, pp. 1693-1702, 1984

Imhoff, M.L., G.W.Petersen, S.G.Sykes, J.R.Irons, "Digital Overlay of Cartographic Information on Landsat Mss Data for Soil Surveys," *Photogrammetric Engineering and Remote Sensing*, Vol 48, no 8, pp 1337-1342, Aug 1982

Irons, J.R., B.L.Markham, R.F.Nelson, D.L.Toll, D.L.Williams, R.S. Latty, R.L.Kennard, M.L.Stauffer, "The Effects of Sensor Advancement on Thematic Mapper Data Classification," *Proceedings of the XVIIIth International Symposium on Remote Sensing of Environment*, Paris, France, pp. 1759-1773, 1984

Irons, J.R., B.L.Markham, R.F.Nelson, D.L.Toll, D.L.Williams, "The effects of spatial resolution on the classification of Thematic Mapper data," *International Journal of Remote Sensing*, vol 6, no 8, pp 1385-1403, 1985

Isaacs, R.G., A.M.Vogelmann, "Multispectral Sensor Data Simulation Modeling Based on the Multiple Scattering LOWTRAN code," *Remote Sensing Environment*, vol 26, pp 75-99, 1988

Kittler, J., J.Foglein, "Contextual Classification of Multispectral Pixel Data," *Image and Vision Computing,* vol 2, no 1, pp 13-29, 1984

Latty, R.S., and R.M. Hoffer, "Computer-based Classification Accuracy due to the Spatial Resolution Using Per-Point versus Per Field Classification Techniques," *Proceedings Seventh International Symposium on Machine Processing of Remotely Sensed Data,* West Lafayette, IN, pp 384-393, 1981

Lauer, D.T., and W.J. Todd, "Landcover Mapping with Merged Landsat RBV and MSS Stereoscopic Images," *Proceedings: ASP Fall Technical Conference*, American Society of Photogrammetry, San Francisco, CA, pp 680-689, 1981

Markham, B.L., J.R.G. Townshend, "Land Cover Classification Accuracy as a Function of Sensor Resolution," *Proceedings of the Fifteenth International Symposium on Remote Sensing of Environment,* Ann Arbor, MI, pp 1075-1090, 1981

Mayers, M., L. Wood, J. Hood, "Adaptive Spatial Filtering," *Technical Papers -- 1988 ACSM-ASPRS Fall Convention*, Virginia Beach, VA, p 99-105, Sept 1988

Merickel, M.B., J.C. Lundgren, S.S.Shen, "A Spatial Processing Algorithm to Reduce the Effects of Mixed Pixels and Increase the Separability Between Classes," *Pattern Recognition*, vol 17, no 5, pp 525-533, 1984

Palmer, J.M., M.G.Tomasko, "Broadband Radiometry with Spectrally selective Detectors," *Optics Letters,* vol 5, no 5, pp 208-210, 1980

Park, S.K., R.A.Schowengerdt, "Image Reconstruction by Parametric Cubic Convolution", *Computer Vision, Graphics, and Image Processing*, vol 23, pp 258-272, 1982

Price, J.C., "Combining Panchromatic and Multispectral Imagery from Dual Resolution Satellite Instruments," *Remote Sensing of Environment*, vol 21, pp 119-128, 1987

Rosenblum, W., "Optimal Selection of Textural and Spectral Features for Scene Segmentation", *MS Thesis*, Rochester Institute of Technology, Rochester, NY, 1990

Sadowski, F.G., J.E.Malila, J.E.Sarno, R.F.Nalepka, "The Influence of Multispectral Scanner Spatial Resolution on Forest Feature Classification," *Proceedings of the 11th International Symposium on Remote Sensing of Environment*, Ann Arbor, MI, 1977, pp 1279-1288

Salvaggio, C.,"Automated Segmentation of Urban Features from Landsat Thematic Imagery for use in Pseudoinvariant Feature Temporal Image Normalization", *MS Thesis*, Rochester Institute of Technology, Rochester, NY, 1987

Schowengerdt, R.A.,"Reconstruction of Multispatial, Multispectral Image Data Using Spatial Frequency Content," *Photogrammetry Engineering and Remote Sensing*, vol46, no 10, pp 1325-1334, Oct 1980

Schowengerdt, R.A.,"Enhanced Thermal Mapping with Landsat and HCMM Digital Data," *Technical Papers: ACSM-ASP, Convention, 48th Annual Meeting*, American Society of Photogrammetry, Denver, CO, pp 414-422, 1982

Schowengerdt, R.A., Techniques for Image Processing and Classification in Remote Sensing, Academic Press, Orlando, FL, 1983

Shimoda, H., K.Fukue, R.Yamaguchi, Z.Zhang, T.Sakata, "Accuracy of Landcover Classification of TM and SPOT data," *Proceedings of IGARSS 1988 Symposium*, Edinburgh, Scotland, pp 529-535, 1988

Slater, P.N., "Survey of Multispectral Imaging Systems for Earth Observations," *Remote Sensing of Environment*, vol 17, no 1, pp 85-102, 1985

Suits, G., W.Malila, T.Weller, "Procedures for Using Signals from One Sensor as Substitutes for Signals of Another," *Remote Sensing of Environment*, vol 25, no 3, pp 395-408, 1988

Tom, T.T., M.J. Carlotto, and D.K. Scholten, "Spatial Sharpening of Thematic Mapper Data using a Multiband Approach," *Optical Engineering*, vol 24, pp 1026-1029, 1985

Walsh, S.J., K.R. Gallager, I.E.Von Essen, J.W.Cooper, "Integration of Digital Terrain Models and Enhanced Landsat Thematic Mapper Digital Data within a Geographic Information System: Hydrologic Analysis of Glacier National Park, Montana," *Technical Papers - 1988 ACSM-ASPRS Fall Convention,* Virginia Beach, VA, pp 175-180, Sept 1988

Warnick, J.S., T.Davis, C.Salvaggio, J.R.Schott, "The Merging of Multi-Date-Multi-Sensor-Multi-Resolution Images for Enhanced Image Analysis," *Final Report #RIT/DIRS 88/89-51-127*, Digital Imaging and Remote Sensing Laboratory, Center for Imaging Science, Rochester Institute of Technology, Rochester, NY, 1989

Welsh, R., "Merging Landsat and SIR-A Image Data in Digital Formats," *Imaging Technology in Research and Development*, July 1984, pp 11-12

Welsh, R., "Cartographic Potential of SPOT Image Data," *Photogrammetric Engineering and Remote Sensing*, vol 51, no 8, pp 1085-1091, 1985

Welsh, R., M. Ehlers, "Merging Multi-Resolution SPOT HRV and Landsat TM Data," *Photogrammetric Engineering and Remote Sensing*, vol 53, pp 301-303, 1987

Woodcock, C.E., S.L. Ryherd, "Generation of Texture Images using Adaptive Windows," *Technical Papers - 1989 ASPRS/ACSM Annual Convention*, Baltimore, MD, Vol 2 - Image Data Processing, pp 11-22, Apr 89

Woodcock, C.E., A.H.Strahler, "The Factor of Scale in Remote Sensing," *Remote Sensing of Environment*, vol 21, pp 311-332, 1987

Appendix A

Classification Results for Original TM Data (30 m)

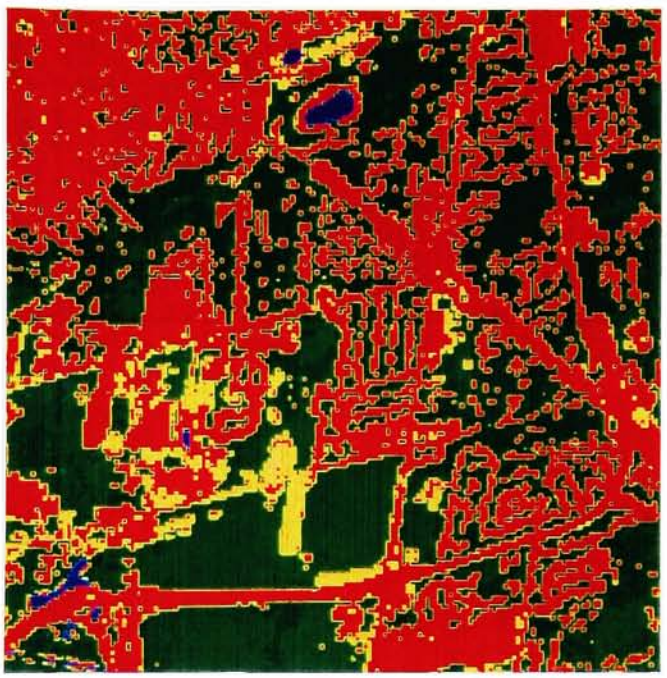

Figure A1. Classification Map for the Original TM Data Set.
Red represents urban; yellow - soil; blue - water;
dark green - trees; light green - grass.

Confusion Matrices on the Original TM Data Set:

Table A1. Using a Random Data Set (100 samples / class)

	urban	soil	water	trees	grass
urban	76.0%	0.0%	0.0%	18.0%	6.0%
soil	28.0%	35.0%	0.0%	10.0%	27.0%
water	0.0%	0.0%	100.0%	0.0%	0.0%
trees	15.0%	0.0%	0.0%	68.0%	17.0%
grass	1.0%	0.0%	0.0%	7.0%	92.0%

overall classification accuracy: 74.2%

Table A2. Using Independent Data Set 1

	urban	soil	water	trees	grass
urban	92.5%	6.6%	0.0%	0.9%	0.0%
soil	0.0%	100.0%	0.0%	0.0%	0.0%
water	0.0%	0.0%	62.3%	37.3%	0.0%
trees	0.5%	0.0%	0.0%	61.9%	37.6%
grass	0.9%	0.0%	0.0%	0.0%	99.1%

overall classification accuracy: 83.2%

Table A3. Using Independent Data Set 2 (50 samples/class)

	urban	soil	water	trees	grass
urban	50.0%	6.0%	0.0%	44.0%	0.0%
soil	0.0%	100.0%	0.0%	0.0%	0.0%
water	18.0%	0.0%	60.0%	22.0%	0.0%
trees	24.0%	0.0%	0.0%	70.0%	6.0%
grass	16.0%	6.0%	0.0%	0.0%	78.0%

overall classification accuracy: 71.6%

Appendix B

Classification Results for Hybrid Data (30 m) using Blurred TM Data (90 m) and Blurred SPOT Data (30 m)

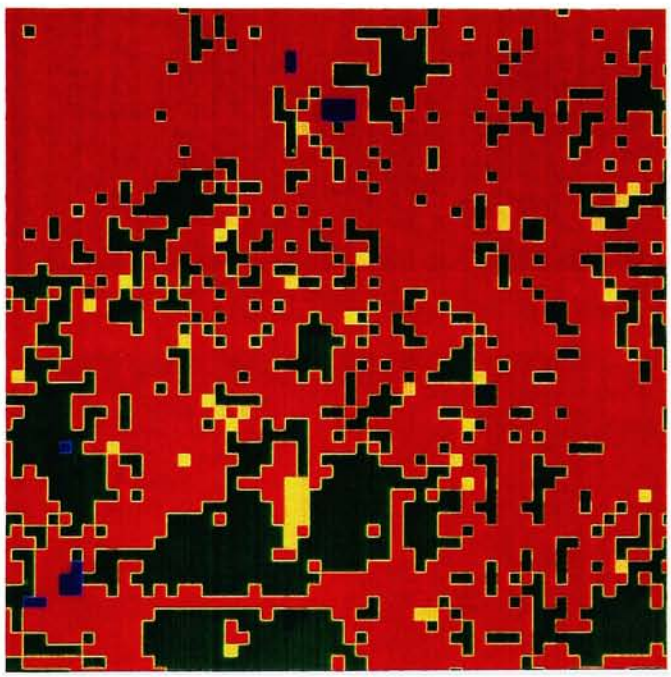

Figure B1. Classification Map for Blurred TM (90 m)
Red represents urban; yellow - soil; blue - water;
dark green - trees; light green - grass.

Confusion Matrices on the Blurred TM Data Set (90 m):

Table B1a. Using Random (50 samples/class)

	urban	soil	water	trees	grass
urban	62.0%	2.0%	4.0%	26.0%	6.0%
soil	22.0%	22.0%	0.0%	32.0%	24.0%
water	0.0%	0.0%	82.0%	0.0%	18.0%
trees	28.0%	2.0%	0.0%	54.0%	16.0%
grass	10.0%	0.0%	0.0%	18.0%	72.0%

overall classification accuracy: 58.4%

Table B1b. Using Independent Data Set 1

	urban	soil	water	trees	grass
urban	73.6%	0.0%	0.0%	5.7%	20.8%
soil	100.0%	0.0%	0.0%	0.0%	0.0%
water	69.8%	0.0%	30.2%	0.0%	0.0%
trees	24.8%	0.0%	0.0%	37.6%	37.6%
grass	9.1%	0.0%	0.0%	0.0%	90.9%

overall classification accuracy: 46.5%

Classification Results for the Original DIRS Method (30m hybrid)

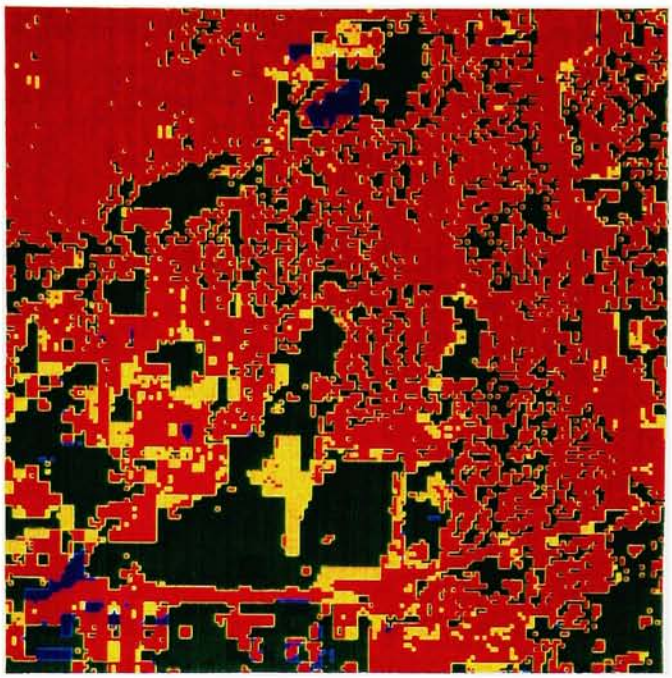

Figure B2. Classification Map for the Original DIRS Method (30 m hybrid). Red represents urban; yellow - soil; blue - water; dark green - trees; light green - grass.

Table B2. Confusion Matrix for the original DIRS Method (30 m hybrid) using Independent Data Set 1

	urban	soil	water	trees	grass
urban	63.2%	34.0%	0.0%	0.9%	1.9%
soil	0.0%	100.0%	0.0%	0.0%	0.0%
water	0.0%	0.0%	88.7%	0.0%	11.3%
trees	15.3%	0.0%	0.3%	14.9%	66.8%
grass	5.5%	0.3%	0.0%	0.0%	94.2%

overall classification accuracy: 72.2%

Classification Results for the DIRS Method using new Weighting for Synthetic Panchromatic Image (30m hybrid)

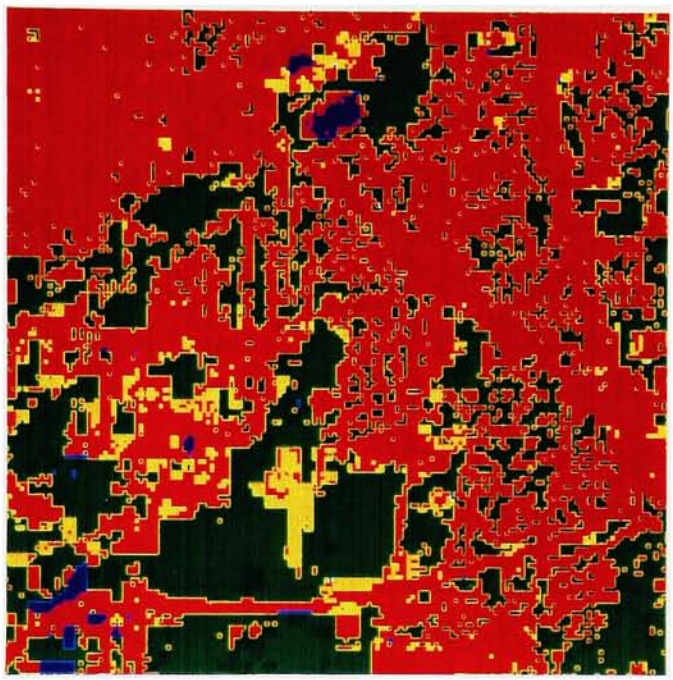

Figure B3. Classification Map for the DIRS Method with New Weighting for Synthetic Pan Image(30 m hybrid). Red represents urban; yellow - soil; blue - water; dark green - trees; light green - grass.

Table B3. Confusion Matrix for DIRS Method with New Weighting for Synthetic Pan Image (30 m hybrid) using Independent Data Set 1

	urban	soil	water	trees	grass
urban	96.2%	1.9%	0.0%	0.0%	1.9%
soil	3.3%	96.7%	0.0%	0.0%	0.0%
water	0.0%	0.0%	100.0%	0.0%	0.0%
trees	2.0%	0.0%	0.0%	27.2%	70.8%
grass	6.4%	0.0%	0.0%	0.0%	93.6%

overall classification accuracy: 82.7%

Classification Results for the DIRS Method with Interpolated TM Input (30m hybrid)

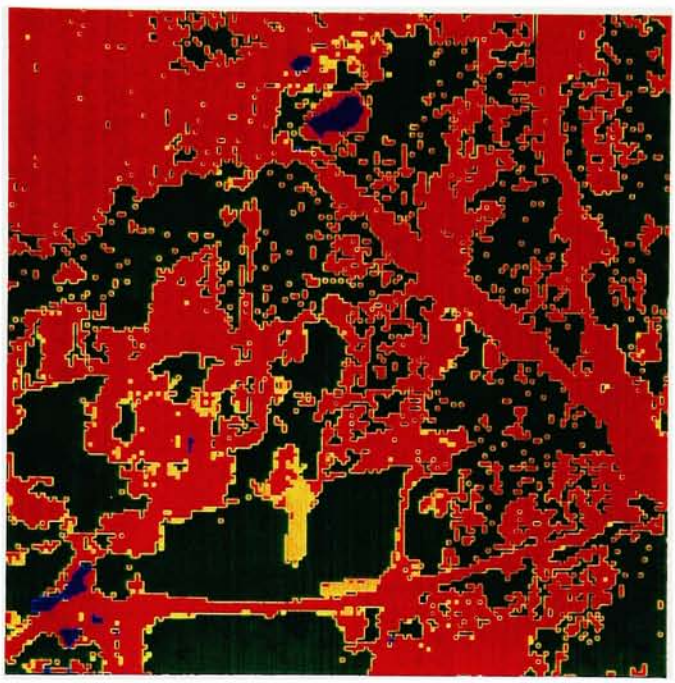

Figure B4. Classification Map for the DIRS Method with Interpolated Input (30 m hybrid)
Red represents urban; yellow - soil; blue - water; dark green - trees; light green - grass.

Table B4. Confusion Matrix for the DIRS Method with Interpolated Input (30 m hybrid) using Independent Data Set 1

	urban	soil	water	trees	grass
urban	95.2%	7.5%	0.0%	0.0%	0.0%
soil	0.0%	100.0%	0.0%	0.0%	0.0%
water	0.0%	0.0%	100.0%	0.0%	0.0%
trees	3.5%	3.5%	0.0%	51.0%	42.1%
grass	0.9%	0.0%	0.0%	0.0%	99.1%

overall classification accuracy: 88.5%

Classification Results for the DIRS Method with Interpolated TM Input and Post-fixing (30m hybrid)

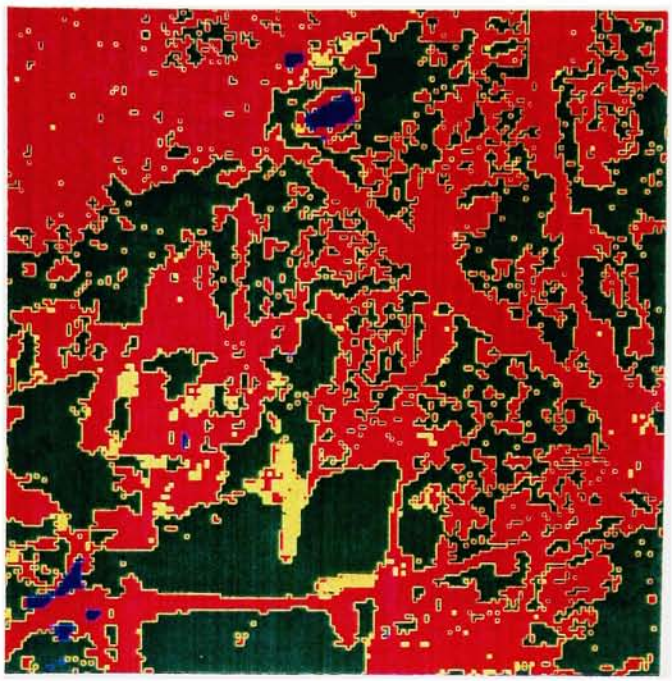

Figure B5. Classification Map for the DIRS Method with Interpolated Input and Post-fixing (30 m hybrid) Red represents urban; yellow - soil; blue - water; dark green - trees; light green - grass.

Table B5. Confusion Matrix for the DIRS Method with Interpolated Input and Post-fixing (30 m hybrid) using Independent Data Set 1

	urban	soil	water	trees	grass
urban	96.2%	0.9%	0.0%	0.9%	1.9%
soil	0.0%	100.0%	0.0%	0.0%	0.0%
water	0.0%	0.0%	88.7%	0.0%	11.3%
trees	4.0%	0.0%	0.0%	22.3%	73.8%
grass	0.3%	0.0%	0.0%	0.0%	99.7%

overall classification accuracy: 81.4%

Classification Results for the DIRS Enhancement 1 Method

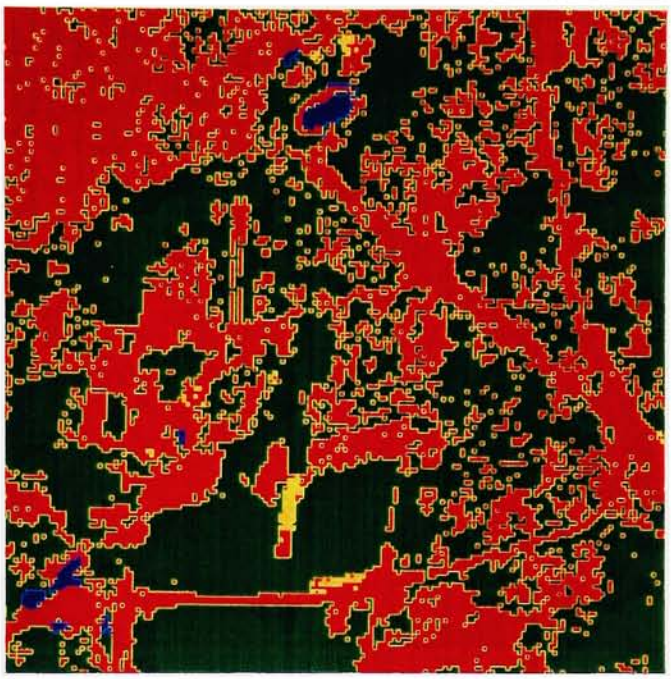

Figure B6. Classification Map for DIRS Enhancement 1 (30 m hybrid)
Red represents urban; yellow - soil; blue - water;
dark green - trees; light green - grass.

Table B6. Confusion Matrix for DIRS Enhancement 1 (30 m hybrid) using Independent Data Set 1

	urban	soil	water	trees	grass
urban	76.4%	0.0%	0.0%	1.9%	21.7%
soil	14.8%	85.2%	0.0%	0.0%	0.0%
water	1.9%	0.0%	90.6%	0.0%	7.5%
trees	1.5%	0.0%	0.0%	9.9%	88.6%
grass	2.1%	0.0%	0.0%	0.0%	97.9%

overall classification accuracy: 72.0%

Classification Results for the DIRS Enhancement 1 Method with Post-fixing (30m hybrid)

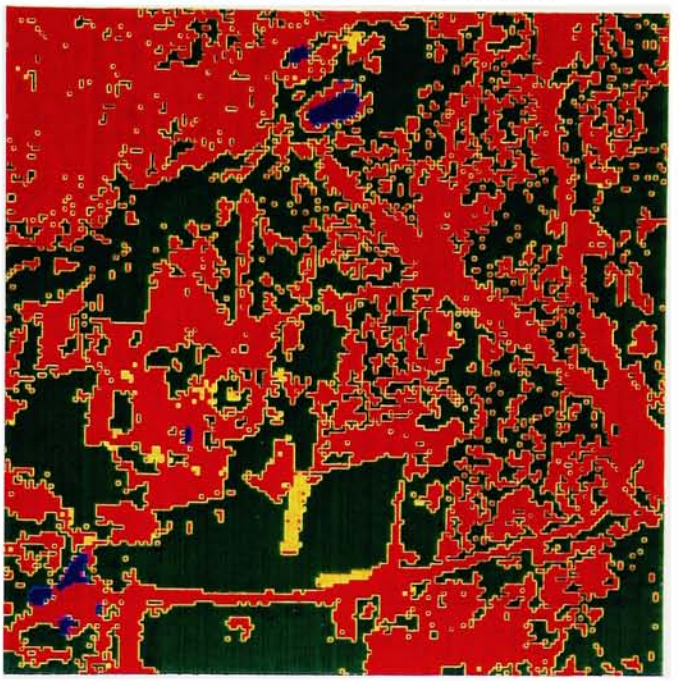

Figure B7. Confusion Matrix for DIRS Enhancement 1 with Post-fixing (30 m hybrid)
Red represents urban; yellow - soil; blue - water; dark green - trees; light green - grass.

Table B7. Confusion Matrix for DIRS Enhancement 1 with Post-fixing (30 m hybrid) using Independent Data Set 1

	urban	soil	water	trees	grass
urban	96.2%	0.0%	0.0%	0.0%	3.8%
soil	6.6%	93.4%	0.0%	0.0%	0.0%
water	1.9%	0.0%	98.1%	0.0%	0.0%
trees	0.5%	0.0%	0.0%	19.3%	80.2%
grass	0.3%	0.0%	0.0%	0.0%	99.7%

overall classification accuracy: 81.3%

Classification Results for the DIRS Enhancement 2 Method (30m hybrid)

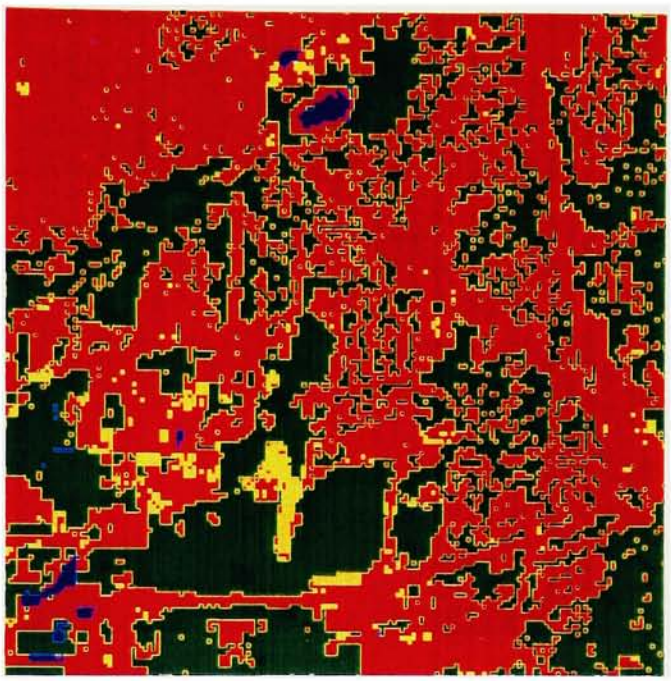

Figure B8. Classification Map for DIRS Enhancement 2 (30 m hybrid)
Red represents urban; yellow - soil; blue - water;
dark green - trees; light green - grass.

Table B8. Confusion Matrix for DIRS Enhancement 2 (30 m hybrid)
using Independent Data Set 1

	urban	soil	water	trees	grass
urban	98.1%	0.0%	0.0%	0.0%	1.9%
soil	4.9%	95.1%	0.0%	0.0%	0.0%
water	11.3%	0.0%	77.3%	0.0%	11.3%
trees	8.9%	0.0%	0.0%	29.7%	61.4%
grass	6.4%	0.0%	0.0%	0.0%	93.6%

overall classification accuracy: 78.8%

Classification Results for the DIRS Enhancement 2 Method with Adjustment for TM4 and TM5 (30m hybrid)

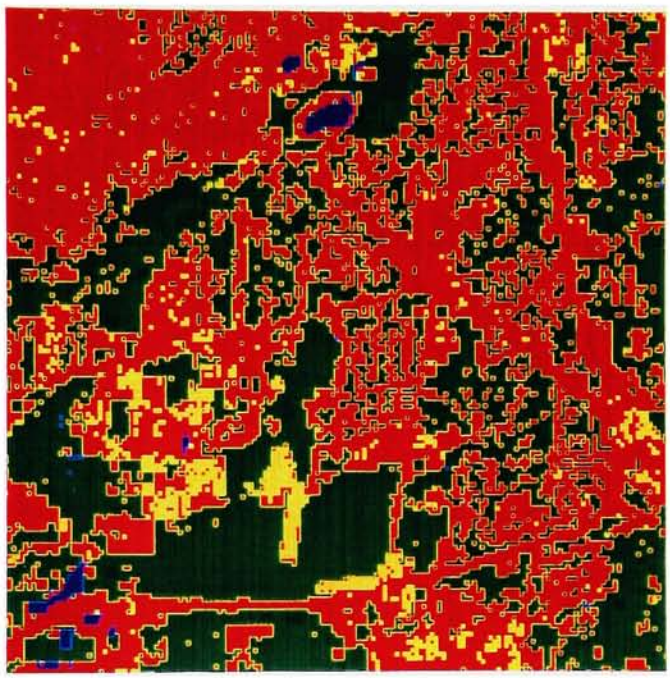

Figure B9. Classification Map for DIRS Enhancement 2 with adjustment for TM4 and TM5 (30 m hybrid) Red represents urban; yellow - soil; blue - water; dark green - trees; light green - grass.

Table B9. Confusion Matrix for DIRS Enhancement 2 with adjustment for TM4 and TM5 (30 m hybrid) using Independent Data Set 1

	urban	soil	water	trees	grass
urban	90.6%	6.6%	0.0%	0.9%	1.9%
soil	3.3%	96.7%	0.0%	0.0%	0.0%
water	11.3%	0.0%	88.7%	0.0%	0.0%
trees	0.5%	0.0%	0.0%	39.6%	59.9%
grass	0.6%	0.0%	0.0%	0.0%	99.4%

overall classification accuracy: 83.0%

Classification Results for Price's Method

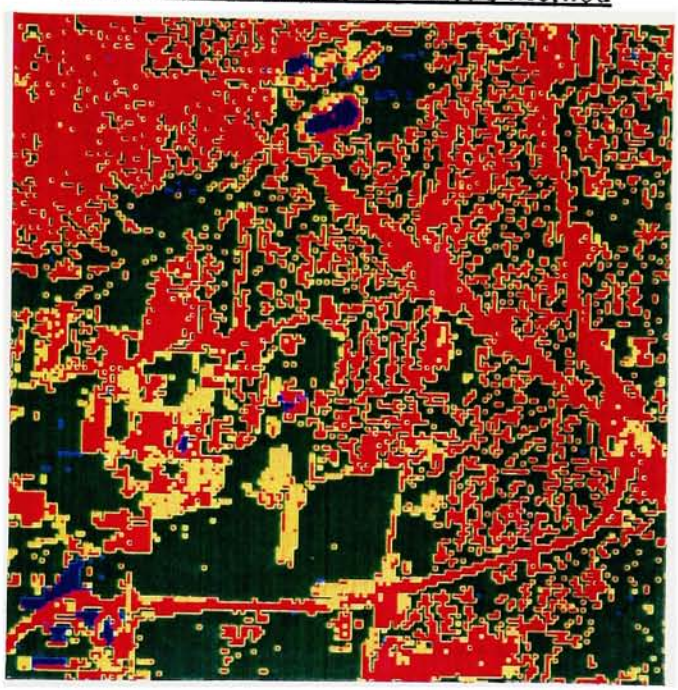

Figure B10. Classification Map for Prices Method
Red represents urban; yellow - soil; blue - water;
dark green - trees; light green - grass.

Table B10. Confusion Matrix for Prices Method using Independent Data Set 1

	urban	soil	water	trees	grass
urban	71.7%	19.8%	0.0%	0.0%	8.5%
soil	3.3%	96.7%	0.0%	0.0%	0.0%
water	0.0%	0.0%	98.1%	0.0%	1.9%
trees	4.5%	0.5%	0.0%	48.0%	47.0%
grass	0.0%	0.9%	0.0%	0.0%	99.1%

overall classification accuracy: 82.7%

Classification Results for Price's Method with Adaptive Weights Modification (30m hybrid)

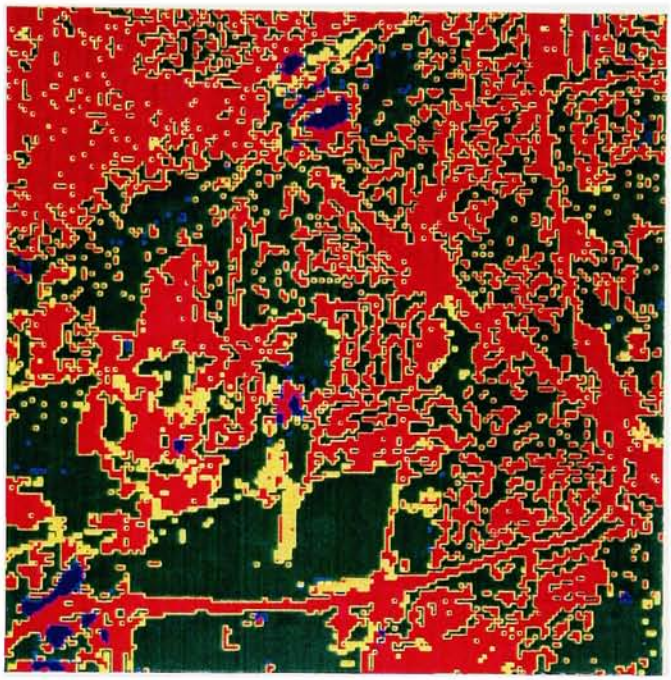

Figure B11. Classification Map for Prices Method with adaptive weights modification
Red represents urban; yellow - soil; blue - water; dark green - trees; light green - grass.

Table B11 -- Confusion Matrix for Prices Method with adaptive weights modification using Independent Data Set 1

	urban	soil	water	trees	grass
urban	76.4%	23.6%	0.0%	0.0%	0.0%
soil	6.6%	93.4%	0.0%	0.0%	0.0%
water	11.3%	0.0%	88.7%	0.0%	0.0%
trees	4.5%	0.5%	14.9%	29.2%	51.0%
grass	0.0%	0.9%	0.0%	0.0%	99.1%

overall classification accuracy: 77.4%

Appendix C

Radiometric Results for the Hybrid Data (30m) using Blurred TM Data (90m) and Blurred SPOT Data (30m)

Table C1. Error Table for blurred TM (90 m)

	error (DC)	error (reflectance)
TM1	7.78	1.09
TM2	4.31	1.63
TM3	7.08	1.58
TM4	11.71	5.12
TM5	8.97	-
TM7	5.95	-

Table C2. Error Table for original DIRS Method (30 m hybrid)

	error (DC)	error (reflectance)
TM1 Estimate	7.81	1.09
TM2 Estimate	3.56	1.34
TM3 Estimate	5.39	1.21
TM4 Estimate	16.21	7.09
TM5 Estimate	9.73	-
TM7 Estimate	5.10	-

Table C3. Error Table for DIRS Method using the new weighting for the Synthetic Pan Image

	error (DC)	error (reflectance)
TM1 Estimate	9.02	1.26
TM2 Estimate	3.78	1.43
TM3 Estimate	5.42	1.21
TM4 Estimate	17.40	7.62
TM5 Estimate	10.45	-
TM7 Estimate	5.16	-

Table C4. Error Table for the DIRS Method with Interpolated Input (30 m hybrid)

	error (DC)	error (reflectance)
TM1 Estimate	8.84	1.23
TM2 Estimate	3.88	1.46
TM3 Estimate	5.53	1.24
TM4 Estimate	16.93	7.41
TM5 Estimate	10.37	-
TM7 Estimate	5.28	-

Table C5. Error Table for the DIRS Method with Interpolated Input and Post-fixing (30 m hybrid)

	error (DC)	error (reflectance)
TM1 Estimate	7.21	1.01
TM2 Estimate	2.98	1.12
TM3 Estimate	4.39	0.98
TM4 Estimate	15.41	6.75
TM5 Estimate	8.79	-
TM7 Estimate	4.31	-

Table C6. Error Table for DIRS Enhancement 1 (30 m hybrid)

	error (DC)	error (reflectance)
TM1 Estimate	8.29	1.16
TM2 Estimate	3.58	1.35
TM3 Estimate	5.36	1.20
TM4 Estimate	16.80	7.35
TM5 Estimate	10.46	-
TM7 Estimate	5.25	-

Table C7. Error Table for DIRS Enhancement 1 with Post-fixing (30 m hybrid)

	error (DC)	error (reflectance)
TM1 Estimate	6.82	0.95
TM2 Estimate	2.89	1.09
TM3 Estimate	4.44	0.99
TM4 Estimate	15.09	6.60
TM5 Estimate	9.04	-
TM7 Estimate	5.19	-

Table C8. Error Table for DIRS Enhancement 2 (30 m hybrid)

	error (DC)	error (reflectance)
TM1 Estimate	6.98	0.97
TM2 Estimate	2.94	1.11
TM3 Estimate	4.67	1.04
TM4 Estimate	16.31	7.14
TM5 Estimate	9.11	-
TM7 Estimate	4.64	-

Table C9. Error Table for DIRS Enhancement 2 with adjustment for TM4 and TM5 (30 m hybrid)

	error (DC)	error (reflectance)
TM1 Estimate	6.98	0.97
TM2 Estimate	2.93	1.11
TM3 Estimate	4.67	1.04
TM4 Estimate	15.07	6.60
TM5 Estimate	9.32	-
TM7 Estimate	4.64	-

Table C10. Error Table for Price Method (30 m hybrid)

	error (DC)	error (reflectance)
TM1 Estimate	5.82	0.81
TM2 Estimate	3.11	1.18
TM3 Estimate	6.00	1.34
TM4 Estimate	12.64	5.53
TM5 Estimate	8.61	-
TM7 Estimate	6.88	-

Table C11. Error Table for Price Method with Adaptive Weights Modification (30 m hybrid)

	error (DC)	error (reflectance)
TM1 Estimate	5.82	0.81
TM2 Estimate	3.11	1.18
TM3 Estimate	6.00	1.34
TM4 Estimate	11.11	4.86
TM5 Estimate	7.80	-
TM7 Estimate	4.59	-

Appendix D

Classification Results for Hybrid Data (30 m) using Blurred TM Data (90 m) and Re-registered Blurred SPOT Data (30 m)

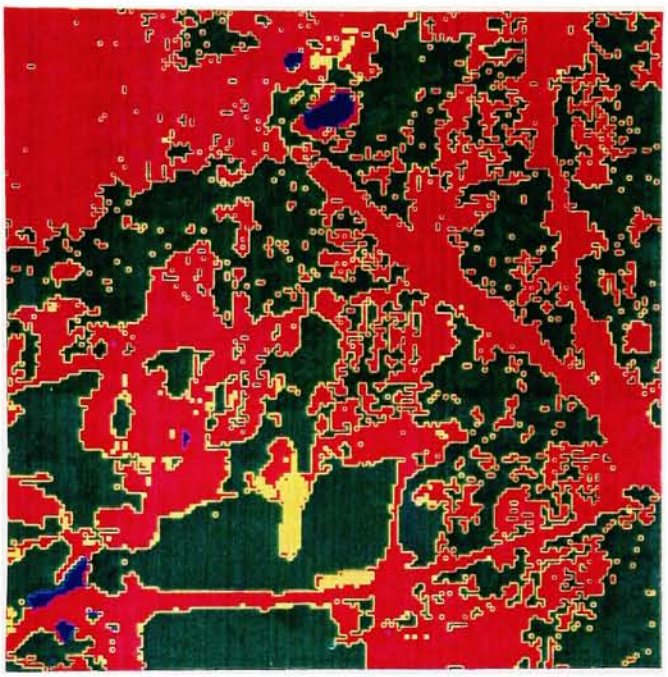

Figure D1. Classification Map for the DIRS Method with Interpolated Input
Red represents urban; yellow -- soil; blue -- water;
dark green -- trees; light green -- grass.

Table D1a. Confusion Matrix using Independent Data Set 1 for the DIRS Method with Interpolated Input and Re-registered SPOT image

	urban	soil	water	trees	grass
urban	95.3%	0.0%	0.0%	2.8%	1.9%
soil	0.0%	100.0%	0.0%	0.0%	0.0%
water	0.0%	0.0%	100.0%	0.0%	0.0%
trees	3.5%	2.5%	0.0%	44.1%	50.0%
grass	2.1%	0.0%	0.0%	0.0%	97.9%

overall classification accuracy: 87.5%

Table D1b. Confusion Matrix using a Random Data Set for the DIRS Method with Interpolated Input and Re-registered SPOT image (50 samples/class)

	urban	soil	water	trees	grass
urban	64.0%	2.0%	0.0%	22.0%	12.0%
soil	10.0%	48.0%	0.0%	16.0%	26.0%
water	0.0%	0.0%	100.0%	0.0%	0.0%
trees	18.0%	0.0%	0.0%	74.0%	8.0%
grass	2.0%	0.0%	0.0%	46.0%	52.0%

overall classification accuracy: 67.6%

Classification Results for the DIRS Method with Interpolated Input, Post-fixing, and a Re-registered SPOT image

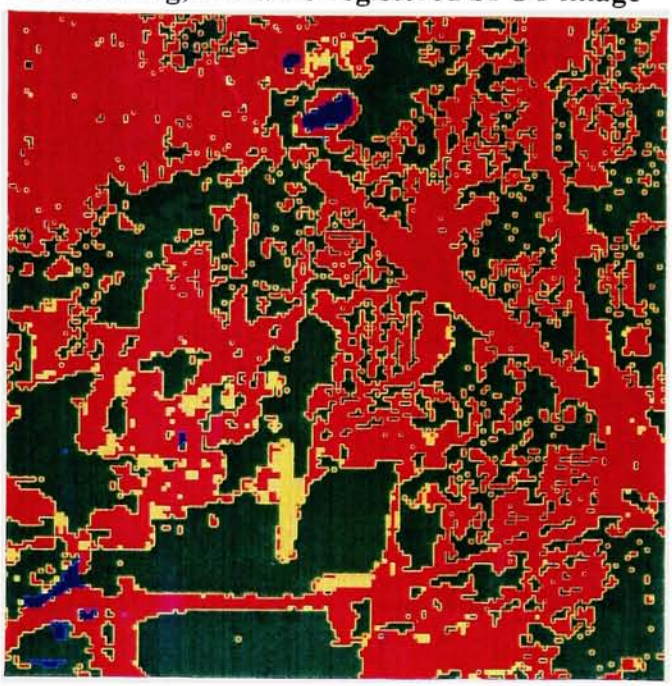

Table D2a. Confusion Matrix using Independent Data Set 1

	urban	soil	water	trees	grass
urban	89.6%	4.7%	0.0%	0.9%	4.7%
soil	0.0%	100.0%	0.0%	0.0%	0.0%
water	0.0%	0.0%	88.7%	0.0%	11.3%
trees	4.0%	0.0%	0.0%	19.3%	76.7%
grass	0.3%	0.0%	0.0%	0.0%	99.7%

overall classification accuracy: 79.5%

Table D2b. Confusion Matrix using a Random Data Set (50 samples/class)

	urban	soil	water	trees	grass
urban	62.0%	0.0%	2.0%	32.0%	4.0%
soil	24.0%	38.0%	0.0%	14.0%	24.0%
water	0.0%	0.0%	100.0%	0.0%	0.0%
trees	14.0%	0.0%	0.0%	82.0%	4.0%
grass	2.0%	0.0%	0.0%	40.0%	58.0%

overall classification accuracy: 68.0%

Classification Results for the DIRS Enhancement 1 Method with Post-fixing and a Re-registered SPOT image

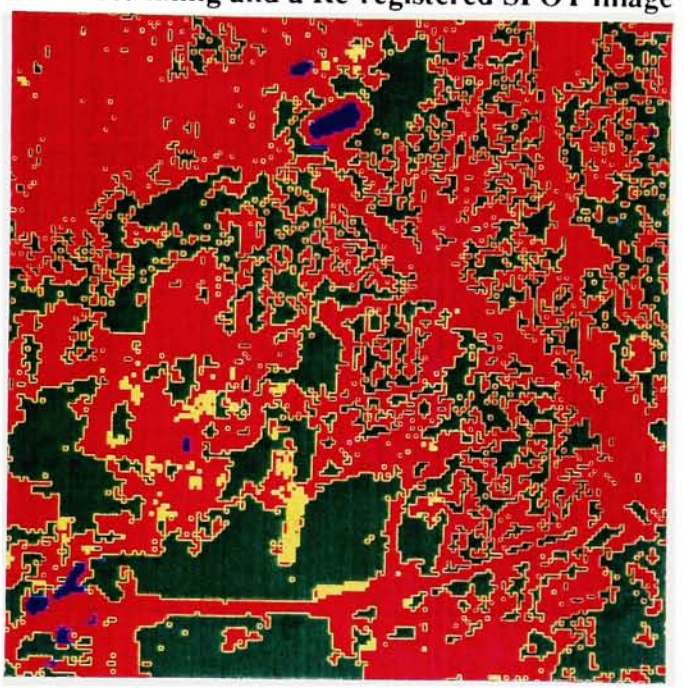

Table D3a. Confusion Matrix using Independent Data Set 1

	urban	soil	water	trees	grass
urban	97.2%	0.0%	0.0%	0.0%	2.8%
soil	11.5%	88.5%	0.0%	0.0%	0.0%
water	0.0%	0.0%	100.0%	0.0%	0.0%
trees	15.8%	0.0%	0.0%	43.6%	40.6%
grass	4.2%	0.0%	0.0%	0.0%	95.8%

overall classification accuracy: 85.0%

Table D3b. Confusion Matrix using a Random Data Set (50 samples/class)

	urban	soil	water	trees	grass
urban	62.0%	0.0%	2.0%	32.0%	4.0%
soil	38.0%	34.0%	2.0%	6.0%	20.0%
water	0.0%	0.0%	92.0%	8.0%	0.0%
trees	22.0%	0.0%	0.0%	66.0%	12.0%
grass	4.0%	0.0%	0.0%	26.0%	70.0%

overall classification accuracy: 64.8%

Classification Results for the DIRS Enhancement 2 Method with TM4, TM5 Modification and Re-registered SPOT image

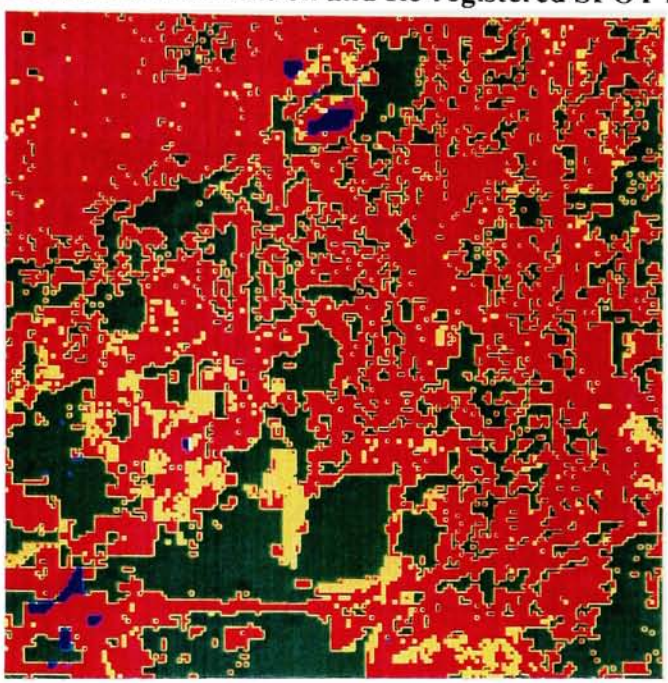

Table D4a. Confusion Matrix using Independent Data Set 1

	urban	soil	water	trees	grass
urban	83.0%	15.1%	0.0%	0.0%	1.9%
soil	4.9%	95.1%	0.0%	0.0%	0.0%
water	22.6%	0.0%	77.4%	0.0%	0.0%
trees	0.5%	0.0%	4.5%	45.0%	50.0%
grass	6.1%	0.0%	0.0%	0.0%	93.9%

overall classification accuracy: 78.9%

Table D4b. Confusion Matrix using a Random Data Set (50 samples/class)

	urban	soil	water	trees	grass
urban	64.0%	0.0%	0.0%	34.0%	2.0%
soil	68.0%	10.0%	0.0%	8.0%	14.0%
water	0.0%	0.0%	96.0%	0.0%	4.0%
trees	6.0%	0.0%	0.0%	86.0%	8.0%
grass	0.0%	0.0%	0.0%	40.0%	60.0%

overall classification accuracy: 63.2%

Classification Results for the Price Method and a Re-registered SPOT image

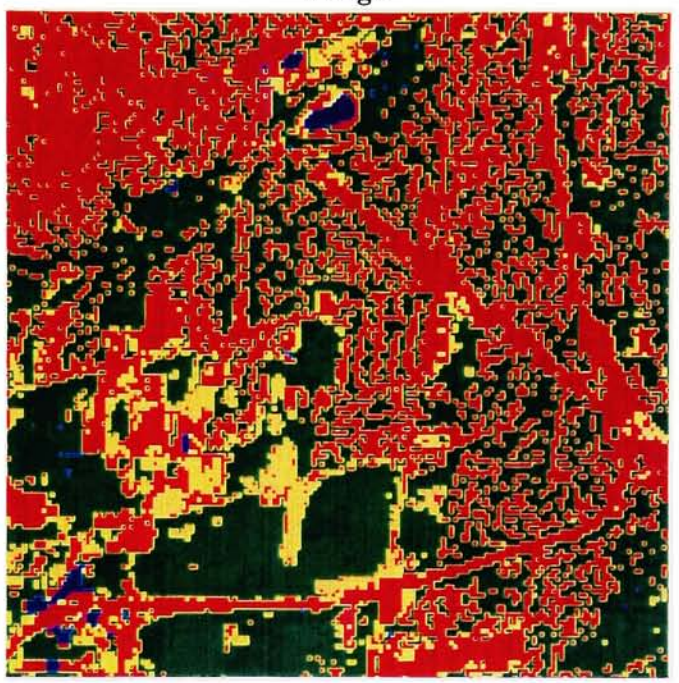

Table D5a. Confusion Matrix using Independent Data Set 1

	urban	soil	water	trees	grass
urban	56.6%	42.5%	0.0%	0.9%	0.0%
soil	3.3%	96.7%	0.0%	0.0%	0.0%
water	0.0%	0.0%	92.5%	0.0%	7.5%
trees	0.5%	4.5%	0.0%	75.2%	19.8%
grass	0.0%	0.9%	0.0%	1.8%	97.3%

overall classification accuracy: 83.7%

Table D5b. Confusion Matrix using a Random Data Set (50 samples/class)

	urban	soil	water	trees	grass
urban	72.0%	0.0%	0.0%	26.0%	2.0%
soil	48.0%	14.0%	0.0%	2.0%	36.0%
water	0.0%	0.0%	88.0%	10.0%	2.0%
trees	14.0%	0.0%	0.0%	70.0%	16.0%
grass	6.0%	0.0%	0.0%	18.0%	76.0%

overall classification accuracy: 64.0%

Classification Results for the Price Method with the Adaptive Weights Modification and a Re-registered SPOT image

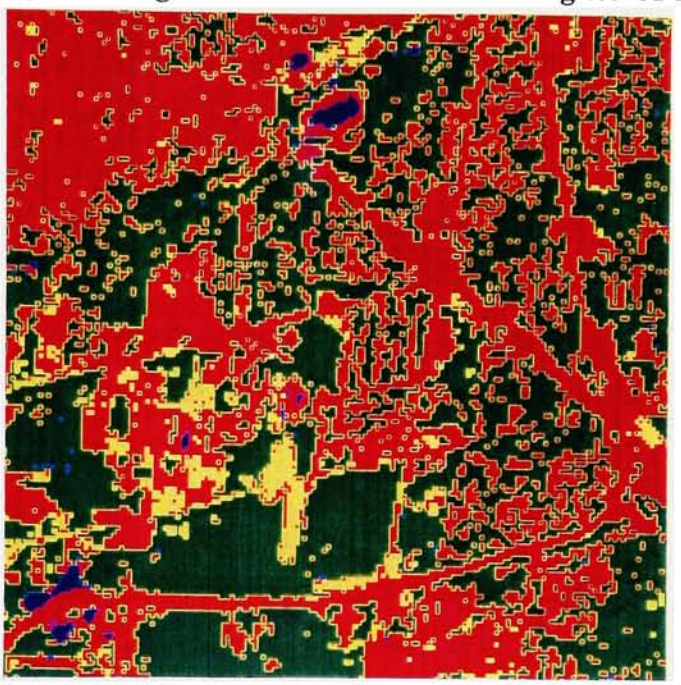

Table D6a. Confusion Matrix using Independent Data Set 1

	urban	soil	water	trees	grass
urban	80.2%	17.9%	0.0%	0.0%	1.9%
soil	1.6%	98.4%	0.0%	0.0%	0.0%
water	11.3%	0.0%	88.7%	0.0%	0.0%
trees	5.0%	0.0%	3.5%	28.2%	63.4%
grass	2.7%	2.1%	0.0%	0.0%	95.2%

overall classification accuracy: 78.1%

Table D6b. Confusion Matrix using a Random Data Set (100 samples/class)

	urban	soil	water	trees	grass
urban	66.0%	1.0%	0.0%	28.0%	5.0%
soil	46.0%	35.0%	0.0%	6.0%	13.0%
water	0.0%	0.0%	76.0%	16.0%	8.0%
trees	14.0%	0.0%	0.0%	83.0%	3.0%
grass	3.0%	0.0%	1.0%	38.0%	58.0%

overall classification accuracy: 63.6%

Appendix E

Radiometric Results for Hybrid Data (30 m) using Blurred TM Data (90 m) and Blurred, Re-registered SPOT Data (30 m)

Table E1 -- Error Table for the DIRS Method with Interpolated Input and Re-registered SPOT image

	error (DC)	error (reflectance)
TM1 Estimate	8.26	1.15
TM2 Estimate	3.65	1.38
TM3 Estimate	5.24	1.17
TM4 Estimate	16.73	7.32
TM5 Estimate	9.93	-
TM7 Estimate	4.98	-

Table E2 -- Error Table for the DIRS Method with Interpolated Input, Post-fixing, and a Re-registered SPOT image

	error (DC)	error (reflectance)
TM1 Estimate	6.51	0.91
TM2 Estimate	2.70	1.02
TM3 Estimate	4.09	0.92
TM4 Estimate	15.37	6.73
TM5 Estimate	8.37	-
TM7 Estimate	4.02	-

Table E3 -- Error Table for the DIRS Enhancement 1 Method with Post-fixing and a Re-registered SPOT image

	error (DC)	error (reflectance)
TM1 Estimate	6.14	0.86
TM2 Estimate	2.61	0.98
TM3 Estimate	4.11	0.92
TM4 Estimate	14.92	6.53
TM5 Estimate	8.71	-
TM7 Estimate	4.20	-

Table E4 -- Error Table for the DIRS Enhancement 2 Method with TM4, TM5 Modification and Re-registered SPOT image

	error (DC)	error (reflectance)
TM1 Estimate	6.26	0.87
TM2 Estimate	2.62	0.99
TM3 Estimate	4.29	0.96
TM4 Estimate	15.13	6.63
TM5 Estimate	9.14	-
TM7 Estimate	4.31	-

Table E5 -- Error Table for the Price Method and a Re-registered SPOT image

	error (DC)	error (reflectance)
TM1 Estimate	5.22	0.73
TM2 Estimate	2.78	1.05
TM3 Estimate	4.95	1.11
TM4 Estimate	12.24	5.36
TM5 Estimate	8.22	-
TM7 Estimate	5.04	-

Table E6 -- Error Table for the Price Method with the adaptive weights modification and a Re-registered SPOT image

	error (DC)	error (reflectance)
TM1 Estimate	5.22	0.73
TM2 Estimate	2.78	1.05
TM3 Estimate	4.95	1.11
TM4 Estimate	10.97	4.80
TM5 Estimate	7.83	-
TM7 Estimate	4.43	-

Appendix F

Classification Results for Hybrid Data (10 m) using TM Data (30 m) and Re-registered SPOT Data (10 m)

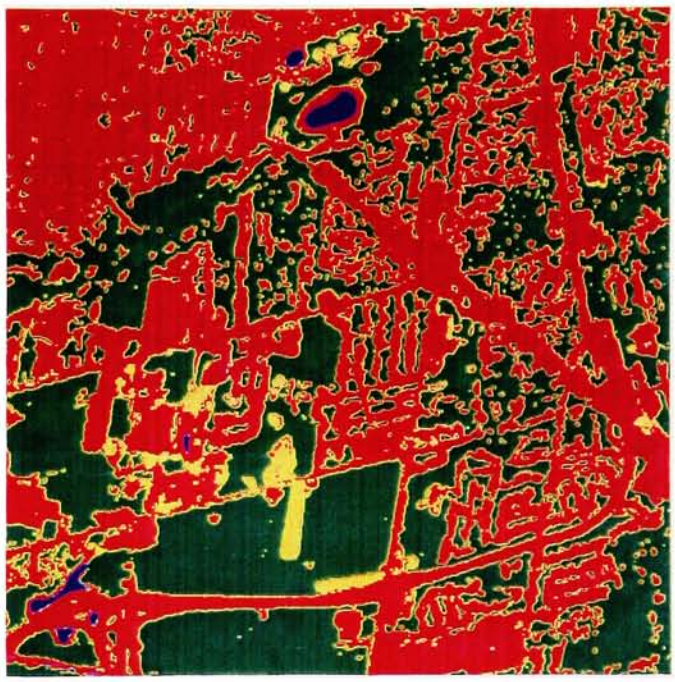

Figure F1. Classification Map for the DIRS Method with Interpolated Input
Red represents urban; yellow -- soil; blue -- water;
dark green -- trees; light green -- grass.

Table F1a. Confusion Matrix using a Random Set (100 samples/class)

	urban	soil	water	trees	grass
urban	72.0%	0.0%	0.0%	23.0%	5.0%
soil	26.0%	66.0%	0.0%	2.0%	6.0%
water	0.0%	0.0%	100.0%	0.0%	0.0%
trees	6.0%	0.0%	0.0%	89.0%	5.0%
grass	1.0%	0.0%	0.0%	22.0%	77.0%

overall classification accuracy: 80.8%

Table F1b. Confusion Matrix using Independent Data Set 1 for the DIRS Method with Interpolated Input and Re-registered SPOT image

	urban	soil	water	trees	grass
urban	98.1%	0.9%	0.0%	0.9%	0.0%
soil	0.0%	100.0%	0.0%	0.0%	0.0%
water	0.0%	0.0%	100.0%	0.0%	0.0%
trees	0.0%	0.0%	0.0%	81.2%	18.8%
grass	0.6%	0.0%	0.0%	0.0%	99.4%

overall classification accuracy: 95.7%

Table F1c. Confusion Matrix using Independent Data Set 2 for the DIRS Method with Interpolated Input and Re-registered SPOT image (50 samples/class)

	urban	soil	water	trees	grass
urban	82.0%	4.0%	0.0%	12.0%	2.0%
soil	0.0%	100.0%	0.0%	0.0%	0.0%
water	24.0%	0.0%	74.0%	2.0%	0.0%
trees	6.0%	0.0%	0.0%	94.0%	0.0%
grass	8.0%	0.0%	0.0%	0.0%	92.0%

overall classification accuracy: 88.4%

Classification Results for the DIRS Method with Interpolated Input, Post-fixing, and a Re-registered SPOT image

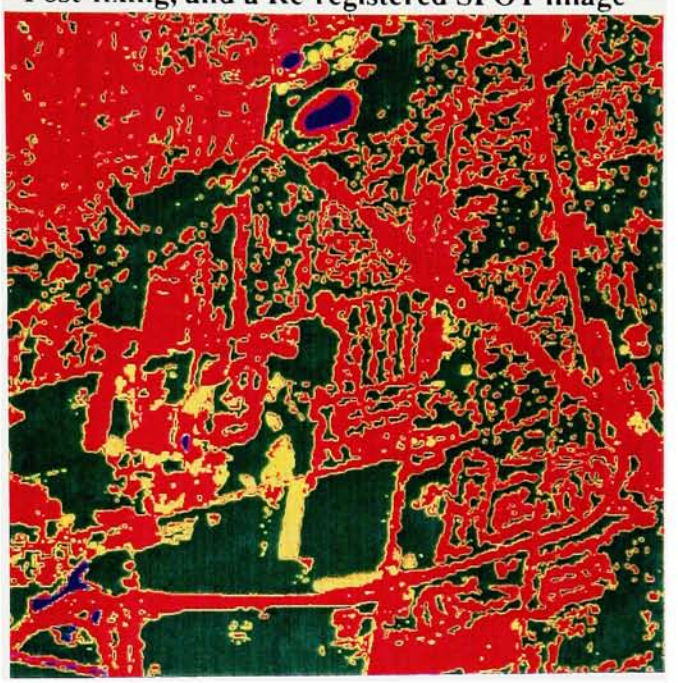

Figure F1. Classification Map for the DIRS Method with Interpolated Input, Post-fixing, and a Re-registered SPOT image
Red represents urban; yellow -- soil; blue -- water;
dark green -- trees; light green -- grass.

Table F2a. Confusion Matrix using a Random Set (100 samples/class)

	urban	soil	water	trees	grass
urban	71.0%	0.0%	2.0%	20.0%	7.0%
soil	33.0%	47.0%	0.0%	8.0%	12.0%
water	0.0%	0.0%	100.0%	0.0%	0.0%
trees	15.0%	0.0%	1.0%	62.0%	22.0%
grass	1.0%	0.0%	0.0%	11.0%	88.0%

overall classification accuracy: 73.6%

Table F2b. Confusion Matrix using Independent Data Set 1 for the DIRS Method with Interpolated Input, Post-fixing, and a Re-registered SPOT image

	urban	soil	water	trees	grass
urban	97.2%	1.9%	0.0%	0.9%	0.0%
soil	0.0%	100.0%	0.0%	0.0%	0.0%
water	0.0%	0.0%	62.3%	37.7%	0.0%
trees	0.0%	0.0%	0.0%	77.7%	22.3%
grass	0.9%	0.0%	0.0%	0.0%	99.1%

overall classification accuracy: 87.3%

Table F2c. Confusion Matrix using Independent Data Set 2 (50 samples/class) for the DIRS Method with Interpolated Input, Post-fixing, and a Re-registered SPOT image

	urban	soil	water	trees	grass
urban	76.0%	6.0%	0.0%	18.0%	0.0%
soil	2.0%	98.0%	0.0%	0.0%	0.0%
water	32.0%	0.0%	62.0%	6.0%	0.0%
trees	20.0%	0.0%	0.0%	78.0%	2.0%
grass	12.0%	0.0%	0.0%	0.0%	88.0%

overall classification accuracy: 80.4%

Classification Results for the DIRS Enhancement 1 Method with Post-fixing and a Re-registered SPOT image

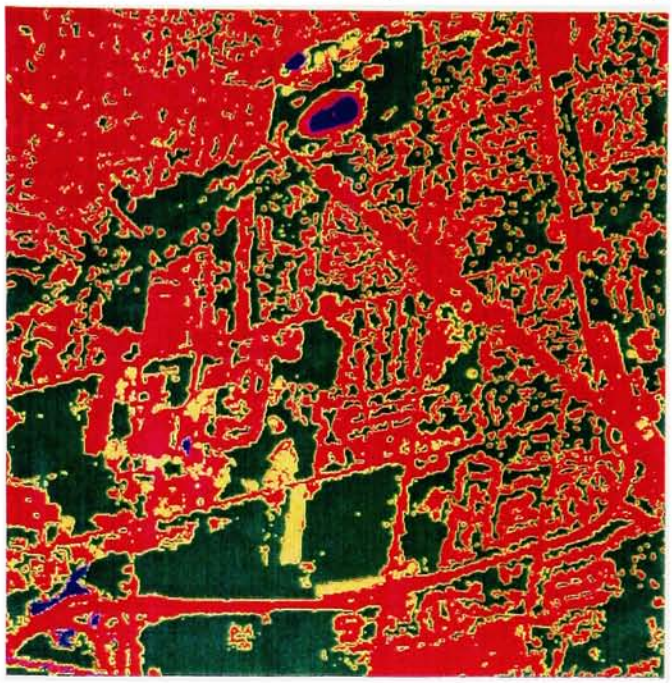

Figure F3. Classification Map for the DIRS Enhancement 1 Method with Post-fixing and a Re-registered SPOT image

Table F3a. Confusion Matrix using a Random Data Set (100 samples/class) for the DIRS Enhancement 1 Method with Post-fixing and a Re-registered SPOT image

	urban	soil	water	trees	grass
urban	74.0%	0.0%	0.0%	18.0%	8.0%
soil	29.0%	66.0%	0.0%	2.0%	3.0%
water	0.0%	0.0%	100.0%	0.0%	0.0%
trees	8.0%	0.0%	0.0%	82.0%	10.0%
grass	1.0%	1.0%	0.0%	16.0%	82.0%

overall classification accuracy: 80.8%

Table F3b. Confusion Matrix using Independent Data Set 1 for the DIRS Enhancement 1 Method with Post-fixing and a Re-registered SPOT image

	urban	soil	water	trees	grass
urban	99.1%	0.0%	0.0%	0.9%	0.0%
soil	0.0%	100.0%	0.0%	0.0%	0.0%
water	0.0%	0.0%	88.7%	11.3%	0.0%
trees	0.0%	0.0%	0.0%	76.7%	23.3%
grass	2.4%	0.0%	0.0%	0.0%	97.6%

overall classification accuracy: 92.4%

Table F3c. Confusion Matrix using Independent Data Set 2 for the DIRS Enhancement 1 Method with Post-fixing and a Re-registered SPOT image

	urban	soil	water	trees	grass
urban	86.0%	2.0%	0.0%	10.0%	2.0%
soil	0.0%	100.0%	0.0%	0.0%	0.0%
water	20.0%	0.0%	72.0%	8.0%	0.0%
trees	18.0%	0.0%	0.0%	80.0%	2.0%
grass	24.0%	0.0%	0.0%	0.0%	76.0%

overall classification accuracy: 82.8%

Classification Results for the DIRS Enhancement 2 Method with TM4, TM5 Modification and Re-registered SPOT image

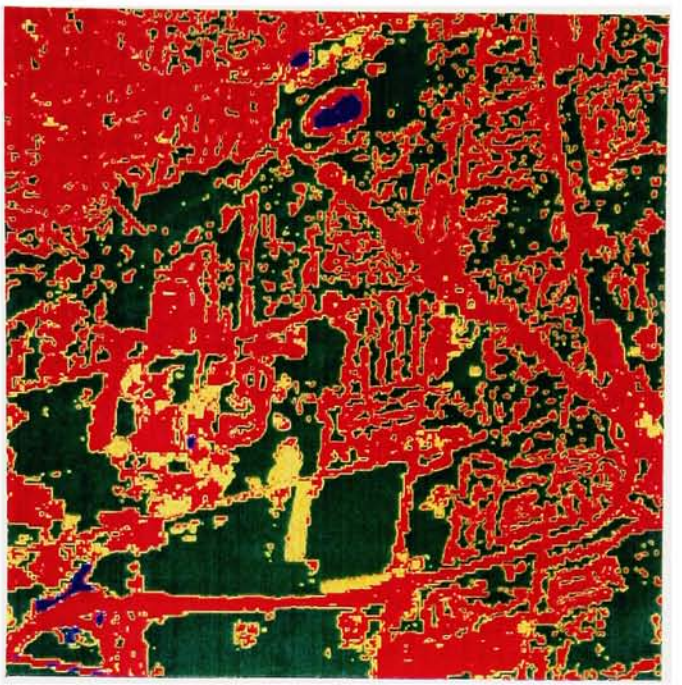

Figure F4. Classification Map for the DIRS Enhancement 2 Method with TM4, TM5 Modification and Re-registered SPOT image

Table F4a. Confusion Matrix using a Random Data Set (100 samples/class) for the DIRS Enhancement 2 Method with TM4, TM5 Modification and Re-registered SPOT image

	urban	soil	water	trees	grass
urban	64.0%	0.0%	0.0%	28.0%	8.0%
soil	47.0%	37.0%	1.0%	3.0%	12.0%
water	0.0%	0.0%	100.0%	0.0%	0.0%
trees	11.0%	0.0%	0.0%	81.0%	8.0%
grass	2.0%	0.0%	0.0%	17.0%	81.0%

overall classification accuracy: 72.6%

Table F4b. Confusion Matrix using Independent Data Set 1 for the DIRS Enhancement 2 Method with TM4, TM5 Modification and Re-registered SPOT image

	urban	soil	water	trees	grass
urban	97.2%	1.9%	0.0%	0.9%	0.0%
soil	0.0%	100.0%	0.0%	0.0%	0.0%
water	1.9%	0.0%	81.1%	17.0%	0.0%
trees	0.0%	0.0%	0.0%	76.2%	23.8%
grass	0.9%	0.0%	0.0%	0.0%	99.1%

overall classification accuracy: 90.7%

Table F4c. Confusion Matrix using Independent Data Set 2 for the DIRS Enhancement 2 Method with TM4, TM5 Modification and Re-registered SPOT image

	urban	soil	water	trees	grass
urban	76.0%	6.0%	0.0%	18.0%	0.0%
soil	4.0%	96.0%	0.0%	0.0%	0.0%
water	32.0%	0.0%	60.0%	6.0%	2.0%
trees	18.0%	0.0%	0.0%	80.0%	2.0%
grass	22.0%	2.0%	0.0%	2.0%	74.0%

overall classification accuracy: 77.2%

Classification Results for the Price Method and a Re-registered SPOT image

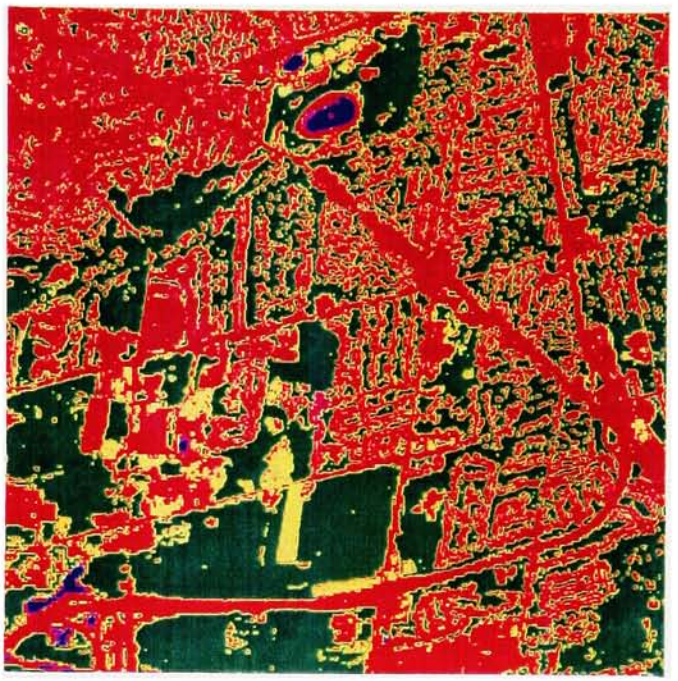

Figure F5. Classification Results for the Price Method and a Re-registered SPOT image

Table F5a. Confusion Matrix using a Random Data Set (100 samples/class) for the Price Method and a Re-registered SPOT image

	urban	soil	water	trees	grass
urban	76.0%	3.0%	1.0%	16.0%	4.0%
soil	26.0%	56.0%	0.0%	1.0%	17.0%
water	0.0%	0.0%	100.0%	0.0%	0.0%
trees	3.0%	0.0%	0.0%	77.0%	20.0%
grass	1.0%	0.0%	0.0%	10.0%	89.0%

overall classification accuracy: 79.6%

Table F5b. Confusion Matrix using Independent Data Set 1 for the Price Method and a Re-registered SPOT image

	urban	soil	water	trees	grass
urban	99.1%	0.0%	0.0%	0.9%	0.0%
soil	0.0%	100.0%	0.0%	0.0%	0.0%
water	9.4%	0.0%	88.7%	1.9%	0.0%
trees	0.0%	0.0%	0.0%	88.6%	11.4%
grass	0.9%	0.0%	0.0%	0.0%	99.1%

overall classification accuracy: 95.1%

Table F5c. Confusion Matrix using Independent Data Set 2 for the Price Method and a Re-registered SPOT image

	urban	soil	water	trees	grass
urban	94.0%	2.0%	0.0%	4.0%	0.0%
soil	2.0%	98.0%	0.0%	0.0%	0.0%
water	26.0%	0.0%	74.0%	0.0%	0.0%
trees	14.0%	0.0%	0.0%	80.0%	6.0%
grass	16.0%	2.0%	0.0%	0.0%	82.0%

overall classification accuracy: 85.6%

Classification Results for the Price Method with the Adaptive Weights Modification and a Re-registered SPOT image

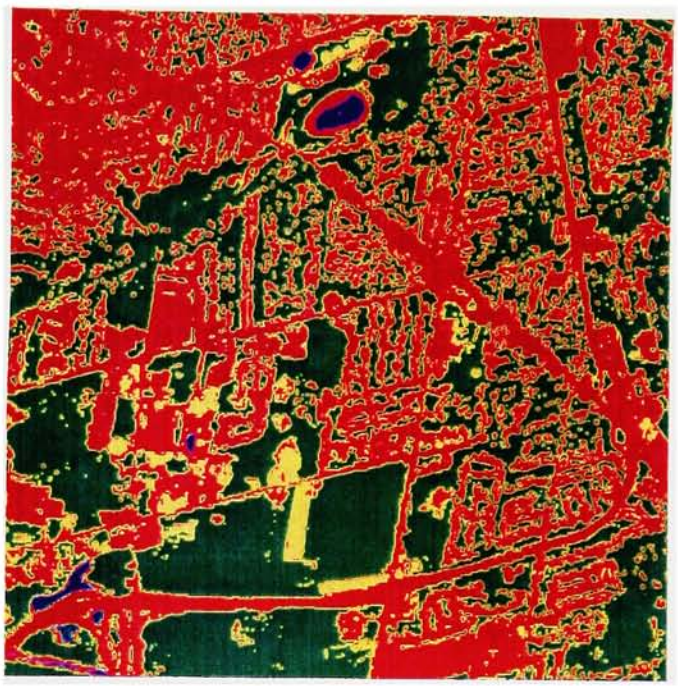

Figure F6. Classification Results for the Price Method with the Adaptive Weights Modification and a Re-registered SPOT image

Table F6a. Confusion Matrix using a Random Data Set (100 samples/class) for the Price Method with the Adaptive Weights Modification and a Re-registered SPOT image

	urban	soil	water	trees	grass
urban	71.0%	0.0%	0.0%	21.0%	8.0%
soil	25.0%	57.0%	0.0%	1.0%	17.0%
water	0.0%	0.0%	100.0%	0.0%	0.0%
trees	4.0%	0.0%	1.0%	88.0%	7.0%
grass	2.0%	1.0%	0.0%	8.0%	89.0%

overall classification accuracy: 81.0%

Table F6b. Confusion Matrix using Independent Data Set 1 for the Price Method with the Adaptive Weights Modification and a Re-registered SPOT image

	urban	soil	water	trees	grass
urban	99.1%	0.0%	0.0%	0.9%	0.0%
soil	0.0%	100.0%	0.0%	0.0%	0.0%
water	0.0%	0.0%	79.2%	20.8%	0.0%
trees	0.0%	0.0%	0.0%	71.8%	28.2%
grass	0.3%	0.9%	0.0%	0.0%	98.8%

overall classification accuracy: 89.8%

Table F6c. Confusion Matrix using Independent Data Set 2 for the Price Method with the Adaptive Weights Modification and a Re-registered SPOT image

	urban	soil	water	trees	grass
urban	90.0%	2.0%	0.0%	8.0%	0.0%
soil	0.0%	100.0%	0.0%	0.0%	0.0%
water	30.0%	0.0%	66.0%	4.0%	0.0%
trees	10.0%	0.0%	0.0%	86.0%	4.0%
grass	16.0%	2.0%	0.0%	0.0%	82.0%

overall classification accuracy: 84.8%

Appendix G

Statistical Tests

I. Determining if the Overall Classification Accuracies from Various Methods are Significantly Different

II. Determining the Threshold Value above which Classification Accuracies are Considered to be Significantly Different than the Input TM Classification Accuracy

I. Determining if the Overall Classification Accuracies from Various Methods are Significantly Different

This statistical test is a check whether the overall classification accuracies from each of the methods are significantly different from one another. It uses an r x c table analysis as presented by Freund [88]. An example is presented for the data in Table 4-8c reproduced below:

Table 4-8c
Summary of Classification Accuracy with
Random Data Set (Re-registered 30m hybrid)

	urban	soil	water	trees	grass	Overall ave
Original TM (30m)	76.0	35.0	100	68.0	92.0	74.2
Blurred TM (90m)	62.0	22.0	82.0	54.0	72.0	58.4
DIRS Method						
- Interpolated Input	64.0	48.0	100	74.0	52.0	67.6
- Interpolated and post-fixed	62.0	38.0	100	82.0	58.0	68.0
DIRS Enhancement 1						
- With post-fix	62.0	34.0	92.0	66.0	70.0	64.8
DIRS Enhancement 2						
- modified for TM4, 5	64.0	10.0	96.0	86.0	60.0	63.2
Price Method						
- LUT	72.0	14.0	88.0	70.0	76.0	64.0
- Adaptive Weights	66.0	35.0	76.0	83.0	58.0	63.6

The steps are as follows:

(A) Reformat the overall classification data into an r x c table format:

Let Method 1 = DIRS Method with Interpolated Input;

Method 2 = DIRS Method with Interpolated Input and Post-fixing;

Method 3 = DIRS Enhancement 1 with Post-fixing;

Method 4 = DIRS Enhancement 2 with TM4 TM5 modification;

Method 5 = Price Method with LUT;

Method 6 = Price Method with Adaptive Weights.

	METHODS					
	1	2	3	4	5	6
classified correctly	67.6	68.0	64.8	63.2	64.0	63.6
classified incorrectly	32.4	32.0	35.2	36.8	36.0	36.4

Since we know the Random data set has 500 total samples, and the Independent Data Set 2 has 250 total samples, the table can be converted from percentages to samples:

	METHODS					
	1	2	3	4	5	6
classified correctly	338	340	324	316	320	318
classified incorrectly	162	160	176	184	180	182

(B) Compute the expected frequency for each cell in the table. The expected frequency is calculated by multiplying the total of the row to which the cell belongs by the total of the column to which it belongs and then dividing by the grand total of the entire table. Since each column adds up to the same total of 500, the expected frequency is the same for every cell in a row. Therefore, the expected frequencies are:

$$e_{row1} = \frac{500 \cdot (1956)}{3000} = 326$$

$$e_{row2} = \frac{500 \cdot (1044)}{3000} = 174$$

(C) Conduct a hypothesis test at the 0.05 level of significance whether the differences among the sample proportions (classification accuracies) are significant.

1. $H_0 : p_1 = p_2 = ... = p_6$ (the sample proportions are the same)

   $H_A :$ $p_1 , p_2 , ..., p_6$ are not all equal

2. $\alpha = 0.05$

3. Reject the null hypothesis if $\chi^2 > 11.070$ where

$$\chi^2 = \sum \frac{(o - e)^2}{e}$$

and 11.070 is the value of $\chi^2_{0.05}$ for (2-1)(6-1) = 5 degrees of freedom; otherwise the differences among the sample proportions are not significant.

4. Since $e_{row1} = 326$, and $e_{row2} = 174$, we can substitute these values into the formula for χ^2 :

$$\chi^2 = \sum \frac{(o - e)^2}{e}$$

$$= \frac{(338 - 326)^2}{326} + \frac{(340 - 326)^2}{326} + \frac{(324 - 326)^2}{326} +$$

$$\frac{(316 - 326)^2}{326} + \frac{(320 - 326)^2}{326} + \frac{(318 - 326)^2}{326} +$$

$$\frac{(162 - 174)^2}{174} + \frac{(160 - 174)^2}{174} + \frac{(176 - 174)^2}{174} +$$

$$\frac{(184 - 174)^2}{174} + \frac{(180 - 174)^2}{174} + \frac{(182 - 174)^2}{174}$$

$$\chi^2 = 4.795$$

5. Since $\chi^2 = 4.795$ does not exceed 11.070, the null hypothesis cannot be rejected. The differences among the 6 classification accuracies are not significant.

II. Determining the Threshold Value above which Classification Accuracies are Considered to be Significantly Different than the Input TM Classification Accuracy.

This test determines if a merging method produces an overall classification accuracy that is statistically better than the classification accuracy obtained from the input (un-merged) TM data set. It calculates a threshold classification accuracy value using standard test statistics regarding the difference between two proportions [Freund 88]. If the classification accuracy obtained from a merging method is greater than this threshold value, then the classification accuracy is considered significantly different.

From Freund [88], the test statistic concerning the difference between two proportions is defined to be:

$$z = \frac{\frac{x_1}{n_1} - \frac{x_2}{n_2}}{\sqrt{\hat{p}\,(1 - \hat{p})\left(\frac{1}{n_1} + \frac{1}{n_2}\right)}} \qquad \text{with} \quad \hat{p} = \frac{x_1 + x_2}{n_1 + n_2} \qquad \text{(G-1)}$$

where: x_i is the number of successes in type i;

n_i is the number of trials in type i.

If we use Table 4-8c as an example again, then:

$$n_1 = n_2 = 500;$$

$$\frac{x_1}{n_1} = 0.584; \quad \text{and} \quad x_1 = 292.$$

If we test at the 0.05 level of significance, then $z_{0.05} = 1.645$.

Solving for x_2 now becomes an exercise in algebra, and x_2 divided by 500 is the classification accuracy threshold. Substituting these values into equation (G-1) we obtain:

$$1.645 = \frac{0.584 - \frac{x_2}{500}}{\sqrt{\left(\frac{292 + x_2}{1000}\right)\left(1 - \frac{292 + x_2}{1000}\right)\left(\frac{2}{500}\right)}}$$

$$\frac{1.645\ (500)}{1000} = \frac{292 - x_2}{\sqrt{(292 + x_2)\ (708 - x_2)\left(\frac{2}{500}\right)}}$$

$$(0.6765)\ (292 + x_2)\ (708 - x_2)\left(\frac{2}{500}\right) = (292 - x_2)^2$$

Multiplying and combining the terms we get:

$$x_2^2 - 583.5466\, x_2 + 84{,}475.9731 = 0$$

Solving with the quadratic equation, $x_2 = 266.17$ and 317.38;

converting to percentages they are: 53.2% and 63.5%.

and the threshold for significance is 63.5%

Appendix H
Input Parameters to Compute the Weighting Factors for a Synthetic Panchromatic Image

I. LOWTRAN 7 Input Parameters

II. Sensor Paramters
- TM1
- TM2
- TM3
- TM4
- SPOT Panchromatic

III. Computed Effective Radiance

IV. Computed Digital Counts

V. Reflectance Spectra

I. LOWTRAN Input Parameters

```
 7  2  2  1  0  0  0  0  0  0  1  1  1  0.000  1.00
IHAZE  1  0  0  0  0  0.000  0.000  0.000  0.000  0.218
33  0  0BUFFALO 6/15/87
 0.218  0.985E+03  0.211E+02  0.131E+02  0.000E+00  0.000E+00ABG
 0.256  0.981E+03  0.197E+02  0.113E+02  0.000E+00  0.000E+00ABG
 0.967  0.903E+03  0.180E+02  0.990E+01  0.000E+00  0.000E+00ABG
 1.072  0.892E+03  0.182E+02  0.500E+01  0.000E+00  0.000E+00ABG
 1.485  0.850E+03  0.176E+02  0.290E+01  0.000E+00  0.000E+00ABG
 2.001  0.800E+03  0.143E+02  0.500E+01  0.000E+00  0.000E+00ABG
 2.246  0.777E+03  0.126E+02  0.610E+01  0.000E+00  0.000E+00ABG
 2.880  0.720E+03  0.660E+01  0.490E+01  0.000E+00  0.000E+00ABG
 3.111  0.700E+03  0.500E+01  0.150E+01  0.000E+00  0.000E+00ABG
 3.300  0.684E+03  0.590E+01 -0.760E+01  0.000E+00  0.000E+00ABG
 3.409  0.675E+03  0.760E+01 -0.224E+02  0.000E+00  0.000E+00ABG
 3.949  0.632E+03  0.530E+01 -0.134E+02  0.000E+00  0.000E+00ABG
 4.185  0.614E+03  0.600E+01 -0.240E+02  0.000E+00  0.000E+00ABG
 4.374  0.600E+03  0.630E+01 -0.236E+02  0.000E+00  0.000E+00ABG
 5.081  0.550E+03  0.110E+01 -0.238E+02  0.000E+00  0.000E+00ABG
 5.839  0.500E+03 -0.450E+01 -0.241E+02  0.000E+00  0.000E+00ABG
 6.659  0.450E+03 -0.107E+02 -0.352E+02  0.000E+00  0.000E+00ABG
 7.552  0.400E+03 -0.178E+02 -0.478E+02  0.000E+00  0.000E+00ABG
 8.539  0.350E+03 -0.255E+02 -0.482E+02  0.000E+00  0.000E+00ABG
 9.634  0.300E+03 -0.344E+02 -0.488E+02  0.000E+00  0.000E+00ABG
10.880  0.250E+03 -0.452E+02 -0.584E+02  0.000E+00  0.000E+00ABG
12.331  0.200E+03 -0.572E+02 -0.704E+02  0.000E+00  0.000E+00ABG
13.168  0.175E+03 -0.593E+02 -0.725E+02  0.000E+00  0.000E+00ABG
14.602  0.139E+03 -0.640E+02 -0.772E+02  0.000E+00  0.000E+00ABG
15.258  0.125E+03 -0.619E+02 -0.751E+02  0.000E+00  0.000E+00ABG
15.933  0.112E+03 -0.650E+02 -0.782E+02  0.000E+00  0.000E+00ABG
16.632  0.100E+03 -0.621E+02 -0.753E+02  0.000E+00  0.000E+00ABG
18.834  0.700E+02 -0.627E+02 -0.759E+02  0.000E+00  0.000E+00ABG
20.949  0.500E+02 -0.544E+02 -0.676E+02  0.000E+00  0.000E+00ABG
22.380  0.400E+02 -0.542E+02 -0.674E+02  0.000E+00  0.000E+00ABG
24.244  0.300E+02 -0.492E+02 -0.624E+02  0.000E+00  0.000E+00ABG
26.939  0.200E+02 -0.434E+02 -0.566E+02  0.000E+00  0.000E+00ABG
```

```
 28.886  0.150E+02 -0.409E+02 -0.541E+02  0.000E+00  0.000E+00ABG
ALTITUDE    0.218  180.000    0.000    0.000    0.000  0
 1  2 166  0
 42.500   79.000    0.000    0.000   15.433    0.000    0.000    0.000
5000.000 40000.000  350.000
 1
```

Where: IHAZE = 1, (visibility of 23 km)
5, (visibility of 5 km)
6, (visibility of 50 km);

ALTITUDE = 705, (altitude in km for the Landsat TM sensor)
832, (altitude in km for the SPOT HRV sensor).

II. Sensor Parameters

Spectral Response for TM band 1

λ (microns)	β(λ)
0.410	0.0000
0.420	0.0007
0.430	0.0027
0.440	0.0370
0.450	0.3391
0.460	0.7200
0.470	0.8206
0.480	0.9026
0.490	0.9472
0.500	0.9891
0.510	0.8293
0.520	0.3187
0.530	0.0465
0.540	0.0162
0.550	0.0052
0.560	0.0031
0.570	0.0000

TM1 gain = 0.0602436
TM1 offset = - 0.15
TM1 Bandwidth = 0.07
(note: should have used TM1 Bandwidth = 0.06)

Spectral Response for TM band 2

λ (microns)	$\beta(\lambda)$
0.500	0.0000
0.510	0.0233
0.520	0.1635
0.530	0.5718
0.540	0.7312
0.550	0.8367
0.560	0.8890
0.570	0.9074
0.580	0.9124
0.590	0.9871
0.600	0.9428
0.610	0.4616
0.620	0.0969
0.630	0.0357
0.640	0.0115
0.650	0.0000

TM2 gain = 0.1175036
TM2 offset = - 0.2804878
TM2 Bandwidth = 0.08

Spectral Response for TM band 3

λ (microns)	$\beta(\lambda)$
0.570	0.0000
0.580	0.0018
0.590	0.0023
0.600	0.0079
0.610	0.0375
0.620	0.2958
0.630	0.5774
0.640	0.8184
0.650	0.9008
0.660	0.9064
0.670	0.9699
0.680	0.9983
0.690	0.7874
0.700	0.1186
0.710	0.0464
0.720	0.0200
0.730	0.0062
0.740	0.0031
0.750	0.0000

TM3 gain = 0.080597
TM3 offset = - 0.119403
TM3 Bandwidth = 0.06

Spectral Response for TM band 4

λ (microns)	β(λ)
0.720	0.0000
0.730	0.0023
0.740	0.0070
0.750	0.0186
0.760	0.0706
0.770	0.2752
0.780	0.6534
0.790	0.9300
0.800	1.0000
0.810	0.9804
0.820	0.9359
0.830	0.9173
0.840	0.9196
0.850	0.9254
0.860	0.8856
0.870	0.8844
0.880	0.8599
0.890	0.7835
0.900	0.7152
0.910	0.2114
0.920	0.0314
0.930	0.0075
0.940	0.0035
0.950	0.0000

TM4 gain = 0.0814399
TM4 offset = - 0.15
TM4 Bandwidth = 0.14
(note: should have used TM4 Bandwidth = 0.12)

Spectral Response for SPOT panchromatic

λ (microns)	β(λ)
0.470	0.000
0.480	0.005
0.490	0.114
0.500	0.347
0.510	0.458
0.520	0.526
0.530	0.637
0.540	0.719
0.550	0.734
0.560	0.746
0.570	0.800
0.580	0.865
0.590	0.912
0.600	0.919
0.610	0.941
0.620	0.932
0.630	0.953
0.640	0.971
0.650	1.000
0.660	0.959
0.670	0.903
0.680	0.803
0.690	0.699
0.700	0.631
0.710	0.601
0.720	0.411
0.730	0.215
0.740	0.085
0.750	0.033
0.760	0.014
0.770	0.006
0.780	0.004
0.790	0.002
0.800	0.000

SPOT gain = 0.99203

SPOT offset = 0

SPOT Bandwidth = 0.17945 W/m^2 sr μm

III. Computed Radiance from LOWTRAN 7 with Integrated Sensor Response (W/cm^2 sr μm)

Atmosphere 1 (IHAZE = 1)

	SPOT	TM1	TM2	TM3	TM4
urban	1.228E-03	4.956E-04	5.604E-04	4.245E-04	4.973E-04
	2.105E-03	7.551E-04	9.536E-04	7.418E-04	8.560E-04
	1.044E-03	4.844E-04	4.917E-04	3.431E-04	3.950E-04
	1.942E-03	7.368E-04	8.805E-04	6.777E-04	7.243E-04
	1.321E-03	5.874E-04	6.164E-04	4.403E-04	4.887E-04
soil	1.392E-03	4.328E-04	5.843E-04	5.309E-04	7.505E-04
	1.731E-03	5.757E-04	7.475E-04	6.410E-04	9.005E-04
	2.139E-03	5.632E-04	8.351E-04	8.720E-04	1.143E-03
	1.941E-03	4.778E-04	7.845E-04	7.766E-04	1.013E-03
	1.209E-03	3.611E-04	4.940E-04	4.747E-04	5.826E-04
water	4.186E-04	5.665E-04	2.251E-04	1.006E-04	7.273E-05
	4.292E-04	3.875E-04	2.318E-04	1.025E-04	7.437E-05
	4.350E-04	3.817E-04	2.361E-04	1.032E-04	7.364E-05
	4.643E-04	3.724E-04	2.550E-04	1.094E-04	8.011E-05
	5.568E-04	3.619E-04	3.065E-04	1.386E-04	1.191E-04
trees	1.068E-03	4.047E-04	4.846E-04	3.122E-04	1.555E-03
	1.527E-03	4.297E-04	6.996E-04	4.703E-04	1.775E-03
	1.181E-03	4.072E-04	5.396E-04	3.516E-04	1.566E-03
	1.307E-03	4.070E-04	5.664E-04	4.303E-04	1.698E-03
	1.045E-03	4.172E-04	5.139E-04	2.634E-04	1.778E-03
grass	9.336E-04	3.950E-04	4.660E-04	2.480E-04	1.287E-03
	7.265E-04	3.246E-04	3.746E-04	1.709E-04	1.208E-03
	1.218E-03	4.645E-04	5.770E-04	3.014E-04	2.085E-03
	1.257E-03	4.756E-04	5.263E-04	4.261E-04	1.967E-03
	1.226E-03	4.541E-04	5.475E-04	3.686E-04	1.949E-03

Atmosphere 2 (IHAZE = 5)

	SPOT	TM1	TM2	TM3	TM4
urban	8.890E-04	3.886E-04	4.106E-04	3.010E-04	3.502E-04
	1.312E-03	4.925E-04	5.919E-04	4.627E-04	5.544E-04
	7.982E-04	3.839E-04	3.787E-04	2.595E-04	2.921E-04
	1.233E-03	4.848E-04	5.584E-04	4.301E-04	4.790E-04
	9.316E-04	4.252E-04	4.362E-04	3.090E-04	3.453E-04
soil	9.732E-04	3.635E-04	4.222E-04	3.555E-04	4.944E-04
	1.135E-03	4.208E-04	4.972E-04	4.116E-04	5.800E-04
	1.341E-03	4.158E-04	5.389E-04	5.294E-04	7.177E-04
	1.243E-03	3.822E-04	5.152E-04	4.808E-04	6.435E-04
	8.858E-04	3.346E-04	3.807E-04	3.268E-04	3.985E-04
water	4.942E-04	4.110E-04	2.552E-04	1.358E-04	1.088E-04
	4.992E-04	3.444E-04	2.583E-04	1.367E-04	1.097E-04
	5.018E-04	3.422E-04	2.603E-04	1.371E-04	1.093E-04
	5.156E-04	3.388E-04	2.690E-04	1.402E-04	1.130E-04
	5.604E-04	3.347E-04	2.928E-04	1.550E-04	1.352E-04
trees	8.139E-04	3.523E-04	3.752E-04	2.441E-04	9.533E-04
	1.037E-03	3.625E-04	4.748E-04	3.245E-04	1.079E-03
	8.683E-04	3.534E-04	4.006E-04	2.642E-04	9.597E-04
	9.318E-04	3.533E-04	4.132E-04	3.045E-04	1.035E-03
	8.002E-04	3.573E-04	3.883E-04	2.191E-04	1.080E-03
grass	7.458E-04	3.482E-04	3.666E-04	2.111E-04	8.002E-04
	6.458E-04	3.199E-04	3.244E-04	1.718E-04	7.551E-04
	8.846E-04	3.763E-04	4.172E-04	2.384E-04	1.256E-03
	9.080E-04	3.805E-04	3.941E-04	3.032E-04	1.188E-03
	8.914E-04	3.722E-04	4.038E-04	2.737E-04	1.178E-03

Atmosphere 3 (IHAZE = 6)

	SPOT	TM1	TM2	TM3	TM4
urban	1.200E-03	4.748E-04	5.445E-04	4.174E-04	4.982E-04
	2.120E-03	7.500E-04	9.583E-04	7.492E-04	8.720E-04
	1.006E-03	4.629E-04	4.722E-04	3.323E-04	3.915E-04
	1.949E-03	7.307E-04	8.813E-04	6.822E-04	7.348E-04
	1.298E-03	5.722E-04	6.035E-04	4.340E-04	4.892E-04
soil	1.372E-03	4.081E-04	5.696E-04	5.287E-04	7.620E-04
	1.728E-03	5.596E-04	7.414E-04	6.438E-04	9.183E-04
	2.154E-03	5.464E-04	8.334E-04	8.851E-04	1.171E-03
	1.947E-03	4.569E-04	7.802E-04	7.855E-04	1.035E-03
	1.180E-03	3.321E-04	4.745E-04	4.700E-04	5.871E-04
water	3.497E-04	5.512E-04	1.916E-04	7.845E-05	5.495E-05
	3.608E-04	3.602E-04	1.986E-04	8.047E-05	5.666E-05
	3.670E-04	3.541E-04	2.031E-04	8.118E-05	5.590E-05
	3.978E-04	3.442E-04	2.230E-04	8.767E-05	6.266E-05
	4.950E-04	3.330E-04	2.772E-04	1.182E-04	1.034E-04
trees	1.033E-03	3.784E-04	4.647E-04	3.000E-04	1.598E-03
	1.515E-03	4.048E-04	6.910E-04	4.654E-04	1.827E-03
	1.151E-03	3.810E-04	5.227E-04	3.413E-04	1.610E-03
	1.283E-03	3.808E-04	5.508E-04	4.235E-04	1.747E-03
	1.009E-03	3.915E-04	4.956E-04	2.489E-04	1.830E-03
grass	8.914E-04	3.681E-04	4.452E-04	2.328E-04	1.320E-03
	6.737E-04	2.935E-04	3.489E-04	1.521E-04	1.238E-03
	1.191E-03	4.417E-04	5.620E-04	2.887E-04	2.149E-03
	1.230E-03	4.535E-04	5.086E-04	4.190E-04	2.026E-03
	.199E-03	4.306E-04	5.310E-04	3.590E-04	2.007E-03

IV. Computed Digital Counts

Atmosphere 1 (IHAZE = 1)

	SPOT	TM1	TM2	TM3	TM4
urban	68	120	62	89	45
	116	182	104	155	77
	58	117	55	72	36
	107	177	96	142	65
	73	142	68	93	45
soil	77	105	65	111	68
	96	139	82	134	81
	118	136	91	182	102
	107	116	86	162	91
	67	88	55	100	53
water	23	137	26	22	8
	24	94	27	23	8
	24	93	28	23	8
	26	91	30	24	9
	31	88	35	30	12
trees	59	98	54	66	138
	84	104	77	99	158
	65	99	60	74	139
	72	99	63	90	151
	58	101	57	56	158
grass	52	96	52	53	115
	40	79	42	37	108
	67	113	64	64	185
	69	115	58	90	174
	68	110	61	78	173

Atmosphere 2 (IHAZE = 5)

	SPOT	TM1	TM2	TM3	TM4
urban	49	95	46	64	33
	73	119	65	97	50
	44	94	43	55	27
	68	117	62	90	44
	52	103	49	65	32
soil	54	89	47	75	45
	63	102	55	87	53
	74	101	60	111	65
	69	93	57	101	58
	49	82	43	69	37
water	27	100	30	30	11
	28	84	30	30	11
	28	84	30	30	11
	29	83	31	30	12
	31	82	34	34	14
trees	45	86	42	52	85
	57	88	53	69	96
	48	86	45	56	86
	52	86	46	64	93
	44	87	44	47	97
grass	41	85	41	45	72
	36	78	37	37	68
	49	92	47	51	112
	50	93	44	64	106
	49	91	45	58	105

Atmosphere 3 (IHAZE = 6)

	SPOT	TM1	TM2	TM3	TM4
urban	66	115	60	88	46
	117	180	104	156	78
	56	112	53	70	36
	108	176	96	143	66
	72	138	67	91	45
soil	76	99	63	111	69
	96	135	81	135	82
	119	132	91	185	105
	108	111	85	164	93
	65	81	53	99	53
water	19	133	23	18	7
	20	88	24	18	7
	20	86	24	18	7
	22	84	26	20	7
	27	81	32	26	11
trees	57	92	52	64	142
	84	98	76	98	162
	64	93	58	72	143
	71	93	61	89	155
	56	95	55	53	162
grass	49	90	50	50	118
	37	72	40	33	110
	66	107	62	61	190
	68	110	56	88	180
	66	105	59	76	178

V. Reflectance Spectra

V. Reflectance Spectra

The following tables contain the reflectance spectra for the 25 targets used in computing the synthetic panchromatic weights. For those spectra which are averages of other signatures, the variance associated at each wavelength is also included. The 25 signatures are:

URBAN:	asphalt ave*
	concrete ave*
	gravel
	roofing asphalt
	slate
SOIL:	clay ave*
	loam dry ave*
	loam wet ave*
	sand ave*
	soil ave*
WATER:	water1 through water4
	water ave*
TREES:	ash ave*
	beech ave*
	maple ave*
	oak ave*
	pine ave*
GRASS:	clover
	coarse grass
	orchard grass
	swamp grass
	grass ave*

* denotes an averaged signature

wavelength (micron)	asphalt ave (%r)	variance (%r)
0.4000	7.2539	4.2078
0.4324	8.5758	4.7523
0.4647	9.5174	5.0668
0.4971	10.4912	5.4329
0.5294	11.3506	5.8412
0.5618	12.2835	6.2126
0.5941	13.0583	6.5111
0.6265	13.6551	6.6112
0.6588	14.2181	6.8261
0.6912	14.6264	6.9133
0.7235	15.0084	7.1620
0.7559	15.2762	7.3441
0.7882	15.5070	7.4223
0.8206	15.7433	7.4260
0.8529	15.9420	7.4292
0.8853	16.1183	7.4500
0.9176	16.3185	7.4710
0.9500	16.5668	7.4837
0.9824	16.8450	7.5006
1.0147	17.1273	7.5359
1.0471	17.3849	7.6019
1.0794	17.5790	7.6872
1.1118	17.6489	7.7207

wavelength (micron)	concrete ave (%r)	variance (%r)
0.4000	14.7078	6.0053
0.4324	17.6116	6.6171
0.4647	19.7129	6.8831
0.4971	21.2464	7.0876
0.5294	23.2163	7.5996
0.5618	25.0887	8.0533
0.5941	26.2880	8.2168
0.6265	27.0557	8.2593
0.6588	27.5655	8.2729
0.6912	27.8814	8.2884
0.7235	28.1160	8.3150
0.7559	28.3200	8.3466
0.7882	28.4864	8.3615
0.8206	28.6126	8.3318
0.8529	28.7264	8.2521
0.8853	28.8753	8.1423
0.9176	29.0510	7.9966
0.9500	29.2245	7.8188
0.9824	29.4779	7.6490
1.0147	29.8235	7.5170
1.0471	30.2322	7.4364
1.0794	30.6663	7.3760
1.1118	31.0389	7.3350

wavelength (micron)	gravel (%r)
0.400	18.000
0.450	20.000
0.500	20.000
0.525	20.000
0.550	22.000
0.600	24.500
0.650	24.500
0.670	24.500
0.700	26.500
0.715	27.000
0.750	25.000
0.800	25.000
0.815	25.000
0.850	22.500
0.865	22.500
0.900	24.000
0.950	25.000
1.000	26.500
1.050	28.000
1.100	29.500

wavelength (micron)	roof asphalt (%r)
0.400	9.000
0.450	9.500
0.500	9.750
0.700	11.000
0.750	11.150
0.800	12.000
0.850	12.500
0.900	12.000
1.000	11.000
1.100	10.500

wavelength (micron)	slate ave (%r)	variance (%r)
0.4000	13.1667	3.2998
0.4292	13.3976	3.2968
0.4583	13.7525	3.3045
0.4875	13.9445	3.3307
0.5167	14.0698	3.3559
0.5458	14.1598	3.4457
0.5750	14.2063	3.6840
0.6042	14.4843	3.7597
0.6333	14.8553	3.6220
0.6625	14.8325	3.6667
0.6917	14.9481	3.5924
0.7208	15.1430	3.4748
0.7500	15.3315	3.3968
0.7792	15.4539	3.4206
0.8083	15.5103	3.5196
0.8375	15.5195	3.6342
0.8667	15.5071	3.7507
0.8958	15.4992	3.8752
0.9250	15.5184	4.0212
0.9542	15.5640	4.1903
0.9833	15.6268	4.3732
1.0125	15.6971	4.5547
1.0417	15.7640	4.7143
1.0708	15.8139	4.8278
1.1000	15.8336	4.8707

wavelength (micron)	clay ave (%r)	variance (%r)
0.4	9.475	6.4169
0.4324	10.3895	6.7527
0.4647	12.033	7.6052
0.4971	13.3854	8.5273
0.5294	14.7924	9.2407
0.5618	18.6361	10.4947
0.5941	26.6893	13.5757
0.6265	30.3166	15.7008
0.6588	32.8111	16.918
0.6912	35.5978	17.0522
0.7235	37.6873	16.8153
0.7559	38.9559	15.8306
0.7882	39.07	15.538
0.8206	39.1095	15.7183
0.8529	38.7008	15.4574
0.8853	38.6528	15.5417
0.9176	38.6716	15.4146
0.95	39.2862	15.8408
0.9824	40.1467	16.2454
1.0147	40.6325	15.6496
1.0471	41.4368	15.2551
1.0794	42.6397	15.5841
1.1118	43.4778	15.9322
1.1441	43.6774	16.1637
1.1765	43.1041	16.2399
1.2088	41.6337	16.2958

wavelength (micron)	loam dry ave (%r)	variance (%r)
0.4000	4.8250	2.6901
0.4324	6.0320	3.5878
0.4647	7.8972	4.979
0.4971	9.9596	6.2457
0.5294	13.5459	8.2032
0.5618	18.6381	11.227
0.5941	23.4690	13.3411
0.6265	26.7455	14.664
0.6588	28.9561	15.435
0.6912	31.0680	15.8183
0.7235	32.8521	16.0029
0.7559	34.0106	15.9468
0.7882	34.3662	15.4817
0.8206	34.3978	14.7332
0.8529	34.1023	13.9781
0.8853	34.1604	13.6261
0.9176	34.1348	13.5397
0.9500	34.2633	13.4116
0.9824	34.5742	13.2416
1.0147	35.1156	13.161
1.0471	35.9354	13.3093
1.0794	37.0586	13.8047
1.1118	38.4470	14.7299
1.1441	40.0378	16.1804
1.1765	41.5871	17.8806
1.2088	42.5748	18.8076

wavelength (micron)	loam wet ave (%r)	variance (%r)
0.4000	3.1167	1.2857
0.4324	3.3001	1.5313
0.4647	3.8405	2.0974
0.4971	4.7867	2.8985
0.5294	6.6116	4.3601
0.5618	9.4394	6.7946
0.5941	12.5652	9.2795
0.6265	14.7714	10.8467
0.6588	16.3326	12.0248
0.6912	17.7031	12.7291
0.7235	18.7446	12.9564
0.7559	19.3152	12.7056
0.7882	19.4697	11.8912
0.8206	19.0534	10.9520
0.8529	18.5257	10.2040
0.8853	18.3156	9.8384
0.9176	18.4599	9.8763
0.9500	18.8830	10.2211
0.9824	19.4982	10.7697
1.0147	20.2187	11.3783
1.0471	20.9563	11.8777
1.0794	21.6055	12.1278
1.1118	22.1714	12.2357
1.1441	22.8341	12.4335
1.1765	23.7957	12.9180
1.2088	25.2523	13.9713

wavelength (micron)	sand ave (%r)	variance (%r)
0.4000	9.7910	6.9012
0.4324	11.0945	6.9322
0.4647	12.4006	7.2508
0.4971	13.8032	7.5379
0.5294	16.0499	7.7878
0.5618	18.2708	7.6676
0.5941	19.8237	7.5009
0.6265	21.5510	7.7226
0.6588	23.3101	7.8350
0.6912	24.8459	7.4841
0.7235	26.2491	7.6764
0.7559	27.7084	8.1159
0.7882	28.9225	8.5884
0.8206	29.9130	8.9397
0.8529	30.7870	9.2115
0.8853	31.7761	9.4635
0.9176	32.5929	9.5225
0.9500	33.4390	9.5676
0.9824	34.3435	9.9087
1.0147	35.2869	10.7863
1.0471	35.8646	11.0431
1.0794	36.4346	10.8028
1.1118	37.0728	10.6271
1.1441	37.7160	10.5012
1.1765	38.0292	10.4641
1.2088	38.6012	10.1514

wavelength (micron)	soil ave (%r)	variance (%r)
0.4000	4.7951	3.3789
0.4324	5.5813	3.8050
0.4647	6.5829	4.5061
0.4971	7.9013	5.6142
0.5294	9.9614	7.1669
0.5618	12.6366	8.8267
0.5941	15.1746	10.5700
0.6265	16.9803	11.9755
0.6588	18.6543	12.9735
0.6912	20.2253	13.3712
0.7235	21.7086	13.7367
0.7559	23.1065	14.1498
0.7882	24.1747	14.3461
0.8206	24.8104	14.2925
0.8529	25.1980	14.1392
0.8853	25.6280	13.9194
0.9176	26.0587	13.8155
0.9500	26.7500	13.8079
0.9824	27.4794	13.8130
1.0147	28.3895	13.9910
1.0471	29.6291	14.3832
1.0794	30.7135	14.6852
1.1118	31.5308	14.7322
1.1441	32.1033	14.5755
1.1765	32.7071	14.5394
1.2088	33.7309	15.0002

wavelength (micron)	water1 (%r)
0.4008	9.7015
0.4090	9.1188
0.4175	8.7248
0.4357	8.9543
0.4556	8.0026
0.4773	7.6746
0.4988	4.1640
0.5115	3.3056
0.5249	2.6529
0.5391	2.1187
0.5540	1.6514
0.5698	1.3312
0.5865	1.0090
0.6042	0.7584
0.6431	0.4790
0.6873	0.3871
0.7380	0.4110
0.7663	0.4344
0.8299	0.4869
0.8658	0.5166
0.9050	0.5489
0.9479	0.5844
0.9950	0.6233
1.0471	0.6664
1.1050	0.7142
1.1696	0.7675

wavelength (micron)	water2 (%r)	water3 (%r)
0.3500	9.5000	8.5000
0.4141	8.3520	7.3093
0.4320	7.4443	6.6690
0.4415	7.3446	6.6499
0.4515	7.5874	6.7585
0.4619	7.4994	6.7574
0.4728	7.1857	6.5176
0.4843	6.2669	5.8943
0.5089	3.7620	3.9381
0.5222	3.0897	3.3250
0.5540	1.9160	2.1596
0.5865	1.2063	1.2317
0.6042	0.9411	0.9832
0.6231	0.7134	0.7657
0.6431	0.5870	0.6346
0.6873	0.4426	0.4414
0.7117	0.4377	0.4167
0.7663	0.4877	0.4642
0.8299	0.5460	0.5197
0.8658	0.5790	0.5510
0.9050	0.6149	0.5851
0.9479	0.6542	0.6225
0.9950	0.6975	0.6636
1.0363	0.7353	0.6995
1.0929	0.7872	0.7489
1.1561	0.8452	0.8039

wavelength (micron)	water4 (%r)
0.3992	7.4657
0.4057	6.7603
0.4320	4.9371
0.4415	4.8927
0.4515	5.1718
0.4619	5.4126
0.4728	5.4186
0.4843	5.3286
0.5089	4.6148
0.5222	4.0431
0.5540	2.8143
0.5865	1.8684
0.6231	1.1221
0.6645	0.7816
0.6873	0.6334
0.7117	0.6040
0.7663	0.6725
0.7968	0.7109
0.8299	0.7524
0.8658	0.7975
0.9050	0.8467
0.9479	0.9005
0.9950	0.9597
1.0363	0.1012
1.0929	0.1083
1.1561	0.1162

wavelength (micron)	water ave (%r)	variance (%r)
0.4000	5.7672	2.4318
0.4324	4.5551	2.4561
0.4647	4.7533	2.3265
0.4971	4.4339	0.6491
0.5294	5.0181	1.9894
0.5618	4.4923	2.9046
0.5941	3.4049	2.7532
0.6265	2.7564	2.6319
0.6588	2.0105	1.9582
0.6912	1.5028	1.4185
0.7235	2.0454	2.4572
0.7559	2.0818	2.4303
0.7882	2.1182	2.4038
0.8206	2.1546	2.3776
0.8529	2.1909	2.3519
0.8853	2.2273	2.3266
0.9176	2.2637	2.3017
0.9500	2.3001	2.2774
0.9824	2.3365	2.2535
1.0147	2.3729	2.2308
1.0471	2.4093	2.2072
1.0794	2.4456	2.1849
1.1118	2.4820	2.1631
1.1441	2.5183	2.1418
1.1765	2.5548	2.1212

wavelength (micron)	ash ave (%r)	variance (%r)
0.4000	5.0125	0.3238
0.4234	4.9661	0.4247
0.4469	5.1264	0.8480
0.4703	5.5450	1.1364
0.4938	6.3108	1.5188
0.5172	8.4325	1.6261
0.5407	10.7217	1.5823
0.5641	10.7408	1.8448
0.5876	9.4564	2.7846
0.6110	9.0323	3.4688
0.6345	8.5204	4.2551
0.6579	8.0063	4.9861
0.6814	8.2313	5.7139
0.7048	21.8191	4.5883
0.7283	39.2243	6.7595
0.7517	46.2806	8.2610
0.7752	49.9668	8.2553
0.7986	51.7098	7.4394
0.8221	53.0270	6.5921
0.8455	54.3608	5.9239
0.8690	55.4814	5.3648
0.8924	56.4352	4.8749
0.9393	58.0869	4.3429
0.9862	58.8730	3.8533
1.0331	60.3809	3.7795
1.0800	61.3854	3.5782

wavelength (micron)	beech ave (%r)	variance (%r)
0.4000	4.8500	0.9394
0.4234	5.3658	1.4039
0.4469	5.7867	1.7304
0.4703	6.1550	1.9747
0.4938	6.7592	2.2864
0.5172	11.1213	4.3175
0.5407	16.6838	5.4089
0.5641	18.5977	4.8492
0.5876	17.0617	3.0501
0.6110	16.8021	2.7648
0.6345	16.3848	3.8047
0.6579	14.2365	5.6858
0.6814	13.0250	7.1986
0.7048	32.6949	1.7470
0.7283	48.6266	5.2838
0.7517	54.9735	6.6395
0.7752	57.5684	5.9558
0.7986	59.2999	4.7611
0.8221	60.8526	3.5106
0.8690	63.3283	1.5286
0.8924	64.2547	1.0458
0.9393	65.4749	0.8854
0.9628	65.4183	1.1004
0.9862	65.4514	1.0546
1.0331	66.3466	0.9209
1.0800	67.1000	1.2450

wavelength (micron)	maple ave (%r)	variance (%r)
0.4000	4.7867	0.4559
0.4234	5.0294	0.8322
0.4469	5.1253	1.2348
0.4703	5.3693	1.5295
0.4938	6.1976	1.5856
0.5172	9.3411	1.9537
0.5407	12.5070	2.9783
0.5641	12.8521	2.9924
0.5876	11.2525	3.5179
0.6110	10.6587	4.5478
0.6345	10.4587	5.6960
0.6579	9.5093	6.8845
0.6814	9.6588	8.0209
0.7048	24.3516	5.7392
0.7283	40.3821	8.5347
0.7517	47.1126	10.7630
0.7752	50.2860	10.6759
0.7986	52.1011	10.0600
0.8221	53.4951	9.4201
0.8690	55.8997	8.4940
0.8924	56.7429	8.1538
0.9159	57.5245	7.9329
0.9628	58.4657	7.4945
1.0097	59.3190	7.5105
1.0331	59.8287	7.6975
1.0800	60.3188	8.0890

wavelength (micron)	oak ave (%r)	variance (%r)
0.4000	4.0429	0.5010
0.4234	4.8187	0.7119
0.4469	5.3397	0.7865
0.4703	5.5008	1.1908
0.4938	6.0075	1.2904
0.5172	9.2896	1.6779
0.5407	12.9003	3.4844
0.5641	13.2204	2.6626
0.5876	12.5584	2.0621
0.6110	12.7182	4.1991
0.6345	12.6137	7.5743
0.6579	12.5229	9.9150
0.6814	14.7312	10.0947
0.7048	27.3688	6.6030
0.7283	42.3325	7.4662
0.7517	50.9876	11.0869
0.7752	54.0828	10.4918
0.7986	55.9306	8.9539
0.8221	57.8067	7.5194
0.8690	61.2838	5.3045
0.9159	63.8494	3.7723
0.9628	65.0181	3.1835
0.9862	65.1896	3.0757
1.0097	65.1379	2.9793
1.0566	64.9464	2.8561
1.0800	64.8637	2.7847

wavelength (micron)	pine ave (%r)	variance (%r)
0.4000	4.2192	0.7970
0.4234	5.1893	0.8867
0.4469	5.9020	0.9486
0.4703	6.0801	0.9306
0.4938	6.3519	0.9108
0.5172	9.5201	1.8357
0.5407	13.2585	2.5531
0.5641	12.4005	2.3609
0.5876	9.5369	1.9395
0.6110	8.0952	1.7418
0.6345	6.8038	1.9908
0.6579	5.6494	1.4920
0.6814	6.1304	1.2907
0.7048	18.7707	3.4072
0.7283	43.4731	7.2556
0.7517	56.8457	12.0020
0.7986	60.6639	12.9094
0.8221	61.5947	12.7374
0.8690	62.2015	12.9853
0.8924	62.0399	12.8182
0.9159	61.3843	12.4189
0.9393	60.3627	11.8626
0.9628	57.8612	10.5839
0.9862	57.1754	10.2476
1.0331	60.2705	11.6057
1.0800	61.8625	11.9252

wavelength (micron)	clover (%r)	coarse grass (%r)
0.40	2.00	4.50
0.50	3.00	6.00
0.56	8.00	11.00
0.62	4.00	7.00
0.68	1.50	5.00
0.76	38.00	40.00
0.78	39.00	42.00
0.80	40.50	43.50
0.86	42.00	45.00
0.96	45.00	45.00
1.02	49.00	47.00
1.12	48.00	47.00

wavelength (micron)	orchard grass (%r)
0.40	9.00
0.50	9.00
0.54	13.30
0.64	7.50
0.70	25.00
0.73	45.00
0.75	60.00
0.78	67.00
0.90	69.50
0.95	69.30
1.08	72.80

wavelength (micron)	swamp grass (%r)
0.40	7.90
0.48	8.00
0.50	8.50
0.52	13.00
0.54	15.50
0.56	15.00
0.60	10.00
0.68	7.00
0.69	6.50
0.70	18.00
0.73	60.00
0.75	70.00
0.78	71.00
0.88	73.00
1.10	74.50

wavelength (micron)	grass ave (%r)	variance (%r)
0.4000	8.6455	3.0086
0.4234	8.1555	2.9210
0.4469	7.3426	2.6931
0.4703	7.0755	2.5241
0.4938	8.2226	2.5462
0.5172	11.3208	3.1860
0.5407	13.9132	3.7150
0.5641	13.5884	3.3290
0.5876	11.2198	2.7514
0.6110	8.3764	2.3623
0.6345	6.7733	2.6845
0.6579	8.4793	4.1997
0.6814	15.5105	5.8306
0.7048	29.6291	7.9555
0.7283	48.3172	10.9784
0.7517	60.6736	11.5657
0.7752	64.8162	12.1918
0.7986	66.5935	12.2972
0.8221	67.7268	12.2363
0.8690	68.4342	12.3458
0.8924	68.2135	12.2043
0.9393	67.1161	11.3917
0.9628	67.0564	10.9687
1.0097	68.9507	10.6680
1.0566	70.8419	10.9669
1.0800	70.7134	10.9599

Appendix I

Computing the Standard Deviation Between Two Values

This appendix shows that the standard deviation between two samples is the absolute value of their differences divided by the square root of two.

Given two samples, x_1 and x_2 ,and their average, $\bar{x} = \frac{x_1 + x_2}{2}$, we can write the definition of the standard deviation between them as:

$$\sigma = \sqrt{\frac{(x_1 - \bar{x})^2 + (x_2 - \bar{x})^2}{n - 1}}$$

since n = 2 samples, the equation can be rewritten as:

$$\sigma = \sqrt{(x_1^2 - 2x_1\bar{x} + \bar{x}^2) + (x_2^2 - 2x_2\bar{x} + \bar{x}^2)}$$

combining terms,

$$\sigma = \sqrt{x_1^2 + x_2^2 + 2\bar{x}^2 - 2\bar{x}(x_1 + x_2)}$$

substituting in $\bar{x}$,

$$\sigma = \sqrt{x_1^2 + x_2^2 + 2\left(\frac{x_1 + x_2}{2}\right)^2 - 2\left(\frac{x_1 + x_2}{2}\right)(x_1 + x_2)}$$

$$\sigma = \sqrt{x_1^2 + x_2^2 - \frac{1}{2}(x_1 + x_2)^2}$$

$$\sigma = \sqrt{\frac{1}{2}(x_1^2 - 2x_1x_2 + x_2^2)}$$

$$\sigma = \sqrt{\frac{(x_1 - x_2)^2}{2}}$$

and

$$\sigma = \frac{|x_1 - x_2|}{\sqrt{2}}$$